

# <sup>1</sup> ATLAS+CMS DARK MATTER FORUM RECOMMENDA- <sup>2</sup> TIONS

<sup>3</sup> Author/contributor list to be added as document is finalized.

<sup>4</sup> May 13, 2015



# 1

## *Introduction*

This document presents recommendations for the MC production and parameter scans for the various simplified models.

What is the motivation for this report?

First, the physics is compelling. Measurements at the energy frontier can make quantitative statements about dark matter.

Second, in Run-1 at the LHC, there was confusion in the community over the interpretation of the data.

Third, there are reasons to strive for uniformity in interpretation in the different experiments. This will ultimately aid in the combination of data, but also facilitates cross checks of results.

What is the format of this report?

First, it describes the signatures and models of interest for dark matter searches.

Secondly, it provides information on the tools to be used to simulate signals.

Finally, it makes a recommendation on a scan of parameters within those models based on supporting material.



24 2

25 *Overall choices for simplified models*

26 General topics:

- 27 • choice of Dark Matter type: Dirac (unless specified otherwise)
- 28     and what we might be missing
- 29 • MFV and what we might be missing



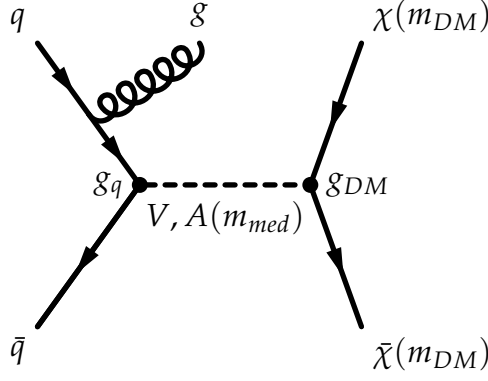


Figure 3.1: Representative Feynman diagram showing the pair production of dark matter particles in association with a parton from the initial state via a vector or axial-vector mediator. The cross section and kinematics depend upon the mediator and dark matter masses, and the mediator couplings to dark matter and quarks respectively:  $(M_{\text{med}}, m_{\text{DM}}, g_{\text{DM}}, g_q)$ .

### 3

## Recommended models for all MET+X analyses

### 3.1 Vector and axial vector mediator, s-channel exchange

A simple extension of the Standard Model (SM) is an additional  $U(1)$  gauge symmetry, where a dark matter (DM) candidate particle has charges only under this new group. Assuming that some SM particles are also charged under this group, then a new vector boson can mediate interactions between the SM and DM.

We consider the case of a DM particle that is a Dirac fermion and where the production proceeds via the exchange of a spin-1 mediator in the  $s$ -channel. We consider vector and axial-vector couplings between the spin-1 mediator and SM and DM fields, with the corresponding interaction Lagrangians:

$$\mathcal{L}_{\text{vector}} = g_q \sum_{q=u,d,s,c,b,t} Z'_\mu \bar{q} \gamma^\mu q + g_{\text{DM}} Z'_\mu \bar{\chi} \gamma^\mu \chi \quad (3.1)$$

$$\mathcal{L}_{\text{axial-vector}} = g_q \sum_{q=u,d,s,c,b,t} Z'_\mu \bar{q} \gamma^\mu \gamma^5 q + g_{\text{DM}} Z'_\mu \bar{\chi} \gamma^\mu \gamma^5 \chi. \quad (3.2)$$

Universal couplings are assumed for all the quarks. It is also possible to consider another model in which mixed vector and axial-vector couplings are considered, for instance the couplings to the quarks are vector whereas those to DM are axial-vector. As a starting point, we consider only the models with the vector couplings only and axial vector couplings only.

We assume that no additional visible or invisible decays contribute to the width of the mediator. This is referred to as the minimal width and it is defined as follows for the vector and axial-

vector models:

$$\Gamma_{\min}^{V/A} = \Gamma_{\tilde{\chi}\chi}^{V/A} + \sum_q \Gamma_{\bar{q}q}^{V/A}. \quad (3.3)$$

The leading order expressions for the partial widths are:

$$\Gamma_{\tilde{\chi}\chi}^V = \frac{g_{\text{DM}}^2 M_{\text{med}}}{12\pi} \left( 1 + \frac{2m_{\text{DM}}^2}{M_{\text{med}}^2} \right) \beta_{\text{DM}} \theta(M_{\text{med}} - 2m_{\text{DM}}) \quad (3.4)$$

$$\Gamma_{\bar{q}q}^V = \frac{3g_q^2 M_{\text{med}}}{12\pi} \left( 1 + \frac{2m_q^2}{M_{\text{med}}^2} \right) \beta_q \theta(M_{\text{med}} - 2m_q) \quad (3.5)$$

$$\Gamma_{\tilde{\chi}\chi}^A = \frac{g_{\text{DM}}^2 M_{\text{med}}}{12\pi} \beta_{\text{DM}}^{3/2} \theta(M_{\text{med}} - 2m_{\text{DM}}) \quad (3.6)$$

$$\Gamma_{\bar{q}q}^A = \frac{3g_q^2 M_{\text{med}}}{12\pi} \beta_q^{3/2} \theta(M_{\text{med}} - 2m_q), \quad (3.7)$$

$\theta(x)$  denotes the Heaviside step function, and  $\beta_f = \sqrt{1 - \frac{4m_f^2}{M_{\text{med}}^2}}$  is the velocity of the fermion  $f$  in the mediator rest frame. Note the color factor 3 in the quark terms. Figure 3.2 shows the minimal width as a function of mediator mass for both vector and axial-vector mediators assuming  $g_q = g_{\text{DM}} = 1$ . With this choice of the couplings, the dominant contribution to the minimal width comes from the quarks due to the color factor enhancement and the large number of them.

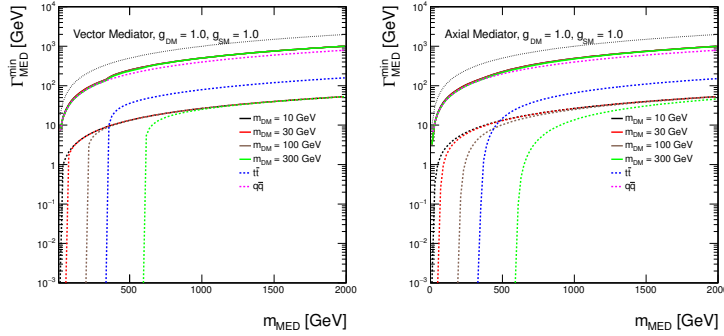


Figure 3.2: Minimal width as a function of mediator mass for vector and axial-vector mediator assuming couplings of 1. The total width is shown as solid lines for Dark Matter masses of 10 GeV, 30 GeV, 100 GeV and 300 GeV in black, red, brown and green, respectively. The individual contributions from Dark Matter are indicated by dotted lines with the same colors. The contribution from all quarks but top is shown as magenta dotted line and the contribution from top quarks only is illustrated by the dotted blue line. The dotted black line shows the extreme case  $\Gamma_{\min} = M_{\text{med}}$ .

The simplified models described here have four free parameters: mediator mass  $M_{\text{med}}$ , Dark Matter mass  $m_{\text{DM}}$ , coupling of the mediator to quarks  $g_q$  and coupling of the mediator to Dark Matter  $g_{\text{DM}}$ . In order to determine an optimal choice of the parameter grid for presentation of the early Run-2 results, dependencies of the kinematic quantities and cross sections on the individual parameters need to be studied. The following paragraphs list the main observations from the scans over the parameters that support the final proposal for the parameter grid.

*Scan over the couplings* Figure 3.3 reveals there are no differences in the shape of the  $\cancel{E}_T$  distribution among the samples where the pair of 10 GeV Dark Matter particles are produced on-shell from



the mediator of 1 TeV, generated with different choice of the coupling strength. The considered coupling values range from 0.1 to 1.45, where the latter value approximates the maximum allowed coupling value, holding  $g_q = g_{DM}$ , such that  $\Gamma_{\min} < M_{\text{med}}$ . Based on similar plots for different choices of mediator and Dark Matter masses, it is concluded that the shapes of kinematic distributions are not altered either for the on-shell Dark Matter production where  $M_{\text{med}} > 2m_{DM}$ , or for the off-shell Dark Matter production where  $M_{\text{med}} < 2m_{DM}$ . Only the cross sections change. Differences in kinematic distributions are expected only close to the transition region where both on-shell and off-shell regimes mix.

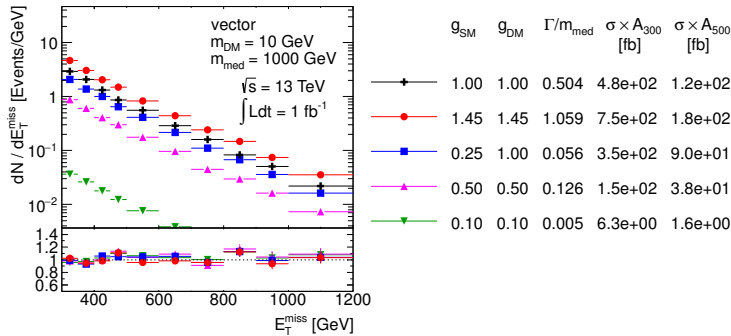


Figure 3.3: Scan over couplings. The  $E_T$  distribution is compared for the vector mediator models using the parameters as indicated. Ratios of the normalized distributions with respect to the first one are shown.  $A_{300}$  and  $A_{500}$  in the table denote the acceptance of the  $E_T > 300$  GeV and  $E_T > 500$  GeV cut, respectively.

The only situation requiring a more careful treatment is the case of extremely heavy and narrow mediators, which can arise for small coupling strengths. Upon close examination, it was determined that this case is not peculiar. However, the complete story is a cautionary tale about understanding the details of tools applied. Figure 3.4 suggests a change in the shape of the  $E_T$  distribution for 5 TeV mediator once  $\Gamma_{\min}/M_{\text{med}}$  gets down to the order of percent or below. This, however, does not come from physics, but is an artifact of the generator implementation, where a cutoff for the regions far away from the mediator mass is often used. This is illustrated in Fig. 3.5 showing the invariant mass of the Dark Matter pair in the samples generated for 7 TeV mediator with different coupling strength. In all cases, it is expected to observe a peak around the mediator mass with a tail extending to  $m_{\tilde{\chi}\tilde{\chi}} \rightarrow 0$ , significantly enhanced by parton distribution functions at low Bjorken  $x$ . For coupling strength 1 and 3, the massive enhancement at  $m_{\tilde{\chi}\tilde{\chi}} \rightarrow 0$  implies the resonant production at  $m_{\tilde{\chi}\tilde{\chi}} = 7$  TeV is statistically suppressed such that barely any events are generated there. However, for narrower mediators with couplings below 1, the peak around 7 TeV is clearly visible in the generated sample and the dominant tail at  $m_{\tilde{\chi}\tilde{\chi}} \rightarrow 0$  is artificially cut off, leading to unphysical cross section predictions and kinematic shapes. This explains why the sample with the narrowest mediator in Fig. 3.4 is heavily suppressed in terms of production cross section and also gives different  $E_T$  shape. In general, for such extreme parameter choices the EFT model should give the correct answer. [TODO: add results of ongoing study.]

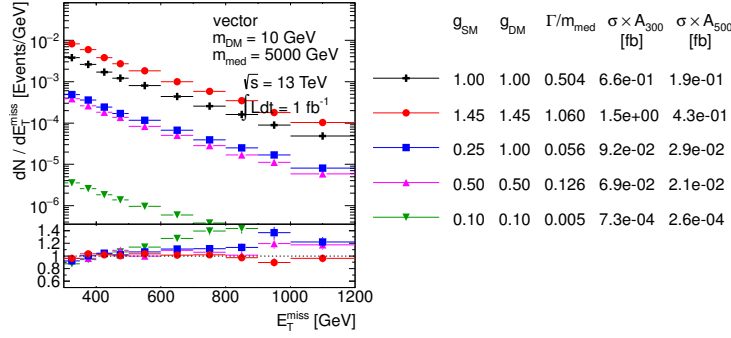


Figure 3.4: Scan over couplings. The  $E_T$  distribution is compared for the vector mediator models using the parameters as indicated. Ratios of the normalized distributions with respect to the first one are shown.  $A_{300}$  and  $A_{500}$  in the table denote the acceptance of the  $E_T > 300$  GeV and  $E_T > 500$  GeV cut, respectively.

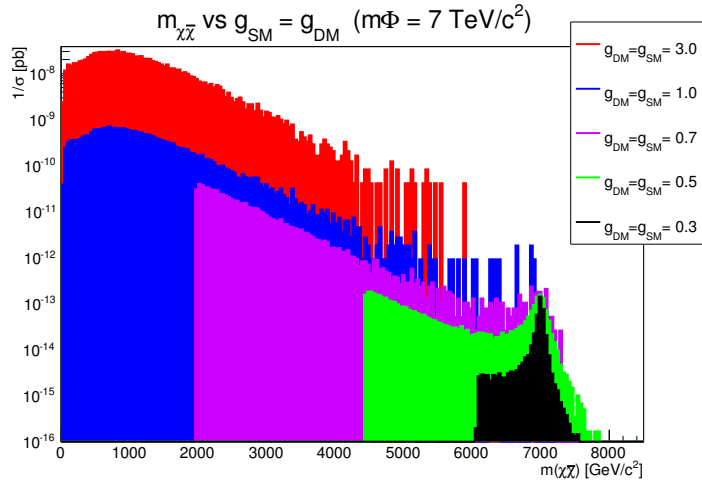


Figure 3.5: Invariant mass of the Dark Matter pair in the samples with  $M_{med} = 7$  TeV and different coupling strengths.

*Scan over the Dark Matter mass* For the fixed mediator mass and couplings, both the cross section and the kinematic distributions remain similar for different Dark Matter masses as long as  $M_{med} > 2m_{DM}$ . This simply reflects the fact that most mediators are produced on-shell, and the details of the invisible decay are unimportant. This is illustrated in Fig. 3.6 for an example of  $M_{med} = 1$  TeV  $10 \text{ GeV} < m_{DM} < 300 \text{ GeV}$ . It is observed that the cross section decreases as the  $m_{DM}$  approaches  $M_{med}/2$ . Once the Dark Matter pair is produced off-shell, the cross section of such simplified model is suppressed and the  $E_T$  spectrum hardens, as demonstrated with the choice of  $m_{DM} = 1$  TeV in the same plot. Figure 3.7 reveals the  $E_T$  spectrum hardens further with increasing  $m_{DM}$ , accompanied by the gradual decrease of the cross section. From these observations one can conclude:

- A coarse binning along  $m_{DM}$  is sufficient at  $M_{med} \gg 2m_{DM}$ .
- Finer binning is needed in order to capture the changes in the cross section and kinematic quantities close to the production threshold on both sides around  $M_{med} = 2m_{DM}$ .
- Due to the significant cross section suppression of the off-shell Dark Matter pair production, it is not necessary to populate the parameter space  $M_{med} \ll 2m_{DM}$  since the LHC is not going to be able to probe the models there.

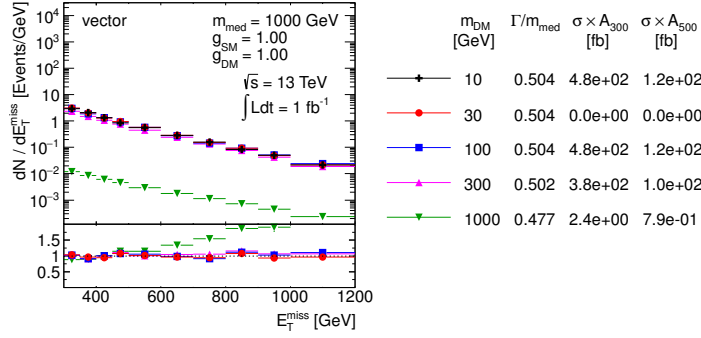


Figure 3.6: Scan over Dark Matter mass. The  $E_T$  distribution is compared for the vector mediator models using the parameters as indicated. Ratios of the normalized distributions with respect to the first one are shown.  $A_{300}$  and  $A_{500}$  in the table denote the acceptance of the  $E_T > 300$  GeV and  $E_T > 500$  GeV cut, respectively.

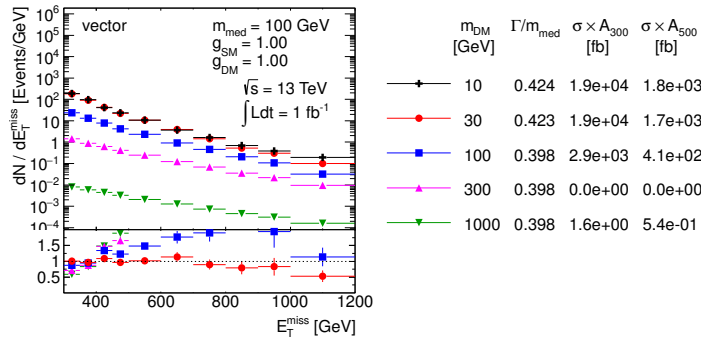


Figure 3.7: Scan over Dark Matter mass. The  $E_T$  distribution is compared for the vector mediator models using the parameters as indicated. Ratios of the normalized distributions with respect to the first one are shown.  $A_{300}$  and  $A_{500}$  in the table denote the acceptance of the  $E_T > 300$  GeV and  $E_T > 500$  GeV cut, respectively.

Scan over the mediator mass Changing the mediator mass for fixed Dark Matter mass and couplings leads to significant differences in cross section and shapes of the kinematic variables for  $M_{med} > 2m_{DM}$  as shown in Fig. 3.8. As expected, higher mediator masses lead to harder  $E_T$  spectra. On the other hand, the  $E_T$  shapes are similar in the off-shell Dark Matter production regime. This is illustrated in Fig. 3.9. Therefore, a coarse binning in  $m_{DM}$  is sufficient at  $M_{med} \ll 2m_{DM}$ .

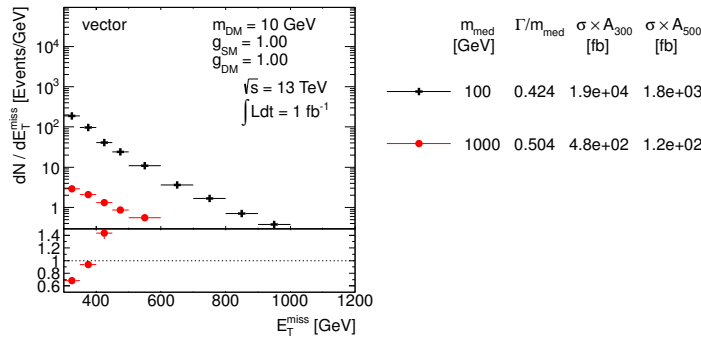


Figure 3.8: Scan over mediator mass. The  $E_T$  distribution is compared for the vector mediator models using the parameters as indicated. Ratios of the normalized distributions with respect to the first one are shown.  $A_{300}$  and  $A_{500}$  in the table denote the acceptance of the  $E_T > 300$  GeV and  $E_T > 500$  GeV cut, respectively.

Proposed parameter grid It is difficult to visualize a four dimensional scan. However, it is convenient to study the parameter dependence, and present results, in two projections: (a) the  $M_{med}-m_{DM}$  plane for a particular choice of the couplings, and (b) the  $g_q-g_{DM}$  plane for a particular choice of the masses.

We choose to display the results in the  $M_{med}-m_{DM}$  plane for the choice of the couplings  $g_q = g_{DM} = 1$ . In order to motivate

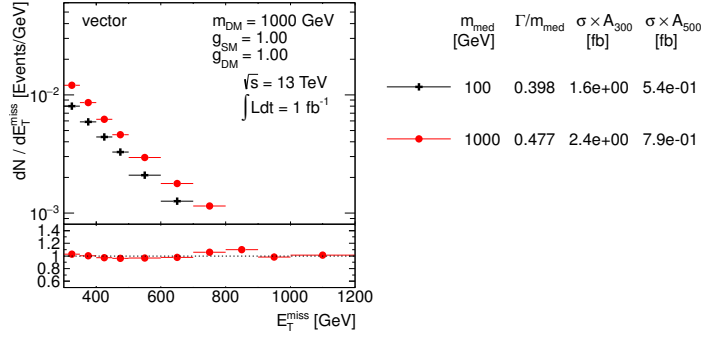


Figure 3.9: Scan over mediator mass. The  $E_T$  distribution is compared for the vector mediator models using the parameters as indicated. Ratios of the normalized distributions with respect to the first one are shown.  $A_{300}$  and  $A_{500}$  in the table denote the acceptance of the  $E_T > 300$  GeV and  $E_T > 500$  GeV cut, respectively.

the highest mediator mass grid point, the expected sensitivity of Run-2 LHC data needs to be taken into account. The expected upper limit at 95% confidence level on the product of cross section, acceptance and efficiency,  $\sigma \times A \times \epsilon$ , in the final Run-1 ATLAS mono-jet analysis [A<sup>+</sup>15] is 51 fb and 7.2 fb for  $E_T > 300$  GeV and  $E_T > 500$  GeV, respectively. The ATLAS 14 TeV prospects [ATL14] predict twice better sensitivity with the first 5 fb<sup>-1</sup> of data already. Given the cross section for V+jets processes increases by roughly a factor 2 when going from  $\sqrt{s} = 8$  TeV to 13 TeV, similar fiducial cross section limits can be expected with the first Run-2 data as from the final Run-1 analysis. The generator level cross section times the acceptance at  $E_T > 500$  GeV for the model with couplings  $g_q = g_{\text{DM}} = 1$ , light Dark Matter of 10 GeV and 1 TeV vector mediator is at the order of 100 fb, i.e. the early Run-2 mono-jet analysis is going to be sensitive to heavier mediators than this. The value of  $\sigma \times A$  at  $E_T > 500$  GeV for 5 TeV vector mediator is at the order of 0.1 fb, therefore this model probably lies beyond the reach of the LHC.

Based on these arguments, the following  $M_{\text{med}}$  grid points are chosen, roughly equidistant in the logarithmic scale: 10 GeV, 20 GeV, 50 GeV, 100 GeV, 200 GeV, 300 GeV, 500 GeV, 1000 GeV and 2000 GeV. Given the fact that significant changes in cross section happen around the  $M_{\text{med}} = 2m_{\text{DM}}$  threshold, the  $m_{\text{DM}}$  grid points are taken at approximately  $M_{\text{med}}/2$ , namely: 10 GeV, 50 GeV, 150 GeV, 500 GeV and 1000 GeV. Points on the on-shell diagonal are always chosen to be 5 GeV away from the threshold, to avoid numerical instabilities in the event generation. The detailed studies of the impact of the parameter changes on the cross section and kinematic distributions presented earlier in this section support removing some of the grid points and rely on interpolation. The optimised grids proposed for the vector and axial-vector mediators are given in Table. 3.1, containing 29 mass points each. One point at very high mediator mass (5 TeV) is added for each of the DM masses scanned, to aid the reinterpretation of results in terms of contact interaction operators (EFTs).

The presentation of the results in the  $g_q$ - $g_{\text{DM}}$  plane for fixed masses benefits from cross section scaling and is discussed in Section 3.3.

$m_{\text{DM}}/\text{GeV}$	$m_{\text{med}}/\text{GeV}$									
1	10	20	50	100	200	300	500	1000	2000	5000
10	10	15	50	100	"	"	"	"	"	"
50	10		50	95	200	300	"	"	"	"
150	10				200	295	500	"	"	"
500	10						500	995	2000	"
1000	10							1000	1995	5000

Table 3.1: Simplified model benchmarks for  $s$ -channel simplified models (spin-1 mediators decaying to Dirac DM fermions in the V and A case, taking the minimum width for  $g_q = g_{\text{DM}} = 1$ )

*Implementation* There are several matrix element implementations of the  $s$ -channel vector mediated DM production. This is available in POWHEG, MADGRAPH and also MCFM. The implementation in POWHEG generates DM pair production with 1 parton at next-to-leading order (NLO), whilst MADGRAPH and MCFM are at leading order (LO). As shown in POWHEG Ref. [HKR13], including NLO corrections result in an enhancement in the cross section as compared to LO and though this is not significant, it does lead to a substantial reduction in the dependence on the choice of the renormalization and factorization scale and hence the theoretical uncertainty on the signal prediction. Since NLO calculations are available for the process in POWHEG, we recommend to proceed with POWHEG as the generator of choice.

### 3.2 Scalar and pseudoscalar mediator, $s$ -channel exchange

One of the most simple UV complete extensions of the effective field theory approach is the addition of a scalar/pseudoscalar mediator between DM and SM. A gauge singlet mediator can have tree-level interactions with a singlet DM particle that is either a Dirac or Majorana fermion, or DM that is a scalar itself. The spin-0 mediator can either be a real or complex scalar; a complex scalar contains both scalar and pseudoscalar particles, whereas the real field only contains the scalar particle. In this document we consider only two of the possible choices for this simplified model: one where the interaction with the SM is mediated by a real scalar, and the second where we consider only a light pseudoscalar, assuming that the associated scalar is decoupled from the low-energy spectrum. The kinematics of the two cases is sufficiently different to suggest that further investigation of the complex scalar case is needed but left for future studies.

Couplings to the SM fermions can be arranged by mixing with the SM Higgs. Such models have interesting connections with Higgs physics, and can be viewed as generalizations of the Higgs portal to DM. The most general scalar mediator models will have renormalizable interactions between the SM Higgs and the new scalar  $\phi$  or pseudoscalar  $a$ , as well as  $\phi/a$  interactions with electroweak gauge bosons. Such interactions are model dependent, often subject to constraints from electroweak precision tests, and would suggest specialized searches which cannot be generalized to a broad class of models (unlike, for instance, the  $E_T + \text{jets}$  searches).

As a result, for this class of minimal simplified models with spin-0 mediators, we will focus primarily on couplings to fermions and loop-induced couplings to gluons.

Minimal Flavor Violation (MFV) implies that scalar couplings to fermions will be proportional to the fermion mass. However, they can differ for up- and down-type quarks and for charged leptons.

Following the assumption that DM is a fermion  $\chi$ , which couples to the SM only through a scalar  $\phi$  or pseudoscalar  $a$ , the most general tree-level interaction Lagrangians compatible with the MFV assumption are [CRTW14, ADR<sup>+</sup>14, BFG15]:

$$\begin{aligned}\mathcal{L}_\phi &= g_\chi \phi \bar{\chi} \chi + \frac{\phi}{\sqrt{2}} \sum_i \left( g_u y_i^u \bar{u}_i u_i + g_d y_i^d \bar{d}_i d_i + g_\ell y_i^\ell \bar{\ell}_i \ell_i \right), \quad (3.8) \\ \mathcal{L}_a &= i g_\chi a \bar{\chi} \gamma_5 \chi + \frac{ia}{\sqrt{2}} \sum_i \left( g_u y_i^u \bar{u}_i \gamma_5 u_i + g_d y_i^d \bar{d}_i \gamma_5 d_i + \right. \\ &\quad \left. g_\ell y_i^\ell \bar{\ell}_i \gamma_5 \ell_i \right). \quad (3.9)\end{aligned}$$

Here the sums run over the all SM generations; the Yukawa couplings  $y_i^f$  are normalized to  $y_i^f = \sqrt{2} m_i^f / v$  where  $v \simeq 246$  GeV represents the Higgs vacuum expectation value (VEV). While the couplings  $g_u, g_d, g_\ell$  to SM fermions are factors multiplying the SM Yukawa structure, we parametrise the DM-mediator coupling as  $g_\chi$ , without any additional Yukawa structure between the mediator and the dark sector.

As already stated we only choose a minimal set of interactions that do not include interactions with the SM Higgs field. For simplicity, we also assume universal SM-mediator couplings  $g_v = g_u = g_d = g_\ell$

Given these simplifications, the minimal set of parameters under consideration is

$$\left\{ m_\chi, m_{\phi/a}, g_\chi, g_v \right\}. \quad (3.10)$$

We choose to consider the minimal mediator width given by

$$\Gamma_{\min}^{S/P} = \Gamma_{\chi\chi}^{S/P} + \sum_q \Gamma_{\bar{q}q}^{S/P} + \Gamma_{gg}^{S/P}, \quad (3.11)$$

with the following LO expressions for the partial widths:

$$\Gamma_{\chi\chi}^S = \frac{g_{\text{DM}}^2 M_{\text{med}}}{8\pi} \beta_{DM}^{3/2} \theta(M_{\text{med}} - 2m_{\text{DM}}) \quad (3.12)$$

$$\Gamma_{\bar{q}q}^S = \frac{3g_q^2 M_{\text{med}}}{8\pi} \frac{m_q^2}{v^2} \beta_q^{3/2} \theta(M_{\text{med}} - 2m_q) \quad (3.13)$$

$$\Gamma_{gg}^S = \frac{g_q^2 \alpha_s^2}{2\pi^3 v^2 M_{\text{med}}} \left| \sum_q m_q^2 F_S \left( \frac{4m_q^2}{M_{\text{med}}^2} \right) \right|^2 \quad (3.14)$$

$$\Gamma_{\chi\chi}^P = \frac{g_{\text{DM}}^2 M_{\text{med}}}{8\pi} \beta_{DM} \theta(M_{\text{med}} - 2m_{\text{DM}}) \quad (3.15)$$

$$\Gamma_{\bar{q}q}^P = \frac{3g_q^2 M_{\text{med}}}{8\pi} \frac{m_q^2}{v^2} \beta_q \theta(M_{\text{med}} - 2m_q) \quad (3.16)$$

$$\Gamma_{gg}^P = \frac{g_q^2 \alpha_s^2}{2\pi^3 v^2 M_{\text{med}}} \left| \sum_q m_q^2 F_P \left( \frac{4m_q^2}{M_{\text{med}}^2} \right) \right|^2, \quad (3.17)$$

with the form factors defined as

$$F_S(x) = 1 + (1 - x) \arctan^2 \left( \frac{1}{\sqrt{x-1}} \right) \quad (3.18)$$

$$F_P(x) = \arctan^2 \left( \frac{1}{\sqrt{x-1}} \right). \quad (3.19)$$

The minimal width for scalar and pseudo-scalar mediators with  $g_q = g_{DM} = 1$  are shown in Fig. 3.10, illustrating the effect of choosing the SM Higgs-like Yukawa couplings for the SM fermions. For the mediator mass above twice the top quark mass  $m_t$ , the minimal width receives the dominant contribution from the top quark. For lighter mediator masses, Dark Matter dominates as the couplings to lighter quarks are Yukawa suppressed.

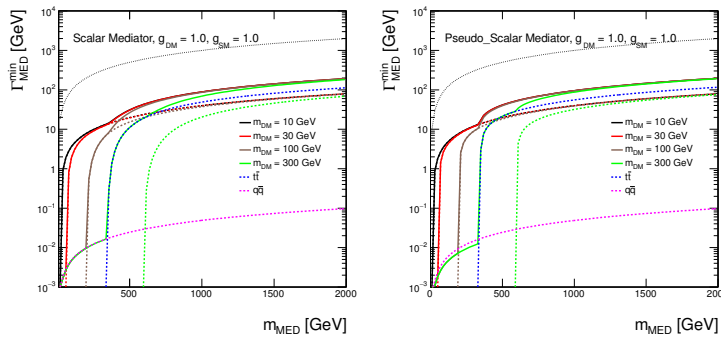


Figure 3.10: Minimal width as a function of mediator mass for scalar and pseudo-scalar mediator assuming couplings of 1. The total width is shown as solid lines for Dark Matter masses of 10 GeV, 30 GeV, 100 GeV and 300 GeV in black, red, brown and green, respectively. The individual contributions from Dark Matter are indicated by dotted lines with the same colors. The contribution from all quarks but top is shown as magenta dotted line and the contribution from top quarks only is illustrated by the dotted blue line. The dotted black line shows the extreme case  $\Gamma_{\min} = M_{\text{med}}$ .

Similarly as in the case of the vector and axial-vector couplings of spin-1 mediators, scans in the parameter space are performed also for the scalar and pseudo-scalar couplings of the spin-0 mediators in order to decide on the optimised parameter grid for the presentation of Run-2 results. Figures 3.11- 3.15 show the scans over the couplings, Dark Matter mass and mediator mass and the same conclusions apply as in Section 3.1.

Since the top quark gives the dominant contribution to the mediator width due to SM Higgs-like Yukawa couplings, the effect of the kinematic threshold at  $M_{\text{med}} = 2m_t$  was studied in detail. A scan over the mediator mass is shown in Fig. 3.15 where  $M_{\text{med}} = 300 \text{ GeV}$  and  $500 \text{ GeV}$  are chosen to be below and above  $2m_t$ . The off-shell Dark Matter production regime is assumed by taking  $m_{DM} = 1 \text{ TeV}$  in order to allow studying solely the effects of the couplings to quarks. No differences in the kinematic distributions are observed and also the cross sections remain similar in this case. Therefore, it is concluded that no significant changes appear for mediator masses around the  $2m_t$  threshold.

The optimized parameter grid in the  $M_{\text{med}}-m_{DM}$  plane for scalar and pseudo-scalar mediators is motivated by similar arguments as in the previous section. Therefore, a similar pattern is followed here, taking again  $g_q = g_{DM} = 1$ . Only the sensitivity to the highest mediator masses has to be revisited. The generator level cross section times the acceptance at  $\cancel{E}_T > 500 \text{ GeV}$  for the model with couplings  $g_q = g_{DM} = 1$ , light Dark Matter of 10 GeV and

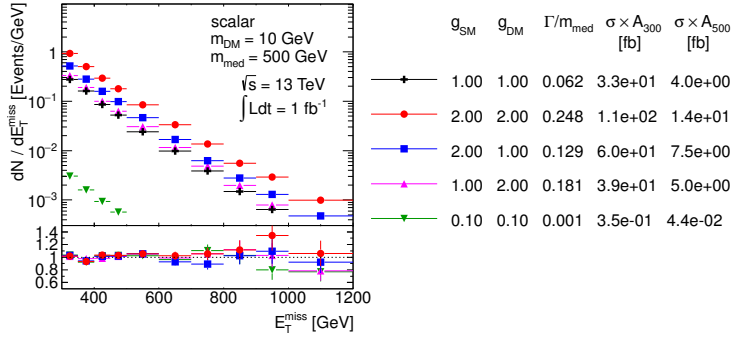


Figure 3.11: Scan over couplings. The  $E_T$  distribution is compared for the scalar mediator models using the parameters as indicated. Ratios of the normalized distributions with respect to the first one are shown.  $A_{300}$  and  $A_{500}$  in the table denote the acceptance of the  $E_T > 300$  GeV and  $E_T > 500$  GeV cut, respectively.

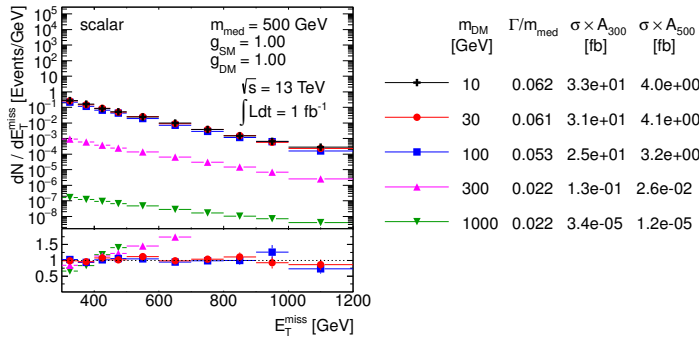


Figure 3.12: Scan over Dark Matter mass. The  $E_T$  distribution is compared for the scalar mediator models using the parameters as indicated. Ratios of the normalized distributions with respect to the first one are shown.  $A_{300}$  and  $A_{500}$  in the table denote the acceptance of the  $E_T > 300$  GeV and  $E_T > 500$  GeV cut, respectively.

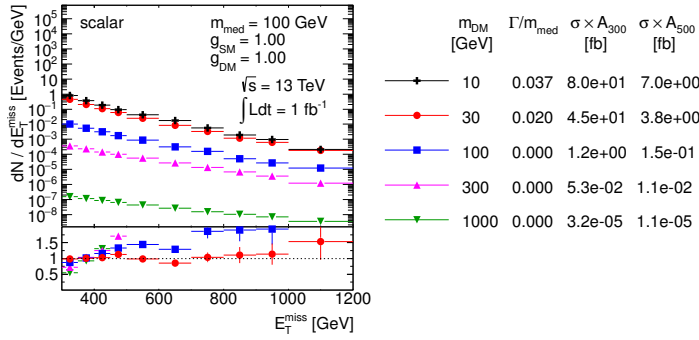


Figure 3.13: Scan over Dark Matter mass. The  $E_T$  distribution is compared for the scalar mediator models using the parameters as indicated. Ratios of the normalized distributions with respect to the first one are shown.  $A_{300}$  and  $A_{500}$  in the table denote the acceptance of the  $E_T > 300$  GeV and  $E_T > 500$  GeV cut, respectively.

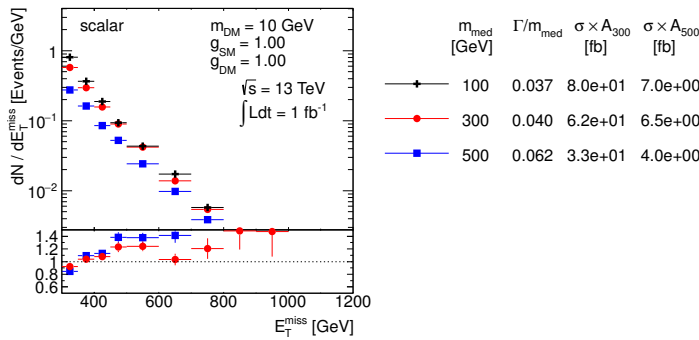


Figure 3.14: Scan over mediator mass. The  $E_T$  distribution is compared for the scalar mediator models using the parameters as indicated. Ratios of the normalized distributions with respect to the first one are shown.  $A_{300}$  and  $A_{500}$  in the table denote the acceptance of the  $E_T > 300$  GeV and  $E_T > 500$  GeV cut, respectively.



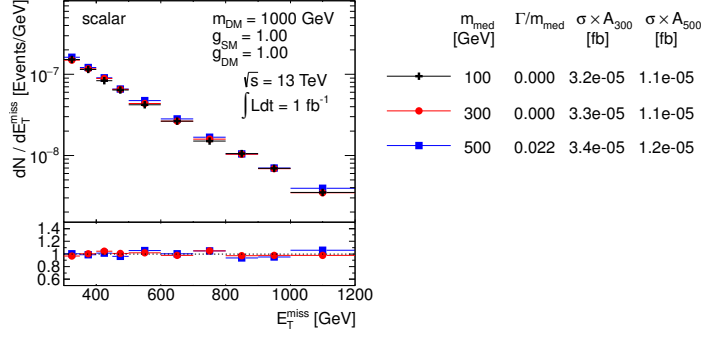


Figure 3.15: Scan over mediator mass. The  $E_T$  distribution is compared for the scalar mediator models using the parameters as indicated. Ratios of the normalized distributions with respect to the first one are shown.  $A_{300}$  and  $A_{500}$  in the table denote the acceptance of the  $E_T > 300$  GeV and  $E_T > 500$  GeV cut, respectively.

500 GeV scalar mediator is at the order of 10 fb, i.e. just at the edge of the early Run-2 sensitivity. Increasing the mediator mass to 1 TeV pushes the product  $\sigma \times A$  down to approximately 0.1 fb, beyond the LHC sensitivity. Therefore, we choose to remove the 2 TeV mediator mass from the grid and present the final grid with 26 mass points only in Fig. 3.2. One point at very high mediator mass (5 TeV) is added for each of the DM masses scanned, to aid the reinterpretation of results in terms of contact interaction operators (EFTs).

$m_{\text{DM}}$ (GeV)	$m_{\text{med}}$ (GeV)								
1	10	20	50	100	200	300	500	1000	5000
10	10	15	50	100					5000
50	10		50	95	200	300			5000
150	10				200	295	500		5000
500	10						500	995	5000
1000	10							1000	5000

Table 3.2: Simplified model benchmarks for  $s$ -channel simplified models (spin-0 mediators decaying to Dirac DM fermions in the scalar and pseudoscalar case, taking the minimum width for  $g_q = g_{\text{DM}} = 1$ )

The proposal for the scan in the  $g_q$ - $g_{\text{DM}}$  plane is described in the following section.

*Implementation* The matrix element implementation of the  $s$ -channel spin-0 mediated DM production is available in POWHEG with the full top-loop calculation at LO [HR15].

### 3.3 Cross section scaling

The aim of the parameter grid optimization is to find out whether certain parts of the parameter space can be omitted and one can rely on the neighboring grid points in order to populate the missing parts. There are two ways of doing this:

- Interpolation is used in-between the grid points that are close enough such that finer granularity is not needed for the presentation purposes, or between the points where smooth or no changes of the results are expected. The latter argument is exactly the one that motivates the reduction of the grid points in the  $M_{\text{med}}-m_{\text{DM}}$  plane.

- Recalculation of the results can be used when the dependencies with respect to the neighboring grid points are known.

The results of the scan over the couplings presented in the previous sections indicate there are no changes in kinematic distributions for different choices of the coupling strengths. This means that the acceptance remains the same in the whole  $g_q$ - $g_{\text{DM}}$  plane and it is sufficient to perform the detector simulation only for one single choice of  $g_q, g_{\text{DM}}$ . The resulting truth-level selection acceptance and the detector reconstruction efficiency can then be applied to all remaining grid points in the  $g_q$ - $g_{\text{DM}}$  plane where only the generator-level cross section needs to be known. This significantly reduces the computing time as the detector response is by far the most expensive part of the Monte Carlo sample production. However, the number of generated samples can be reduced even further if a parameterization of the cross section dependence from one grid point to another exists.

Let us now elaborate on a cross section scaling procedure. The propagator on the s-channel exchange is written in a Breit-Wigner form as  $\frac{1}{q^2 - M_{\text{med}}^2 + iM_{\text{med}}\Gamma}$ , where  $q$  is the momentum transfer calculated from the two partons entering the hard process after the initial state radiation, which is equivalent to the invariant mass of the Dark Matter pair. The size of the momentum transfer with respect to the mediator mass allows to classify the production in the following way:

- off-shell production when  $q^2 \gg M_{\text{med}}^2$  leading to suppressed cross sections,
- on-shell production when  $q^2 \sim M_{\text{med}}^2$  leading to enhanced cross sections,
- effective field theory (EFT) limit when  $q^2 \ll M_{\text{med}}^2$ .

All three categories can be distinguished in Fig. 3.16 showing the upper limit on the interaction scale  $M^* \equiv M_{\text{med}}/\sqrt{g_q g_{\text{DM}}}$  for vector mediator. In the case of the off-shell production and the EFT limit, the first term in the propagator dominates which reduces the dependence on the mediator width. Therefore, in these cases one can approximate the cross section as

$$\sigma \propto g_q^2 g_{\text{DM}}^2. \quad (3.20)$$

The on-shell production regime is the most interesting one as it gives the best chances for a discovery at the LHC given the cross section enhancement. The propagator term with the width cannot be neglected in this case and, in the narrow width approximation which requires  $\Gamma \ll M_{\text{med}}$ , one can integrate

$$\int \frac{ds}{(s - M_{\text{med}}^2)^2 + M_{\text{med}}^2 \Gamma^2} = \frac{\pi}{M_{\text{med}} \Gamma} \quad (3.21)$$

which further implies the cross section scaling

$$\sigma \propto \frac{g_q^2 g_{\text{DM}}^2}{\Gamma}. \quad (3.22)$$

The narrow with approximation is important here as it ensures an integration over parton distribution functions (PDFs) can be neglected. In other words, it is assumed the integrant in Eq. 3.21 is non-zero only for a small region of  $s$ , such that the PDFs can be taken to be constant in this range. Since  $\Gamma \sim g_q^2 + g_{DM}^2$ , one can simplify this rule in the extreme cases as follows

$$\sigma \propto \frac{g_q^2 g_{DM}^2}{g_q^2 + g_{DM}^2} \xrightarrow{g_q \ll g_{DM}} g_q^2 \quad (3.23)$$

$$\sigma \propto \frac{g_q^2 g_{DM}^2}{g_q^2 + g_{DM}^2} \xrightarrow{g_q \gg g_{DM}} g_{DM}^2 \quad (3.24)$$

However, it is important to keep in mind that there is no simple scaling rule for how the cross section changes with the Dark Matter mass and the mediator mass, or for mediators with a large width, because PDFs matter in such cases as well. Therefore, the scaling procedure outlined above is expected to work only for fixed masses and fixed mediator width, assuming the narrow width approximation applies.

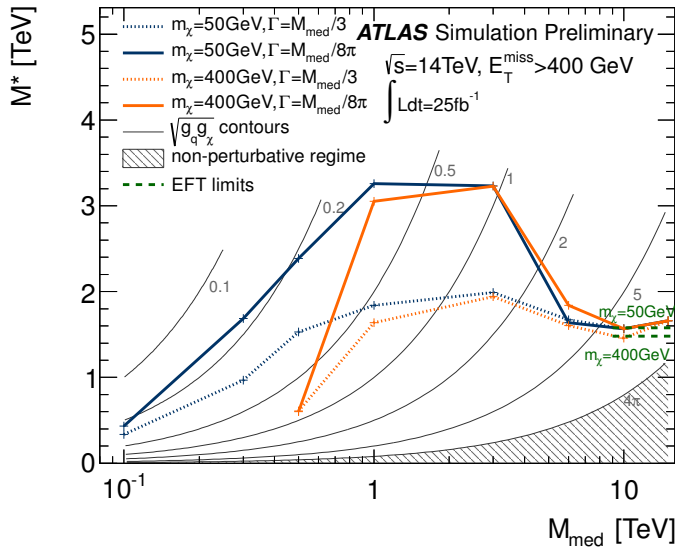


Figure 3.16: Comparison of the 95% CL lower limits on the scale of the interaction of a  $Z'$ -like simplified model at 14 TeV, in terms of the mediator mass. Corresponding limits from EFT models are shown on the same plot as green dashed lines to show equivalence between the two models for high mediator masses. Taken from Ref. [ATL14].

Figures 3.17 and 3.18 show the minimal width in the  $g_q$ - $g_{DM}$  plane for all vector, axial-vector, scalar and pseudo-scalar mediators for  $M_{med} = 100$  GeV and 1000 GeV, respectively, taking  $m_{DM} = 10$  GeV. The individual colors indicate the lines of constant width along which the cross section scaling works. For vector and axial-vector mediators, the minimal width is predominantly defined by  $g_q$  due to the number of quark flavors and the color factor. On the contrary, both the Standard Model and Dark Matter partial width have comparable contributions in case of scalar and pseudo-scalar mediators if the top quark channel is open ( $M_{med} > 2m_t$ ). However, mostly  $g_{DM}$  defines the minimal width for  $M_{med} < 2m_t$  due to the Yukawa-suppressed light quark couplings.

The performance of the cross section scaling is demonstrated in Fig. 3.19 where two mass points  $M_{med} = 100$  GeV and 1 TeV with

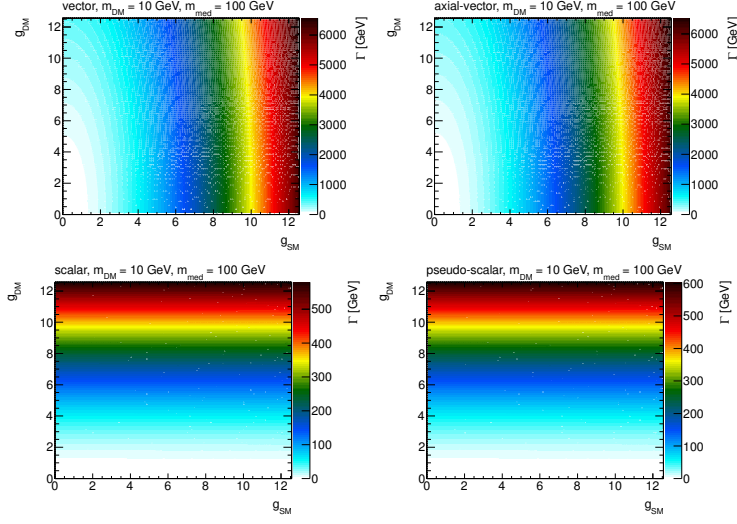


Figure 3.17: Minimal width for vector, axial-vector, scalar and pseudo-scalar mediators as a function of the individual couplings  $g_q$  and  $g_{DM}$ , assuming  $M_{med} = 100$  GeV and  $m_{DM} = 10$  GeV.

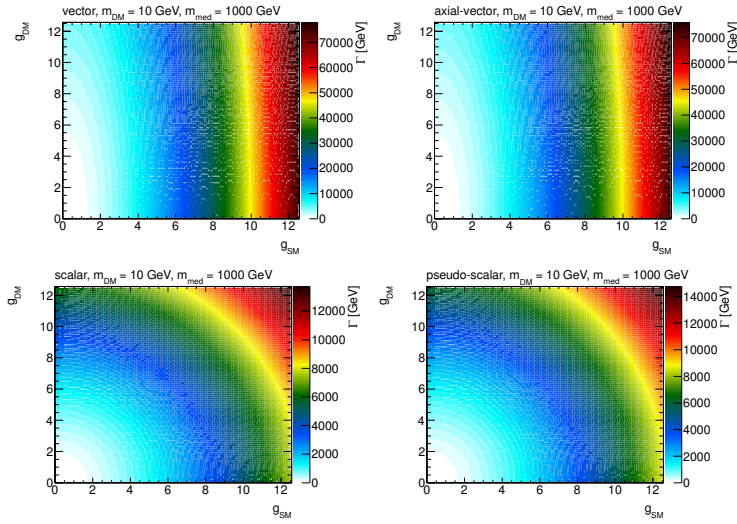


Figure 3.18: Minimal width for vector, axial-vector, scalar and pseudo-scalar mediators as a function of the individual couplings  $g_q$  and  $g_{DM}$ , assuming  $M_{med} = 1$  TeV and  $m_{DM} = 10$  GeV.

$m_{\text{DM}} = 10 \text{ GeV}$  are chosen and rescaled from the starting point  
 $g_q = g_{\text{DM}} = 1$  according to Eq. 3.22 to populate the whole  $g_q$ - $g_{\text{DM}}$   
plane. This means the width is not kept constant in this test and  
this is done in purpose in order to point out deviations from the  
scaling when the width is altered. For each mass point, the rescaled  
cross section is compared to the generator cross section and the  
ratio of the two is plotted. For the given choice of the mass points,  
the scaling seems to work approximately with the precision of  
 $\sim 20\%$  in the region where  $\Gamma_{\text{min}} < M_{\text{med}}$ . Constant colors indicate  
the lines along which the cross section scaling works precisely and  
there is a remarkable resemblance of the patterns shown in the  
plots of the mediator width. To prove the scaling along the lines  
of constant width works, one such line is chosen in Fig. 3.20 for a  
scalar mediator, defined by  $M_{\text{med}} = 300 \text{ GeV}$ ,  $m_{\text{DM}} = 100 \text{ GeV}$ ,  
 $g_q = g_{\text{DM}} = 1$ , and the rescaled and generated cross sections are  
found to agree within 3%.

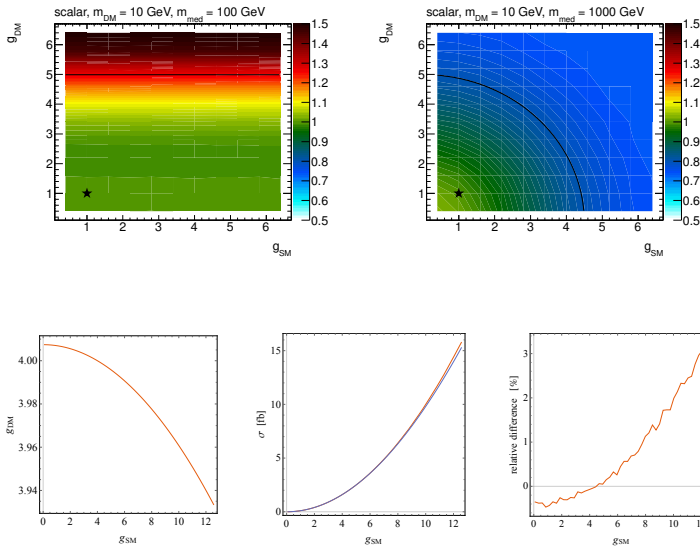


Figure 3.19: Ratio of the rescaled and generated cross sections in the  $g_q$ - $g_{\text{DM}}$  plane. The point at  $g_q = g_{\text{DM}} = 1$ , taken as a reference for the rescaling, is denoted by a star symbol. Scalar model with  $M_{\text{med}} = 100 \text{ GeV}$  (left) and  $1 \text{ TeV}$  (right) is plotted for  $m_{\text{DM}} = 10 \text{ GeV}$ . The limiting case  $\Gamma_{\text{min}} = M_{\text{med}}$  is shown as a black line.

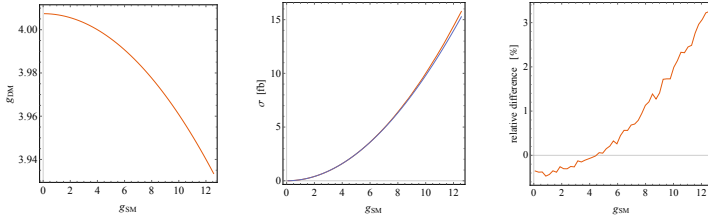


Figure 3.20: Scaling along the lines of constant width. The line of constant width for  $M_{\text{med}} = 300 \text{ GeV}$  and  $m_{\text{DM}} = 100 \text{ GeV}$ , intercepting  $g_q = g_{\text{DM}} = 4$  is shown on left. The generated and rescaled cross sections are compared in the middle, the corresponding ratio is shown on right.

*Proposed parameter grid* We propose to present the results in the  
 $g_q$ - $g_{\text{DM}}$  plane using the following prescription:

- Since the shapes of kinematic quantities do not change for different couplings, use the acceptance and efficiency for the available  $m_{\text{DM}} = 50 \text{ GeV}$ ,  $M_{\text{med}} = 300 \text{ GeV}$ ,  $g_q = g_{\text{DM}} = 1$  grid point from the  $M_{\text{med}}$ - $m_{\text{DM}}$  plane for the scalar and pseudo-scalar mediator. In case of the vector and axial-vector mediator, use the grid point  $m_{\text{DM}} = 50 \text{ GeV}$ ,  $M_{\text{med}} = 1 \text{ TeV}$ ,  $g_q = g_{\text{DM}} = 1$ .
- Generate additional samples in order to get generator cross sections only. For scalar and pseudo-scalar mediator, choose  $m_{\text{DM}} = 50 \text{ GeV}$ ,  $M_{\text{med}} = 300 \text{ GeV}$  with the following values for  $g_q = g_{\text{DM}}$ : 0.1, 2, 3, 4, 5, 6. For vector and axial vector mediator, choose  $m_{\text{DM}} = 50 \text{ GeV}$ ,  $M_{\text{med}} = 1 \text{ TeV}$  with the following values for  $g_q = g_{\text{DM}}$ : 0.1, 0.25, 0.5, 0.75, 1.25, 1.5. The upper values are defined by the minimal width reaching the mediator mass.

- Rescale the generator cross sections along the lines of constant width in order to populate the whole  $g_q$ - $g_{DM}$  plane.

*Rescaling to different mediator width* In general there may be an interest to consider larger mediator masses than  $\Gamma_{\min}$  in order to accommodate further couplings of the mediator. The cross section scaling method described above can be used to reinterpret the results presented for the minimal width, since multiplying the width by factor  $n$  is equivalent to changing the coupling strength by factor  $\sqrt{n}$ , i.e.

$$\sigma(g_q, g_{DM}, n\Gamma_{\min}(g_q, g_{DM})) \propto \frac{g_q^2 g_{DM}^2}{\Gamma_{\min}(\sqrt{n}g_q, \sqrt{n}g_{DM})} . \quad (3.25)$$

The cross section for the sample with couplings  $g_q$  and  $g_{DM}$  and modified mediator width  $\Gamma = n\Gamma_{\min}$  can therefore be rescaled from a sample generated with the minimal width corresponding to the couplings scaled by  $\sqrt{n}$  as described in the following formula.

$$\sigma(g_q, g_{DM}, n\Gamma_{\min}(g_q, g_{DM})) = \frac{1}{n^2} \sigma(\sqrt{n}g_q, \sqrt{n}g_{DM}, \Gamma_{\min}(\sqrt{n}g_q, \sqrt{n}g_{DM})) \quad (3.26)$$

Here, it is again assumed the narrow width approximation applies. The advantage of doing this is in the fact that no event selection and detector response needs to be simulated since the changes in couplings do not have an effect on the shapes of kinematic distributions.

### 3.3.1 POWHEG settings

This section describes specific settings for the Dark Matter models needed to run the POWHEG generation.

- The POWHEG implementation allows to generate a single sample that provides sufficient statistics in all signal regions. POWHEG generates weighted events and the `bornsuppfact` parameter is used to set the event suppression factor according to

$$F(k_T) = \frac{k_T^2}{k_T^2 + \text{bornsuppfact}^2} . \quad (3.27)$$

In this way, the events at, for instance low  $E_T$ , are suppressed and receive higher event weights which ensures higher statistics at high  $E_T$ . We recommend to set `bornsuppfact` to 1000.

- The `bornktmin` parameter allows to suppress the low  $E_T$  region even further by starting the generation at a certain value of  $k_T$ . It is recommended to set this parameter to half the lower analysis  $E_T$  cut, for the event selection used in the CMS/ATLAS monojet analyses for instance the proposed value for `bornktmin` is 150. However, this parameter should be set keeping in mind the event selection of all the analyses that will use these signal samples and hence a threshold lower than 150 may be required.

- Set runningwidth to 0.
- Set mass\_low and mass\_high to -1.
- The minimal values for ncall1, itmx1, ncall2, itmx2 are 250000, 5, 1000000, 5 for the DMV model, respectively. In order to increase speed, set foldsci and foldy to 2 and keep foldphi at 1.
- The minimal values for ncall1, itmx1, ncall2, itmx2 are 100000, 5, 100000, 5 for the DMS\_tloop model, respectively.
- Allow negative weights for the DMV model by setting withnegweights to 1.
- Since the DMS\_tloop model is a leading order process, set L0events and bornonly are set to 1 internally.

**[Comment on proper PDF sets to use, concerns about sea quark PDF in b-initiated diagrams (perhaps the latter belongs in the b-flavored DM section)]**

### 3.4 Colored scalar mediator, $t$ -channel exchange

An alternative set of simplified models exist where the mediator is exchanged in the  $t$ -channel, thereby coupling the quark and dark matter particle directly. Under the assumption that  $\chi$  is a Standard Model (SM) singlet, the mediating particle, labeled  $\phi$ , is necessarily charged and coloured. This model is parallel to, and partially motivated by, the squark of the MSSM, but in this case the  $\chi$  is chosen to be Dirac. An important difference with respect to the MSSM is that **[illustrate that diagram is no longer forced to be small. Should forum provide formulae to relate our parameters to MSSM searches?]**. Following the example of Ref. [PVZ14], the interaction Lagrangian is written as

$$\mathcal{L}_{\text{int}} = g \sum_{i=1,2,3} (\phi_L^i \bar{Q}_L^i + \phi_{uR}^i \bar{u}_R^i + \phi_{dR}^i \bar{d}_R^i) \chi \quad (3.28)$$

**(Note: [PVZ14] uses only  $i = 1, 2$ , but I think it's fine to extend this to 3 here.)** where  $Q_L^i$ ,  $u_R^i$  and  $d_R^i$  are the SM quarks and  $\phi_L^i$ ,  $\phi_{uR}^i$  and  $\phi_{dR}^i$  are the corresponding mediators, which (unlike the  $s$ -channel mediators) must be heavier than  $\chi$ . These mediators have SM gauge representations under  $(SU(3), SU(2))_Y$  of  $(3, 2)_{-1/6}$ ,  $(3, 1)_{2/3}$  and  $(3, 1)_{-1/3}$  respectively. Variations of the model previously studied include coupling to the left-handed quarks only [CEHL14, BDSJ<sup>+</sup>14], to the  $\phi_{uR}^i$  [DNRT13] or  $\phi_{dR}^i$  [PVZ14, A<sup>+</sup>14b], or some combination [BB13, AWZ14].

Minimal Flavour Violation (MFV) requires that the mediator masses for each flavour be equal; the same logic also applies to the couplings  $g$ . The available parameters are then

$$\{m_\chi, M_\phi, g\}. \quad (3.29)$$

447 In practice, the third mediator mass and coupling could be sep-  
 448 arated from the other two, if higher order corrections to the MFV  
 449 prediction arise due to the large top Yukawa coupling – a common  
 450 variation is then to define this split between the first two genera-  
 451 tions and the third, so the parameters are extended to

$$\{m_\chi, M_{\phi_{1,2}}, M_{\phi_3}, g_{1,2}, g_3\}. \quad (3.30)$$

452 The width of each mediator is expressed, using the example of  
 453 decay to an up quark, as

$$\begin{aligned} \Gamma(\phi_i \rightarrow \bar{u}_i \chi) &= \frac{g_i^2}{16\pi M_{\phi_i}^3} (M_{\phi_i}^2 - m_{u_i}^2 - m_\chi^2) \\ &\times \sqrt{M_{\phi_i}^4 + m_{u_i}^4 + m_\chi^4 - 2M_{\phi_i}^2 m_{u_i}^2 - 2M_{\phi_i}^2 m_\chi^2 - 2m_{u_i}^2 m_\chi^2}, \end{aligned} \quad (3.31)$$

454 this reduces to

$$\frac{g_i^2 M_{\phi_i}}{16\pi} \left(1 - \frac{m_\chi^2}{M_{\phi_i}^2}\right)^2 \quad (3.32)$$

455 in the limit  $M_{\phi_i}, m_\chi \gg m_{u_i}$ .

456 An interesting point of difference with the  $s$ -channel simplified  
 457 models is that the mediator can radiate a SM object, such as a jet  
 458 or gauge boson, thus providing three separate mono- $X$  diagrams  
 459 which must be considered together in calculations. This model can  
 460 also give a signal in the di-jet + MET channel when, for example,  
 461 the  $\chi$  is exchanged in the  $t$ -channel and the resulting  $\phi$  pair each  
 462 decay to a jet +  $\chi$ .



## 4

# *Specific models for signatures with heavy flavor quarks*

### 4.1 $b\bar{b}$ +MET models

### 4.2 Models with a single $b$ -quark + MET

### 4.3 $t\bar{t}$ +MET models

As described in Section 3.2, a model with a scalar/pseudoscalar particle mediating the DM-SM interactions is one of the simplest UV completions of our EFT models.

#### 4.3.1 Parameter scan

As discussed in Sec. 3.2, the MFV assumption for spin-0 mediators leads to quark mass dependent Yukawa couplings, and therefore dominant couplings to top quarks. This motivates dedicated DM+ $t\bar{t}$  searches. The benchmark chosen for these searches follows the assumptions mentioned in the previous Section: we consider a Dirac fermion DM particle, universal couplings to quarks, and minimum mediator width.

The benchmark points scanning the model parameters have been selected to ensure that the kinematic features of the parameter space are sufficiently represented. Detailed studies were performed to identify points in the  $m_{\text{DM}}, m_{\phi,a}, g_{\text{DM}}, g_q$  (and  $\Gamma_{\phi,a}$ ) parameter space that differ significantly from each other in terms of expected detector acceptance. Because missing transverse momentum is the key observable for searches, the mediator  $p_T$  spectra is taken to represent the main kinematics of a model. Another consideration in determining the set of benchmarks is to focus on the phase space where we expect the searches to be sensitive during the 2015 LHC run. Based on a projected integrated luminosity of  $30 \text{ fb}^{-1}$  expected for 2015, we disregard model points with a cross section times branching ratio smaller than  $0.1 \text{ fb}$ .

#### 4.3.2 Parameter scan

The kinematics is most dependent on the masses  $m_{\text{DM}}$  and  $m_{\phi,a}$ . Figure 4.1 and 4.2 show typical dependencies for scalar and pseudoscalar couplings respectively. Typically, the mediator  $p_T$  spectra

broadens with larger  $m_{\phi,a}$ . The kinematics are also quite different  
 between on-shell and off-shell production. Furthermore, the kinematic  
 differences between scalar and pseudoscalar are large with light  
 mediator masses and are reduced for larger masses. It is therefore  
 important to benchmark points covering on-shell and off-shell  
 production with sufficient granularity.

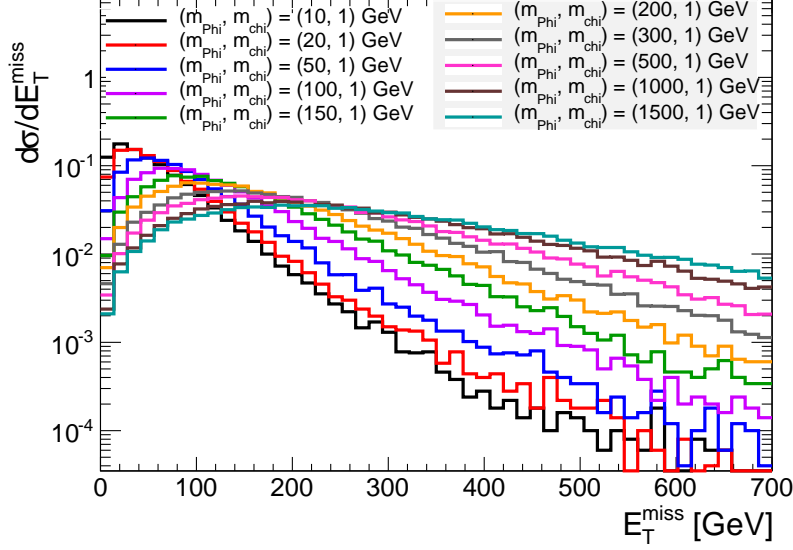


Figure 4.1: Example of the dependence of the kinematics on the scalar mediator mass. The Dark Matter mass is fixed to be 1 GeV.

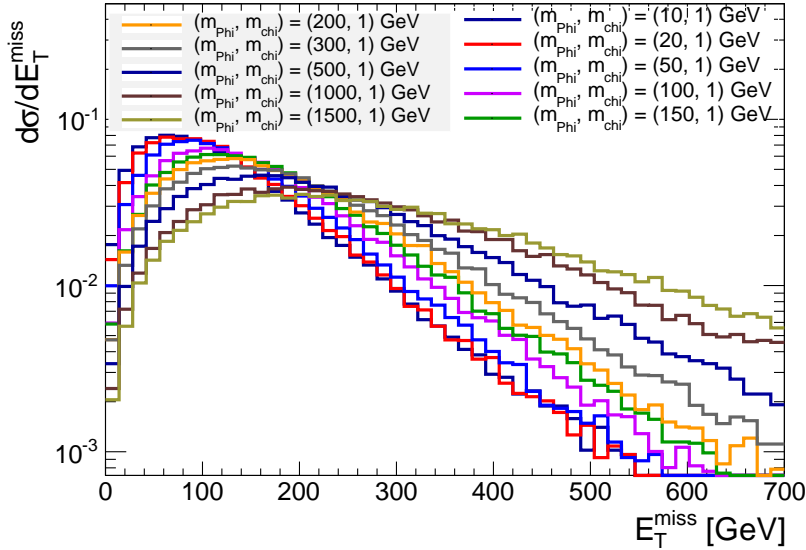


Figure 4.2: Example of the dependence of the kinematics on the pseudoscalar mediator mass. The Dark Matter mass is fixed to be 1 GeV.

Typically only weak dependencies on width or equivalently couplings  
 are observed (see Fig 4.4), except for large mediator masses of  $\sim 1.5$  TeV  
 or for very small couplings of  $\sim 10^{-2}$ . These regimes

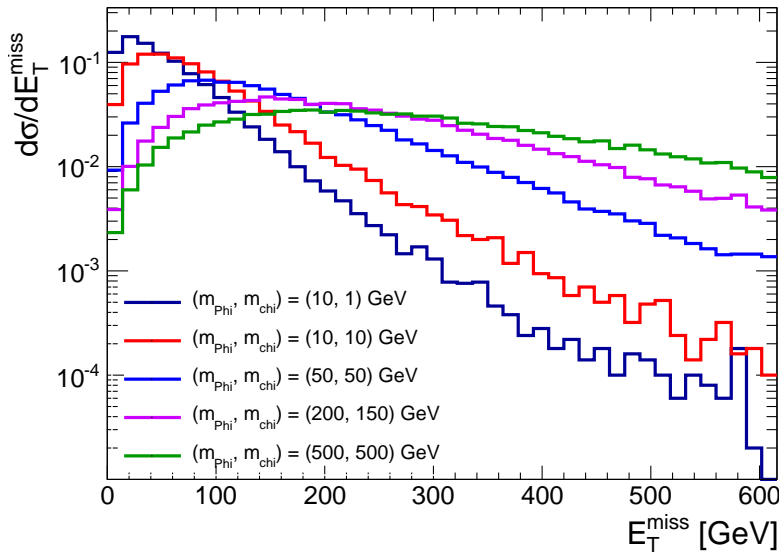


Figure 4.3: Example of the dependence of the kinematic for points of the grid proposed in Tab. 3.2 close to the  $m_{\phi,\chi} \sim 2m_\chi$  limit.<sup>3</sup>

where width effects are significant have production cross sections that are too small to be relevant for  $30 \text{ fb}^{-1}$  and are not considered here. However, with the full Run-2 dataset, such models may be within reach. The weak dependence on the typical width values can be understood as the parton distribution function are the dominant effect on mediator production. In other words, for couplings  $\sim O(1)$  the width is large enough that the  $p_T$  of the mediator is determined mainly by the PDF.

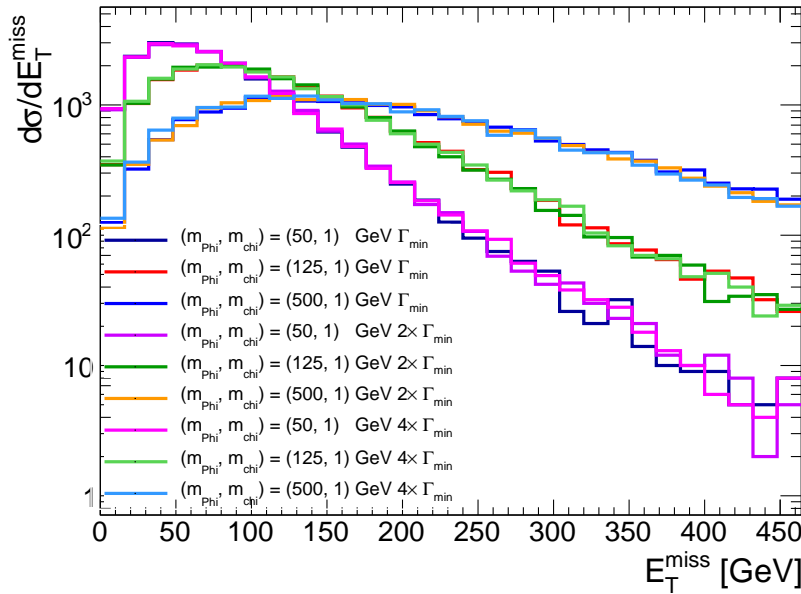


Figure 4.4: Study of the dependence of kinematics on the width of a scalar mediator. The width is increased up to four times the minimal width for each mediator and dark matter mass combination.

Another case where the width can impact the kinematics is when  $m_{\phi,a}$  is slightly larger than  $2m_\chi$ . Here, the width determines the relative contribution between on-shell and off-shell production. An example is given in Fig. 4.5. In our recommendations we propose to use for simplicity the minimal width, as this represents the most conservative choice to interpret the LHC results. [TODO: mention larger widths too]

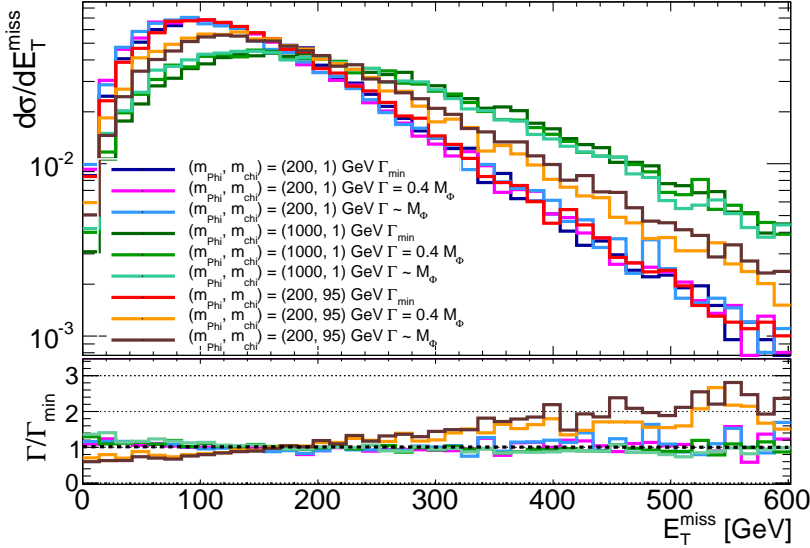


Figure 4.5: Dependence of the kinematics on the width of a scalar mediator. The width is increased up to the mediator mass. Choices of mediator and dark matter masses such that  $m_{\phi,a}$  is slightly larger than  $2m_\chi$  is the only case that shows a sizeable variation of the kinematics as a function of the width.

Given that the kinematics are similar for all couplings  $\sim O(1)$ , we recommend to generate only samples with  $g_{\text{DM}} = g_q = 1$ . It follows from this that these benchmark points should be a good approximation for non-unity couplings and for  $g_{\text{DM}} \neq g_q$ , provided that the sample is rescaled to the appropriate cross section times branching ratio. While the simple scaling function  $\sigma' * BR' = [\sigma * BR] * (g'_q/g_q)^2 * (g'_{\text{DM}}/g_{\text{DM}})^2 * (\Gamma/\Gamma')$  is sufficient for a limited range of coupling values (see Fig. 4.6 for example), we also choose to provide instead a table of cross section times branching ratio values over a large range of couplings to support interpretation of search results (see the Appendix C). The table lists couplings from  $g = 0.1$  to  $g = 3.5$ , where the upper limit is chosen to close to the perturbative limit.

The points for the parameter scan chosen for this model are listed in Table 3.2, chosen to be harmonized with those for other analyses employing the same scalar model as benchmark. Based on the sensitivity considerations above, DM masses are only simulated up to 500 GeV, leading to a total of 24 benchmark points.

In addition to the considerations discussed in the preceding subsections, very light DM fermions are included ( $m_{\text{DM}} = 10 \text{ GeV}$ ) as this is a region where colliders have a complementary sensitivity to current direct detection experiments.

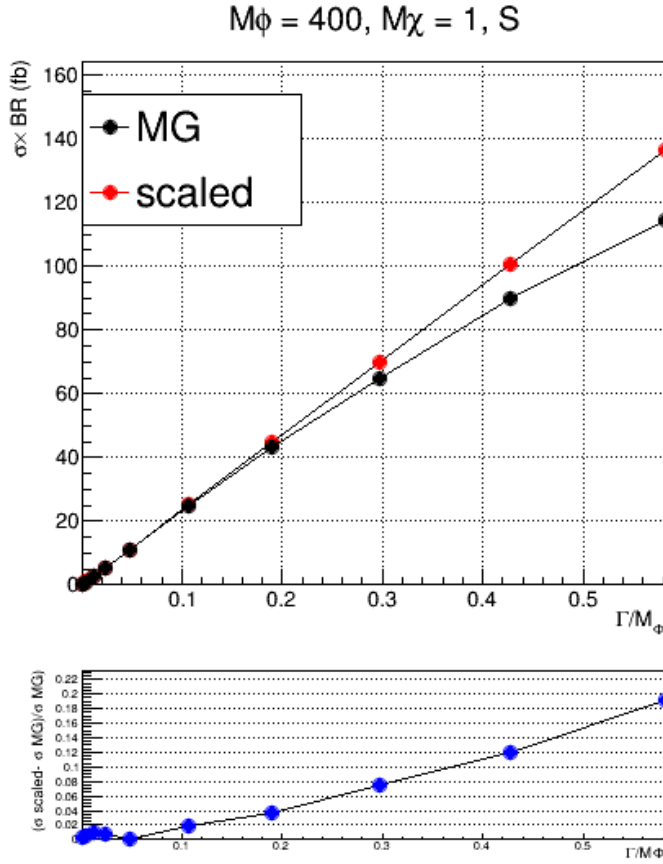


Figure 4.6: An example comparing a simple cross section scaling versus the computation from the generator, for a scalar model with  $m_\phi = 400$  GeV,  $m_{\text{DM}} = 1$  GeV and all couplings set to unity. In this example, the scaling relationship holds for  $\Gamma_\phi/m_\phi$  below 0.2, beyond which finite width effects become important and the simple scaling breaks down.

#### 4.4 Models with a single top-quark + MET

Many different theories predict final states with a single top and associated missing transverse momentum (monotop), some of them including dark matter candidates. A simplified model encompassing the processes leading to this phenomenology is described in Refs. [AFM11, AAB<sup>+</sup>14, BCDF15], and is adopted as one of the benchmarks for Run 2 LHC searches.

A dark matter candidate  $\chi$  and a new particle  $M$  (vector or scalar) are added to the SM, in a theory that respects the  $\text{SU}(2)_L \times \text{U}(1)_Y$  symmetry and produces a single top quark in association with either the DM particle or a new particle decaying invisibly.

Within this model, two distinct processes can lead to monotop production:

- resonant production, as shown in the diagram of Fig. 4.7 (a), where a scalar ( $S$  in the figure,  $\phi$  in the following) or vector ( $X$ ) field are exchanged in the s-channel, and decay into the a spin 1/2 invisible DM candidate (called  $f_{\text{met}}$  in the figure) and a top quark;

- non-resonant production, as shown in the diagrams of Fig. 4.7 (b) and (c), where a flavor-changing interaction produces a top quark in association with a new colored scalar ( $\Phi$ ) or vector ( $V$ ). The new colored particles, called  $v_{met}$  in the figure, decay invisibly, e.g. to a pair of DM particles.  $v_{met}$  can also decay into a top quark and an up quark, leading to a same-sign top quark final state; a detailed study of the complementarity of this signature is beyond the scope of this Forum report.

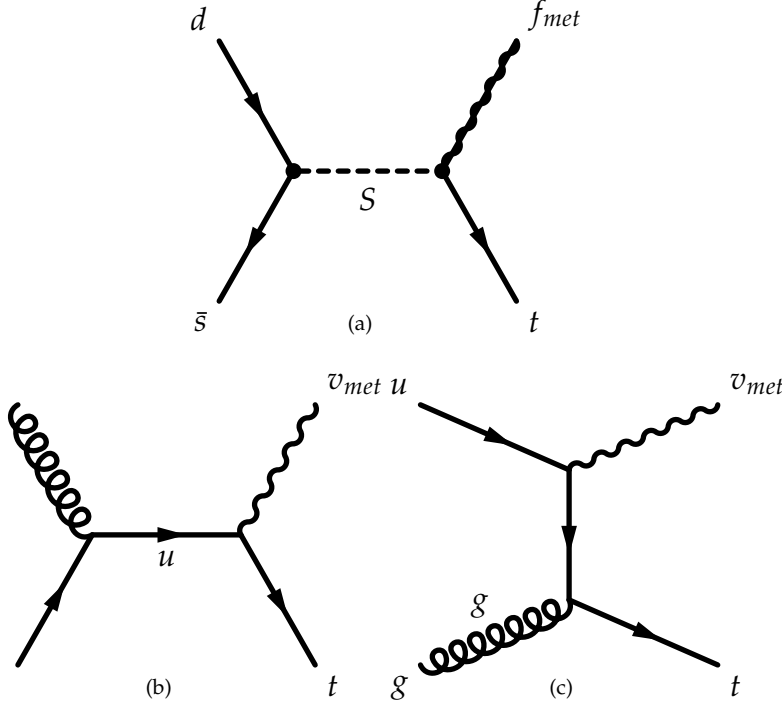


Figure 4.7: Feynman diagram of leading order processes leading to monotop events: production of a coloured scalar resonance  $S$  decaying into a top quark and a spin-1/2 fermion  $f_{met}$  (a),  $s$ - (b) and  $t$ -channel (b) non resonant production of a top quark in association with a spin-1 boson  $v_{met}$ .

In the following, resonant and non-resonant production are treated independently as separate benchmarks. Only the case of a scalar resonance is considered for the resonant model, while the case of vector resonances is left for future studies.

#### RESONANT PRODUCTION

In this case, a colored 2/3-charged scalar ( $\phi^\pm$ ) is produced resonantly and decays into a top quark and a spin-1/2 invisible particle,  $\chi$ . The dynamics of the new sector is described by the following Lagrangian:

$$\mathcal{L} = \left[ \phi \bar{d}^c \left[ a_{SR}^q + b_{SR}^q \gamma_5 \right] d + \phi \bar{u} \left[ a_{SR}^{1/2} + b_{SR}^{1/2} \gamma_5 \right] \chi \right. \\ \left. + X_\mu \bar{d}^c \gamma^\mu \left[ a_{VR}^q + b_{VR}^q \gamma_5 \right] d + X_\mu \bar{u} \gamma^\mu \left[ a_{VR}^{1/2} + b_{VR}^{1/2} \gamma_5 \right] \chi + \text{h.c.} \right] \quad (4.1)$$

where  $u$  ( $d$ ) stands for any  $up$ -quark ( $down$ -quark), the index  $S$  ( $V$ ) stands for scalar (vector) field, and the index  $q$  runs over the three quark generations.

In the notation of [AAB<sup>+</sup>14], the couplings of the new colored fields to down-type quarks are embedded into the  $3 \times 3$  matrices

$a_{\{S,V\}R}^q$  (scalar/vector couplings) and  $b_{\{S,V\}R}^q$  (pseudoscalar/axial vector couplings) while those to the DM candidate  $\chi$  and one single up-type quarks are given by the three-component vectors  $a_{\{S,V\}R}^{1/2}$  and  $b_{\{S,V\}R}^{1/2}$  in flavor space.

In the following, we only consider the model with a new colored scalar, as the requirement of invariance under  $SU(2)_L XU(1)_Y$  would require the introduction of further particles in the case of a new colored vector [BCDF15].

#### NON-RESONANT PRODUCTION

For the non-resonant production, the top quark is produced in association with the new particle: either a new scalar ( $\phi$ ) or a new vector ( $V$ ). For simplicity, we only consider the case of a vector new particle, as the scalar case would involve a mixing with the SM Higgs boson and therefore a larger parameter space. The Lagrangian describing the dynamics of the non-resonant case is:

$$\mathcal{L} = \left[ \phi \bar{u} \left[ a_{FC}^0 + b_{FC}^0 \gamma_5 \right] u + V_\mu \bar{u} \gamma^\mu \left[ a_{FC}^1 + b_{FC}^1 \gamma_5 \right] u + \text{h.c.} \right] \quad (4.2)$$

The strength of the interactions among these two states and a pair of up-type quarks is modeled via two  $3 \times 3$  matrices in flavor space  $a_{FC}^{\{0,1\}}$  for the scalar/vector couplings and  $b_{FC}^{\{0,1\}}$  for the pseudoscalar/axial vector couplings.

#### MODEL PARAMETERS AND ASSUMPTIONS

The models considered as benchmarks for the first LHC searches contain further assumptions in terms of the flavour and chiral structure of the model with respect to the full Lagrangians of equations (4.1) and (4.2). These assumptions are qualitatively discussed below.

*Assumptions in the flavour and chiral structure of the models* We only consider right-handed quark components, in order to simplify the model phenomenology. The representation of the left-handed components under the  $SU(2)_L$  symmetry would lead to a coupling to *down*-type quarks, since the effective theory is invariant under  $SU(2)_L \times U(1)_Y$  gauge symmetry. Having a coupling between the new particle and *down*-type quarks would complicate the collider phenomenology, adding the  $V \rightarrow b\bar{d} + \bar{b}d$  decay mode in addition to the invisible decay mode. This in turn sets the scalar (vector) and pseudoscalar (axial vector) matrices to have elements of equal values.

Furthermore, in order to be visible at the LHC in the monotop final state, these models must include a strong coupling between the new particle  $\phi$  and  $t\chi$ . The same kind of assumption exists for the non-resonant production. This means that only the couplings between the new scalar resonance and light quarks ( $a_{VR}, a_{SR}$ ), and the couplings between the new vector, the top quark and light

quarks ( $a_{FC}$ ), are set to non-zero values

$$(a_{VR}^q)_{11} = (a_{VR}^{1/2})_3 = a \quad (4.3)$$

## IMPLEMENTATION

This Section describes the notations used in the MadGraph model convention, in term of the ones introduced in the previous Section.

The Madgraph model [Fuk] used for these benchmarks corresponds to the Lagrangian from [AFM11]. Each coupling constant of this model can be set via the parameter card and the blocks which are relevant for the two models used for the experimental searches are described below. The relevant parameters in the MadGraph parameter cards, also expressed in the notation introduced in the previous Section, are as follows for the two models considered.

### 1. Resonant scalar model described by the Lagrangian (4.1)

- AQS and BQS:  $3 \times 3$  matrices (flavour space) fixing the coupling of the scalar  $\phi$  ( $S$  stands for scalar) and *down*-type quarks ( $Q$  stands for quarks), previously called  $a/b_{SR}$ .
- A12S and B12S:  $3 \times 1$  matrices (flavour space) fixing the coupling of the DM candidate  $\chi$  (where 12 stands for spin-1/2 fermion) and *up*-type quarks, previously called  $a_{VR}^{1/2}$ .
- particle names: the scalar  $\phi^\pm$  is labeled  $S$  and the fermion  $\chi$  is  $f_{met}$

### 2. Non-resonant vectorial model described by the Lagrangian (4.2)

- A1FC and B1FC:  $3 \times 3$  matrices (flavour space) fixing the coupling of the vector  $V$  (1 stands for vector) and *up*-type quarks, previously called  $a_{FC}^0$ .
- particle name: the vector  $V$  is labelled  $v_{met}$ , while the dark matter candidate  $\chi$  is not implemented (as this model assumes  $\text{BR}(V \rightarrow \chi\chi) = 100\%$ )

The width of the scalar resonance and of the new vector are set to only the allowed decays in the models, namely a DM candidate and a top quark for the resonant model.

## PARAMETER SCAN

The relevant parameters for the resonant model are:

- The mass of the new scalar  $\phi$ ;
- The mass of the DM candidate  $\chi$ ;
- The coupling of the new scalar to the DM candidate and top quark  $a$ , related to the width of the scalar in the minimal width assumption;

The relevant parameters for the non-resonant model are:



- The mass of the new vector  $V$ ;
- The mass of the DM candidate  $\chi$ ;
- The coupling of the new vector to the up and top quark  $a$ , related to the width of the scalar in the minimal width assumption;
- The coupling of the new vector to the DM candidate  $\chi$ , related to the branching fraction of the vector into invisible and visible particle, and as a consequence to the width of the vector.

It has been checked for the non-resonant model that the relevant kinematics does not change when changing the width of the resonance. Figures 4.8, 4.9 and 4.10 show the  $V$  mass distribution, the transverse momentum for  $V$  and for the top quark from the  $V \rightarrow t\bar{t}$  decay, for different  $V$  masses and widths. These figures are relevant independently of the  $V$  decay mode (be it visible or invisible).

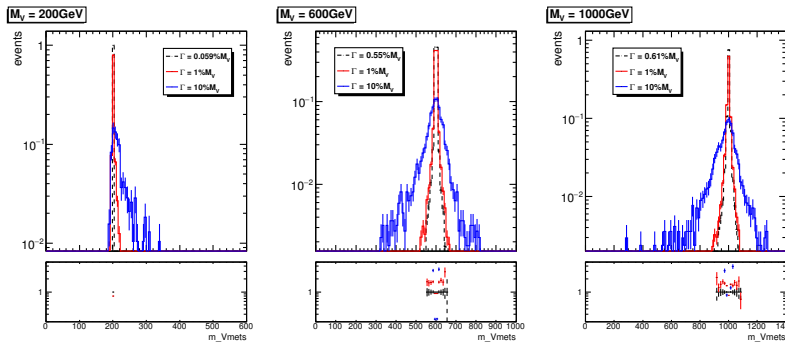


Figure 4.8: Distribution of  $V$  invariant mass for the  $gu \rightarrow tV(\rightarrow t\bar{t})$  (on-shell  $V$ ) for  $m_V = 200, 600, 1000$  GeV (from left to right) and for three different visible decay width (computed from Madgraph directly according to the allowed decays and their couplings, 1% and 10%).

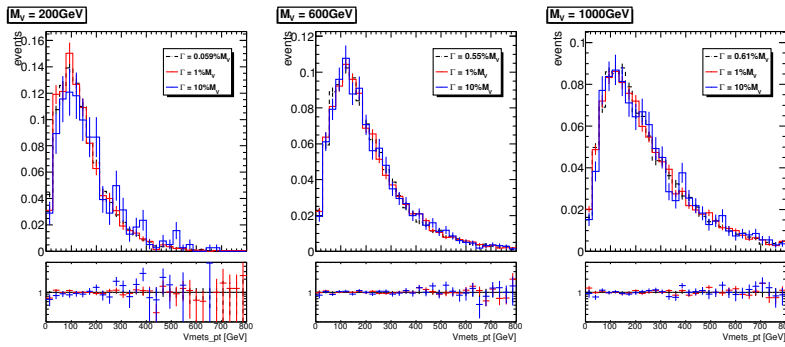


Figure 4.9: Distribution of the  $V$   $p_T$  for the  $gu \rightarrow tV(\rightarrow t\bar{t})$  (on-shell  $V$ ) for  $m_V = 200, 600, 1000$  GeV (from left to right) and for three different visible decay width (computed from Madgraph directly, 1% and 10%).

The limited timescale allowed to reach a consensus for the recommendations contained in this document has not allowed further studies on the parameter scan of these models. The two Collaborations have however agreed to continue studying these models and agree on a common parameter scan, following the same path as for other models described in this document.

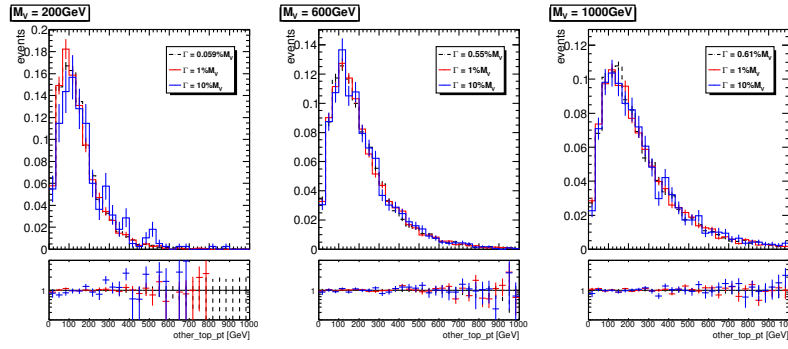


Figure 4.10: Distribution of the top quark  $p_T$  produced in association with  $V$  in  $gu \rightarrow tV$  for  $m_V = 200, 600, 1000$  GeV (from left to right) and for three different visible decay width (computed from Madgraph directly, 1% and 10%).

## Specific models for signatures with EW bosons

In this Section, we consider models with a photon, a W boson, a Z boson or a Higgs boson in the final state, accompanied by Dark Matter particles that either couple directly to the boson or are mediated by a new particle. The experimental signature is identified as  $V+MET$ .

These models are interesting both as some are demanded by gauge coupling relations in models where the gluon provides the experimentally detectable signature, and also as stand-alone models with final states that cannot be generated by the models in Section 3.

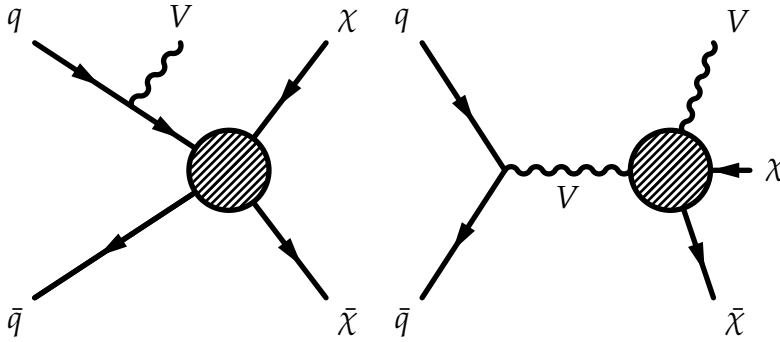


Figure 5.1: Sketch of benchmark models including a contact interaction for  $V+MET$  searches, adapted from [NCC<sup>+</sup>14].

The models considered can be divided in four categories:

*Models including a contact operator, where the boson is radiated from the initial state*

As depicted in the left diagram of Figure 5.1, these models follow the nomenclature and theory for the EFT benchmarks commonly used by MET+X searches [GIR<sup>+</sup>10]. These models have been used in past experimental searches [Kha14, Aad14b, K<sup>+</sup>14, Aad14b, A<sup>+</sup>14a, Aad14a], and they will not be described here.

*Simplified models with a boson radiated either from the initial state or from the mediator*

These models follow those already described in Section 3, replacing the gluon with a boson.

*Models including a contact operator, where the boson is directly coupled to DM*

Shown on the right-hand side of Figure 5.1, these models allow for a contact interaction vertex that directly couples the boson to Dark Matter.

*V-specific simplified models* These models postulate direct couplings of new mediators to bosons, e.g. they couple the Higgs boson to a new vector or to a new scalar [CDM<sup>+</sup><sub>14</sub>, BLW<sub>14</sub>].

The following Sections describe the models within these categories, the parameters for each of the benchmark models chosen, the studies towards the choices of the parameters to be scanned, and finally point to the location of their Matrix Element implementation.

### 5.1 *Simplified models with boson radiation*

Searches in the jet+MET final state are generally more sensitive with respect to final states including bosons, due to the much larger rates of signal events featuring quark or gluon radiation with respect to radiation of bosons [ZBW<sub>13</sub>], in combination with the low branching ratios if leptons from boson decays are required in the final state. The rates for the Higgs boson radiation is too low for these models to be considered a viable benchmark [CDM<sup>+</sup><sub>14</sub>]. However, the presence of photons leptons from W and Z decays and W or Z bosons decaying hadronically allows to reject the background more effectively, making Z/gamma/W+MET searches still worth comparing with searches in the jet+MET final state.

#### 5.1.1 *Vector mediator exchanged in the s-channel*

The case for searches with W bosons in the final state has so far been strengthened by the presence of particular choices of couplings between the WIMP and the up and down quarks which enhance W radiation [BT<sub>13</sub>], in the case of the exchange of a vector mediator in the s-channel. Run-1 searches have considered three sample cases for the product of up and down quark couplings to the mediator  $\xi$ :

- No couplings between mediator and either up or down quarks ( $\xi = 0$ );
- Same coupling between mediator and each of the quark types ( $\xi = 1$ );
- Coupling of opposite sign between mediator and each of the quark types ( $\xi = -1$ ).

The  $\xi = -1$  case leads to a large increase in the cross-section of the process, and modifies the spectrum of missing transverse energy or transverse mass used for the searches. The sensitivity of the W+MET search for this benchmark in this case surpasses that of the jet+MET search. However, as shown in Ref. [BCD<sup>+</sup><sub>15</sub>], the cross-section increase is due to the production of longitudinally polarized W bosons, as a consequence of a violation of electroweak gauge symmetries. Unless further particles are introduced (in a fashion similar to the Higgs boson in the Standard Model), choosing a

value of  $\xi = -1$  for this simplified model will lead to a manifest violation of unitarity at LHC energies. The simplified model with a vector mediator exchanged in the s-channel model can still be considered as a benchmark for searches with a W boson if  $\xi = 1$ . We leave the study of further models with cross-section enhancements due to different couplings to up and down quarks for studies beyond the early LHC searches covered in this document. An example of such model is the case of both DM and SM Higgs charged under a new  $U(1)'$ , with a small mass mixing between SM Z-boson and the new Zprime. This leads to different effective DM couplings to  $u_L$  and  $d_L$ , proportional to their coupling to the Z boson, detailed in Appendix B.

The scan in the parameters that characterize this simplified model for EW boson + MET searches follow what already detailed in Section 3.

As in the case of the jet+MET models, the width does not have a significant impact on the kinematic distributions relevant for those searches. An example of the particle-level analysis acceptance using the generator-level cuts from Ref. [Aad15] for the photon+MET analysis, but raising the photon  $p_T$  cut to 150 GeV is shown in Figure 5.2, comparing a width that is set to  $\Gamma = M_{med}/3$  to the minimal width (the ratio between the two widths ranges from 1.05 to 1.5 with increasing mediator masses).

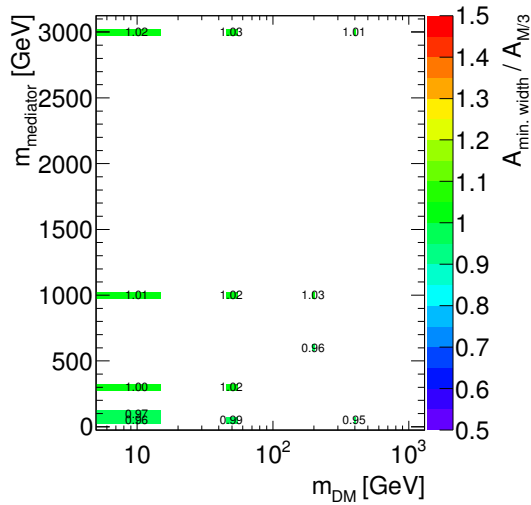


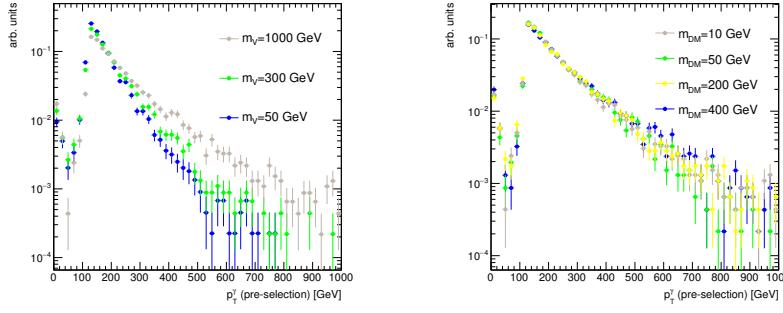
Figure 5.2: Analysis acceptance for the photon+MET analysis when varying the mediator width, in the case of a vector mediator exchanged in the s-channel

Examples of relevant kinematic distributions for selected benchmark points are shown in Fig. 5.10. leading-order cross-sections for the chosen benchmark points are shown in Appendix B.

### 5.1.2 Colored scalar mediator exchanged in the s-channel

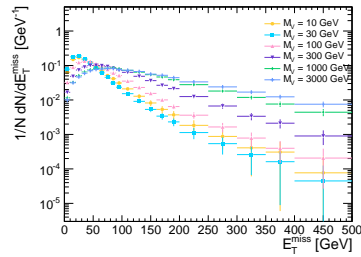
The model parameters with emission of an EW boson follow those in Section 3.

Figure 5.4 shows the MET distribution for the hadronic Z+MET final state, with varying dark matter and mediator mass, before

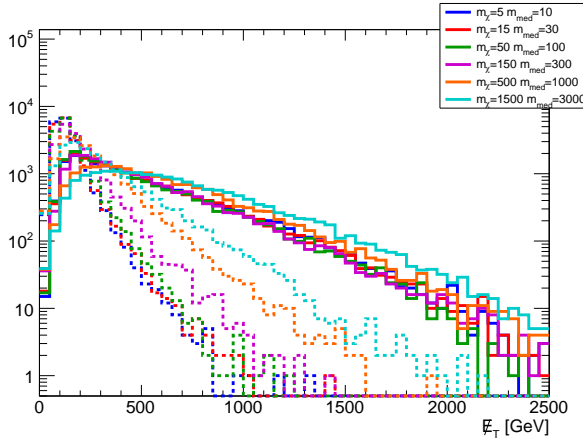


(a) Missing transverse momentum distribution for the photon+MET final state, for different mediator mass choices, for a DM mass of 10 GeV.

(b) Leading photon transverse momentum distribution for the photon+MET final state, for different DM mass choices, with a mediator mass of 1 TeV.



(c) Missing transverse momentum distribution for the leptonic Z+MET final state, for different mediator mass choices, for a DM mass of 15 GeV



(d) Missing transverse momentum distribution for the hadronic W+MET final state.

Figure 5.3: Kinematic distributions relevant for searches with W, Z and photons in the final state, for the simplified model with a vector mediator exchanged in the  $s$ -channel.

any selection. The acceptance for a series of simplified analysis cuts  
(MET > 350 GeV, leading jet  $p_T > 40$  GeV, minimum azimuthal angle  
between jet and MET > 0.4) applied at the generator level is shown  
in Figure 5.5. The parameter scan is still under discussion.

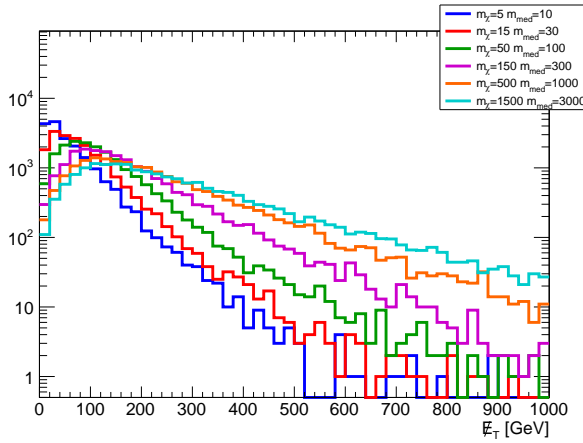


Figure 5.4: Missing transverse momentum distribution for the hadronic Z+MET final state, for the simplified model with a colored scalar mediator exchanged in the  $t$ -channel.

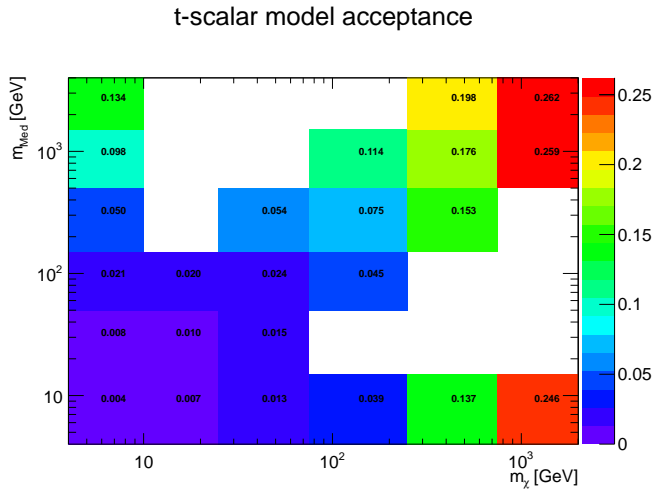


Figure 5.5: Acceptance table for the hadronic Z+MET final state, for the simplified model with a colored scalar mediator exchanged in the  $t$ -channel.

### 5.1.3 Model implementation

These models are generated at leading order with MadGraph 2.2.2, using Pythia8 for the parton shower. Parameter cards can be found on the Forum SVN repository [? ].

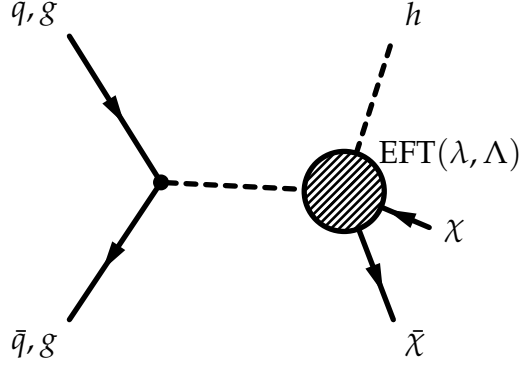
## 5.2 EFT models with direct DM-boson couplings

A complete list of effective operators with direct DM/boson couplings for Dirac DM, up to dimension 7, can be found in [CHLR13].

### 5.2.1 Dimension 5 operators

The lowest dimension benchmark operators we may consider are effective dimension 5, such as the one depicted in Figure 5.6.

Following the notation of [CNS<sup>+</sup>13], models from this category have a Lagrangian that includes terms such as:



$$\frac{m_W^2}{\Lambda_5^3} \bar{\chi} \chi W^{+\mu} W_\mu^- + \frac{m_Z^2}{2\Lambda_5^3} \bar{\chi} \chi Z^\mu Z_\mu . \quad (5.1)$$

Figure 5.6: Diagram for a dimension 5 operator giving rise to a Higgs+MET signature.

where  $m_Z$  and  $m_W$  are the masses of the  $Z$  and  $W$  boson,  $W^\mu$  and  $Z^\mu$  are the fields of the gauge bosons,  $\chi$  denote the Dark Matter fields and  $\Lambda_5$  is the effective field theory scale. Note that these operators are of true dimension 7, but reduce to effective dimension 5 once Higgs vevs, contained in the  $W$  and  $Z$  mass terms, are inserted. As such, one expects these operators would naturally arise in UV complete models where Dark Matter interacts via a Higgs portal where heavy mediators would couple to the Higgs or other fields in an extended Higgs sector. In such models the full theory may be expected to contain additional operators with Higgs-Dark Matter couplings. Concentrating for the moment on mono-gauge boson signals, the above operator induces signatures with MET in conjunction with  $Z$  and  $W$  bosons at tree level, while at loop level it induces couplings to photon pairs and  $Z\gamma$  through  $W$  loops. In these models, a clear relation exists between final states with photons, EW bosons and Higgs boson.

As shown in Fig. 5.7 kinematics of this model can be approximated by that of a simplified model including a high-mass scalar mediator exchanged in the s-channel. For this reason, the list of benchmark models with direct boson-DM couplings for photon,  $Z$  and  $W$  only includes dimension 7 operators: the scalar model with initial state radiation of an EW boson is already recommended and its results can be rescaled. The Higgs+MET analysis however will to use this model, as it would not be sensitive to a scalar mediator model.

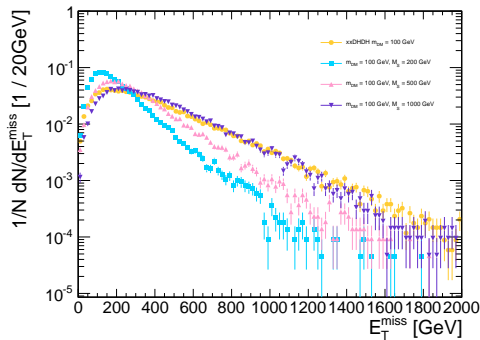


Figure 5.7: Comparison of the missing transverse momentum for the simplified model where a scalar mediator is exchanged in the s-channel and the model including a dimension-5 scalar contact operator, in the leptonic  $Z$ +MET final state



### 5.2.1.1 Parameter scan

### 5.2.2 Dimension 7 operators

The dimension-7 benchmark models contain the  $SU(2)_L \times U(1)_Y$  gauge-invariant couplings between DM fields and the kinetic terms of the EW bosons. The CP-conserving scalar couplings of this type can be written as

$$\frac{c_1}{\Lambda_S^3} \bar{\chi} \chi B_{\mu\nu} B^{\mu\nu} + \frac{c_2}{\Lambda_S^3} \bar{\chi} \chi W_{\mu\nu}^i W^{i,\mu\nu}. \quad (5.2)$$

Here  $B_{\mu\nu} = \partial_\mu B_\nu - \partial_\nu B_\mu$  and  $W_{\mu\nu}^i = \partial_\mu W_\nu^i - \partial_\nu W_\mu^i + g_2 \epsilon^{ijk} W_\mu^j W_\nu^k$  are the  $U(1)_Y$  and  $SU(2)_L$  field strength tensor, respectively, and  $g_2$  denotes the weak coupling constant. In the case of the pseudoscalar couplings, one has instead

$$\frac{c_1}{\Lambda_P^3} \bar{\chi} \gamma_5 \chi B_{\mu\nu} \tilde{B}^{\mu\nu} + \frac{c_2}{\Lambda_P^3} \bar{\chi} \gamma_5 \chi W_{\mu\nu}^i \tilde{W}^{i,\mu\nu}, \quad (5.3)$$

where  $\tilde{B}_{\mu\nu} = 1/2 \epsilon_{\mu\nu\lambda\rho} B^{\lambda\rho}$  and  $\tilde{W}_{\mu\nu}^i = 1/2 \epsilon_{\mu\nu\lambda\rho} W^{i,\lambda\rho}$  are the dual field strength tensors. In addition to the CP-conserving interactions (5.2) and (5.3), there are also four CP-violating couplings that are obtained from the above operators by the replacement  $\bar{\chi} \chi \leftrightarrow \bar{\chi} \gamma_5 \chi$ .

The effective interactions introduced in (5.2) and (5.3) appear in models of Rayleigh DM [? ]. Ultraviolet completions where the operators are generated through loops of states charged under  $U(1)_Y$  and/or  $SU(2)_L$  have been proposed in [? ] and their LHC signatures have been studied in [? ]. If these new charged particles are light, the high- $p_T$  gauge bosons that participate in the MET processes considered here are able to resolve the substructure of the loops. This generically suppresses the cross sections compared to the EFT predictions [? ], and thus will weaken the bounds on the interaction strengths of DM and the EW gauge bosons to some extent. Furthermore, the light charged mediators may be produced on-shell in  $pp$  collisions, rendering direct LHC searches potentially more restrictive than MET searches. Making the above statements precise would require further studies beyond the timescale of this forum.

Since for  $\Lambda_S = \Lambda_P$  the effective interactions (5.2) and (5.3) predict essentially the same value of the mono-photon, mono- $Z$  and mono- $W$  cross section [CNS<sup>+</sup>13, CHH15], we consider below only the former couplings. We emphasise however that measurements of the jet-jet azimuthal angle difference in MET+2 $j$  events may be used to disentangle whether DM couples more strongly to the combination  $B_{\mu\nu} B^{\mu\nu}$  ( $W_{\mu\nu}^i W^{i,\mu\nu}$ ) or the product  $B_{\mu\nu} \tilde{B}^{\mu\nu}$  ( $W_{\mu\nu}^i \tilde{W}^{i,\mu\nu}$ ) of field strength tensors [CHLR13, CHH15].

After EW symmetry breaking the interactions (5.2) induce direct couplings between pairs of DM particles and gauge bosons. The corresponding Feynman rule reads

$$\frac{4i}{\Lambda_S^3} g_{V_1 V_2} (p_1^{\mu_2} p_2^{\mu_1} - g^{\mu_1 \mu_2} p_1 \cdot p_2), \quad (5.4)$$

where  $p_i$  ( $\mu_i$ ) denotes the momentum (Lorentz index) of the vector field  $V_i$  and for simplicity the spinors associated with the DM fields have been dropped. The couplings  $g_{V_i V_j}$  take the form

$$\begin{aligned} g_{\gamma\gamma} &= c_w^2 c_1 + s_w^2 c_2, \\ g_{\gamma Z} &= -s_w c_w (c_1 - c_2), \\ g_{ZZ} &= s_w^2 c_1 + c_w^2 c_2, \\ g_{WW} &= c_2, \end{aligned} \tag{5.5}$$

with  $s_w$  ( $c_w$ ) the sine (cosine) of the weak mixing angle. Note that our coefficients  $c_1$  and  $c_2$  are identical to the coefficients  $C_B$  and  $C_W$  used in [CHH15], while they are related via  $k_1 = \frac{1}{c_w^2} c_1$  and  $k_2 = \frac{1}{s_w^2} c_2$  to the coefficients  $k_1$  and  $k_2$  introduced in [CNS<sup>+</sup>13].

The coefficients  $c_1$  and  $c_2$  appearing in (5.5) determine the relative importance of each of the MET channels and their correlations. For example, one observes that:

- Only  $c_2$  enters the coupling between DM and  $W$  bosons, meaning that only models with  $c_2 \neq 0$  predict a mono- $W$  signal;
- If  $c_1 = c_2$  the mono-photon (mono- $Z$ ) signal does not receive contributions from diagrams involving  $Z$  (photon) exchange;
- Since numerically  $c_w^2/s_w^2 \simeq 3.3$  the mono-photon channel is particularly sensitive to  $c_1$ .

The kinematic distributions for dimension-7 scalar and pseudoscalar operators only shows small differences, as shown in Fig. 5.8.



Figure 5.8: Comparison of the missing transverse momentum for the scalar and pseudoscalar operators with direct interaction between DM and photon, in the photon+MET final state

Similarly, the differences in kinematics for the various signatures are negligible when changing the coefficients  $k_1$  and  $k_2$ , as shown in Figure ?? . Only the case  $k_1 = k_2 = 1$  is generated as benchmark; other cases are left for reinterpretation as they will only need a rescaling of the cross-sections shown in Appendix B for the various DM mass points considered.

Examples of relevant kinematic distributions for selected benchmark points are shown in Fig. 5.10.

*Completion and validity of EW contact operators* [TODO: mention here discussion with Liantao yesterday]



(a) Missing transverse momentum distribution for the photon+MET final state.



(b) Missing transverse momentum distribution for the leptonic Z+MET final state.



(c) Transverse mass ( $m_T$ ) for the leptonic W+MET final state.

Figure 5.9: Kinematic distributions relevant for searches with W, Z and photons in the final state, for for the scalar and pseudoscalar operators representing direct interactions between DM and bosons.

As an example of a simplified model corresponding to the dimension-5 EFT operator described above, we consider a Higgs portal with a scalar mediator. Models of this kind are among the most concise versions of simplified models that produce couplings of Dark Matter to pairs of gauge-bosons. Scalar fields may couple directly to pairs of electroweak gauge bosons, but must carry part of the electroweak vev. One may thus consider a simple model where Dark Matter couples to a scalar singlet mediator, which mixes with the fields in the Higgs sector.

$$L \subset m_s S^2 + \lambda S^2 H^2 + \lambda' S H^2 + y S \chi \bar{\chi} \quad (5.6)$$

Where H is a field in the Higgs sector that contains part of the electroweak vev, S is a heavy scalar singlet and  $\chi$  is a Dark Matter field. There is then an S channel diagram where DM pairs couple to the singlet field S, which then mixes with a Higgs-sector field, and couples to W and Z bosons. This diagram contains 2 insertions of EW symmetry breaking fields, corresponding in form to the effective dimension-5 operator in the previous section.

### 5.2.3 Model implementation

These models are generated at leading order with MadGraph 2.2.2, using Pythia8 for the parton shower. Parameter cards can be found on the Forum SVN repository: [?] for dimension 5 operators and [?] for dimension 7.



(a) Missing transverse momentum distribution for the photon+MET final state.



(b) Missing transverse momentum distribution for the leptonic Z+MET final state.



(c) Transverse mass ( $m_T$ ) for the leptonic W+MET final state.



(d) Fat [Insert algorithm] jet mass ( $m_T$ ) for the hadronic W+MET final state.

Figure 5.10: Kinematic distributions relevant for searches with W, Z and photons in the final state, for the simplified model with a vector mediator exchanged in the  $s$ -channel.

### 5.3 Specific simplified models including EW bosons, tailored to Higgs+MET searches

Three benchmark simplified models [CDM<sup>+</sup><sub>14</sub>, BLW<sub>14</sub>] are recommended for Higgs+MET searches:

- A model where a vector mediator ( $Z'_B$ ) is exchanged in the  $s$ -channel, radiates a Higgs or a Z boson and decays into two DM particles (Fig. 5.11 (a));
- A model where a scalar mediator  $S$  couples to the SM only through the SM Higgs and decays to two DM particles (Fig. 5.12);
- A model where a vector  $Z'$  is produced resonantly and decays into a Higgs boson plus an intermediate heavy pseudoscalar particle  $A^0$ , in turn decaying into two DM particles (Fig. 5.11 (b)).

These models have a distinct kinematics, as shown in the comparison of the MET spectra in Fig. 5.13, for high and low mediator masses. Figure ?? shows the MET distribution for models with

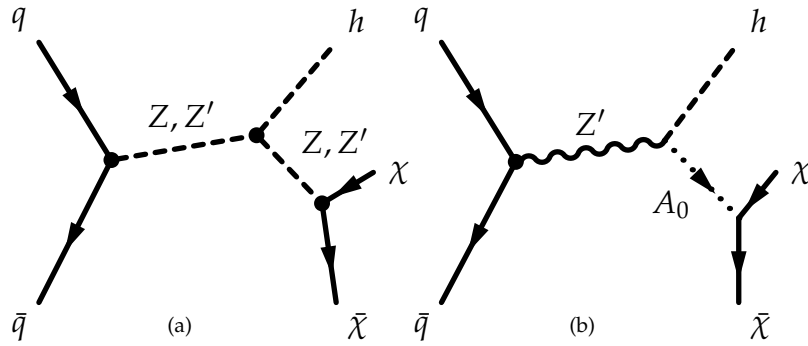


Figure 5.11: Feynman diagrams of leading order processes leading to Higgs+MET events: a model with a vector mediator ( $Z'$ ) coupling with DM and with the Higgs boson  $h$  ??, and a 2HDM model with a new invisibly decaying pseudoscalar  $A^0$  from the decay of an on-shell resonance  $Z'$  giving rise to a Higgs+MET signature ??.

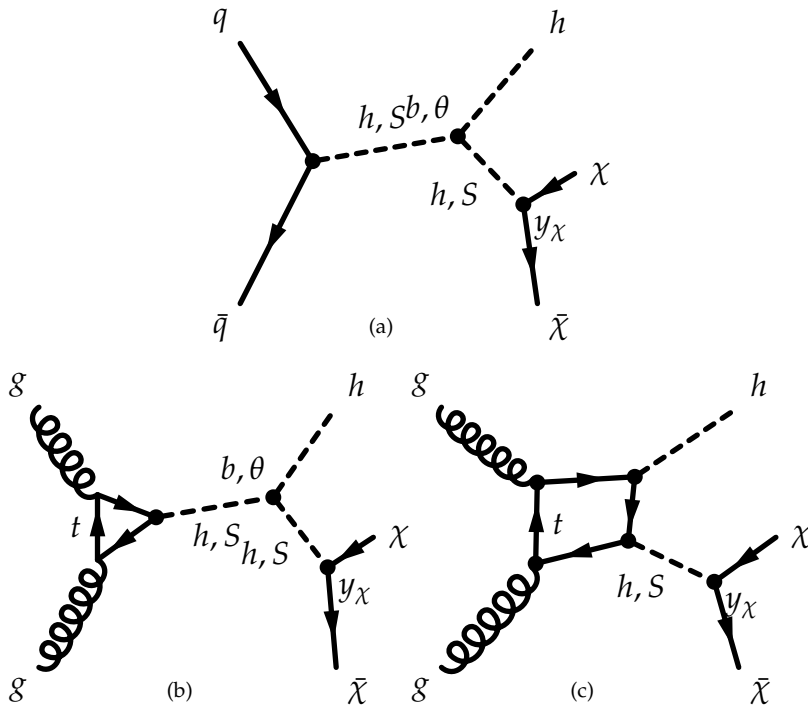


Figure 5.12: Feynman diagrams of leading order processes leading to Higgs+MET events for a model with a scalar mediator ( $S$ ) coupling with DM and with the Higgs boson  $h$ .

high mediator masses ( $m_S = 1$  TeV,  $m_{Z'} = 1$  TeV,  $m_{A^0} = 1$  TeV) and DM mass of either 50 ( $Z'_B$  and  $A^0$  models) or 65 GeV (scalar mediator model). Figure ?? shows the MET distribution for models with low mediator masses ( $m_{Z'_B} = 100$  GeV,  $m_{Z'} = 1$  TeV,  $m_{A^0} = 100$  GeV) and DM mass of 1 TeV for all models.

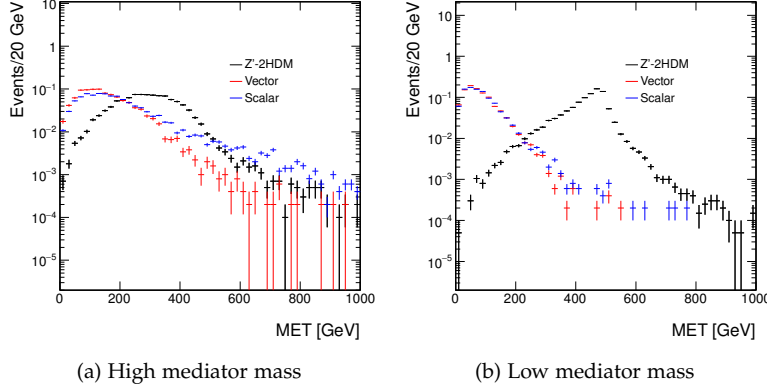


Figure 5.13: Comparison of the missing transverse momentum distributions at generator level in different simplified models leading to a Higgs+MET signature. The model parameter settings are detailed in the text.

### 5.3.1 MET+Higgs from a baryonic $Z'$

[TODO for AB: add baryonic Higgs diagram]

The first model, shown in Fig. ?? postulates a new gauge boson  $Z'$  corresponding to a new  $U(1)_B$  baryon number symmetry. The stable baryonic states included in this model are the DM candidate particles. The mass of the  $Z'$  boson is acquired through a baryonic Higgs  $h_B$ , which mixes with the SM Higgs boson. The interactions between the  $Z'$ , the quarks and the DM are described by the following Lagrangian:

$$L = g_q \bar{q} \gamma^\mu q Z'_\mu + g_\chi \bar{\chi} \gamma^\mu \chi Z'_\mu. \quad (5.7)$$

The quark couplings  $g_q$  are fixed to be equal to one third of the gauge coupling  $g_B$ , while the DM coupling to the  $Z'$  are proportional to the baryon number and to the gauge coupling ( $g_{chi} = B g_B$ ). No leptonic couples of the  $Z'$  are allowed, thus evading dilepton constraints. After incorporating the mixing of the baryonic and SM Higgs bosons, this model is described by the following Lagrangian term at energies below  $m_{Z'}$ :

$$L_{\text{eff}} = -\frac{g_q g_\chi}{m_{Z'}^2} \bar{q} \gamma^\mu q \bar{\chi} \gamma_\mu \chi \left( 1 + \frac{g_{hZ'Z'}}{m_{Z'}^2} h \right), \quad (5.8)$$

The first term of this equation gives rise to a term that is equivalent to the radiation of a jet (or another EW gauge boson) in the initial state. The second term describes the interaction between the  $Z'$  and the SM Higgs boson, via the coupling  $g_{hZ'Z'} = \frac{m_{Z'}^2 \sin \theta}{v_B}$ , where  $\sin \theta$  is the mixing angle between the Higgs and the  $Z'$  and  $v_B$  is the Baryonic Higgs vev.

#### 5.3.1.1 Parameter scan

Overall, this model is described by six parameters:

1. the mediator mass  $m_{\text{med}}$ , (also referred to as  $m_{Z'}$ )
2. mass of dark matter,  $m_{DM}$
3. coupling of  $Z'$  mediator to dark matter,  $g_{DM}$
4. coupling of the mediator to quarks,  $g_q$
5. mixing angle between baryonic Higgs and SM-like Higgs boson,  $\sin \theta$
6. coupling of the mediator to SM-like Higgs boson,  $g_{hZ'Z'}$

The width of the mediator is calculated using all possible decays, namely to quarks, to pairs of DM particles if kinematically allowed,

The dependence of the missing transverse momentum (MET) on the model parameters is studied by varying the parameters one at a time. The variation of parameters other than  $m_{\text{med}}$  and  $m_{DM}$  does not result in significant variations of the MET spectrum, as shown in Figures 5.14. Figure 5.15 shows that for an on-shell mediator, varying  $m_{DM}$  with the other parameters fixed does not affect the MET distribution, while the distribution broadens significantly in the case of an off-shell mediator. For this reason, the same grid in  $m_{\text{med}}$ ,  $m_{DM}$  as for the vector mediator of the jet+MET search (Table ??) is chosen as a starting point. The coupling  $g_{hZ'Z'}$ , along with  $g_q$  and  $g_{DM}$ , are subject to perturbativity bounds:

$$g_q, g_\chi < 4\pi$$

and

$$g_{hZ'Z'} < \sqrt{4\pi} m_{Z'} \sin \theta$$

The value  $g_{hZ'Z'}/m_{Z'} = 1.0$  is chosen as a benchmark value for the generation of Monte Carlo samples since it maximizes the cross section (as shown in the following paragraph) without violating the bounds. The mediator-DM coupling  $g_{DM}$  is fixed to 1, and the mediator-quark  $g_q$  coupling is fixed to  $1/3$ . Since the kinematics does not change as a function of these parameters, results for other values of  $g_{hZ'Z'}/m_{Z'}$ ,  $g_{DM}$  and  $g_q$  can be obtained through rescaling by the appropriate cross sections.

More detailed studies are required to estimate the reach of the analysis with respect to all points in the grid and therefore decide on a smaller set of grid points to be generated; those are left to the individual analyses.

#### 5.3.1.2 Cross-section scaling

The dependence of the cross section of the  $pp \rightarrow H\chi\bar{\chi}$  process on  $g_{hZ'Z'}$  is shown in Figure 5.16. The curves have been fitted to second-order polynomials. For  $m_{\text{med}} = 100$  GeV, the fit function is

$$y = -0.12 - 3.4 \times 10^{-3}x + 2.7 \times 10^{-4}x^2$$

. For  $m_{\text{med}} = 1$  TeV, the fit function is

$$y = 0.0012 - 2.4 \times 10^{-7}x + 1.5 \times 10^{-7}x^2$$

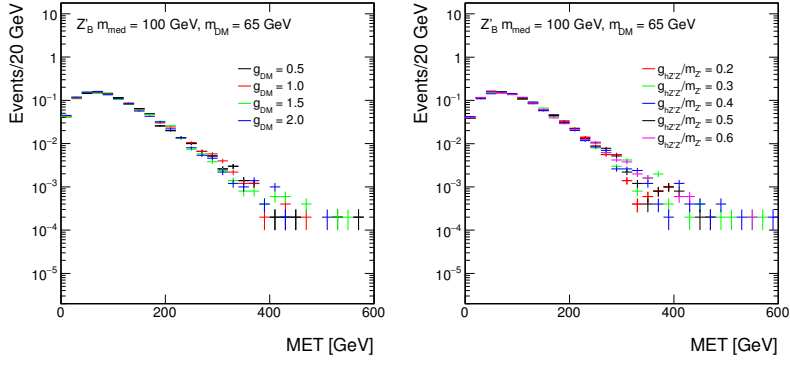


Figure 5.14: Missing transverse momentum distributions at generator level in the vector mediator scenario for different values of: the mediator-dark matter coupling  $g_{\text{DM}}$  (left), and the coupling between the mediator and the SM-like Higgs boson, scaled by the mediator mass,  $g_{hZ'Z'}/m_{Z'}$  (right).

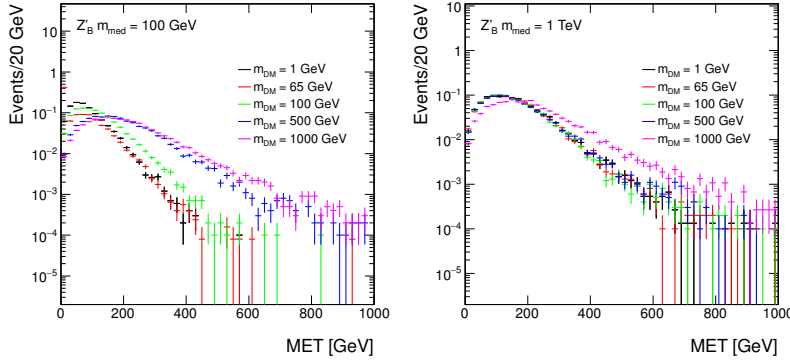


Figure 5.15: Missing transverse momentum distributions at generator level in the vector mediator scenario: for different values of the dark matter mass  $m_{\text{DM}}$  and a mediator mass of  $m_{\text{med}} = 100$  GeV (left) and  $m_{\text{med}} = 1$  TeV (right).

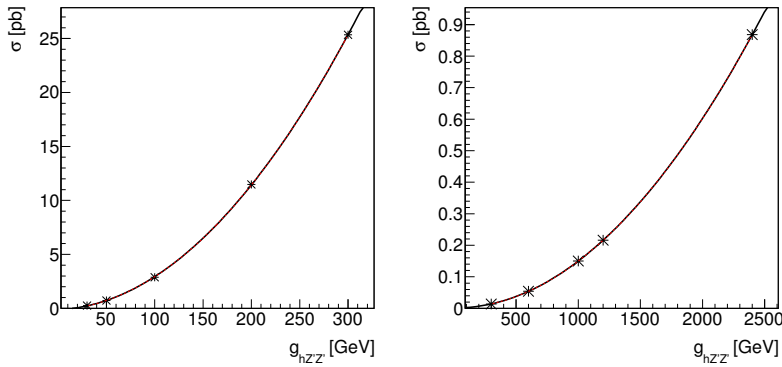


Figure 5.16: Cross section of the  $pp \rightarrow H\chi\chi$  process as a function of  $g_{hZ'Z'}$  for  $m_{Z'} = 100$  GeV (left) and  $m_{Z'} = 1$  TeV (right). The fit functions are shown in the text.



### 5.3.2 MET+Higgs from a scalar mediator

A real scalar singlet  $S$  coupling to DM can be introduced as a portal between SM and the dark sector through the Higgs field. The new scalar mixes with the SM Higgs boson, and couples to DM through a Yukawa term  $y_\chi$ . The relevant terms in the scalar potential are

$$V \supset a|H|^2S + b|H|^2S^2 + \lambda_h|H|^4 \\ \longrightarrow \frac{1}{2}a(h+v)^2S + \frac{1}{2}b(h+v)^2S^2 + \frac{\lambda_h}{4}(h+v)^4, \quad (5.9)$$

where  $a, b$  are new physics couplings and  $\lambda_h$  is the Higgs quartic.

The additional Lagrangian terms for this model are:

$$L \supset -y_\chi \bar{\chi}\chi(\cos\theta S - \sin\theta h) - \frac{m_q}{v} \bar{q}q(\cos\theta h + \sin\theta S) \quad (5.10)$$

where  $\theta$  is the mixing angle between the Higgs boson and the new scalar.

Mono-Higgs signals in this model arise through processes shown in Fig. ??(a,b), or through the radiation of a Higgs boson from the  $t$  quark in the production loop. The first two processes depend on the  $h^2S$  and  $hS^2$  cubic terms in Eq. (5.9). At leading order in  $\sin\theta$ , these terms are

$$V_{\text{cubic}} \approx \frac{\sin\theta}{v} (2m_h^2 + m_S^2) h^2S + bvhS^2 + \dots \quad (5.11)$$

with  $a$  and  $\lambda_h$  expressed in terms of  $\sin\theta$  and  $m_h^2$ , respectively. At leading order of  $\sin\theta$ , the  $h^2S$  term is fixed once the mass eigenvalues  $m_h, m_S$  and mixing angle are specified. The  $hS^2$  term is not fixed and remains a free parameter of the model, depending on the new physics coupling  $b$ .

#### 5.3.2.1 Parameter scan

This model is described by five parameters:

1. the Yukawa coupling of heavy scalar to dark matter (DM),  $g_{DM}$  (also referred to as  $y_\chi$ )
2. the mixing angle between heavy scalar and SM-like Higgs boson,  $\sin\theta$ ;
3. the new physics coupling,  $b$ ;
4. mass of heavy scalar,  $m_S$ , also termed  $m_{\text{med}}$ ;
5. mass of dark matter,  $m_{DM}$ ;

The mixing angle is constrained from current Higgs data to satisfy  $\cos\theta = 1$  within 10% and therefore  $\sin\theta \lesssim 0.4$ . This provides a starting point for the parameter scan in this model: we recommend to set  $\sin\theta = 0.3$ . Figure 5.18 shows that there is no dependence of the kinematics from the value of this angle, and different values can be obtained via rescaling the results for this mixing angle according to the relevant cross-section. It can also be observed from

Figures 5.19 and 5.17 that the kinematics of this model follows that of the equivalent jet+MET model: only small changes are observed in the on-shell region, while the relevant distributions diverge when the mediator is off-shell. For this reason, the same grid in  $m_{\text{med}}$ ,  $m_{\text{DM}}$  as for the scalar mediator of the jet+MET search (Table ??) is chosen as a starting point. The Yukawa coupling to DM  $y_{\text{DM}}$  is set to 1, the new physics coupling between scalar and SM Higgs  $b = 3$ . Results for other values can be obtained via a rescaling of the results for these parameters. More detailed studies are required to estimate the reach of the analysis with respect to all points in the grid and therefore decide on a smaller set of grid points to be generated; those are left to the individual analyses. [TODO: can we get sensitivity to all the points for all signatures?]

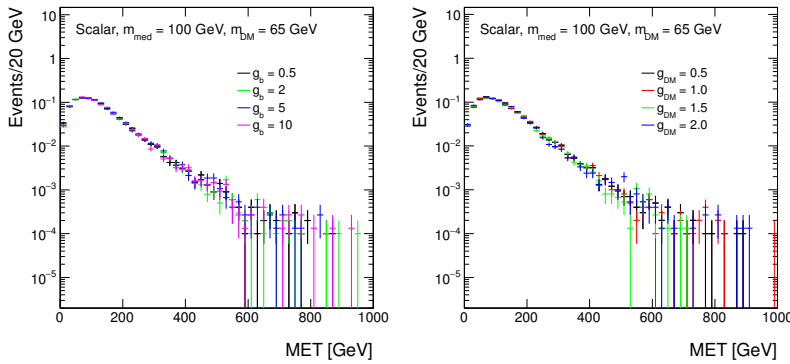


Figure 5.17: Missing transverse momentum distributions at generator level in the scalar mediator scenario, for different values of: the new physics coupling  $g_b$  (left), and the mediator-dark matter coupling  $g_{\text{DM}}$  (right).

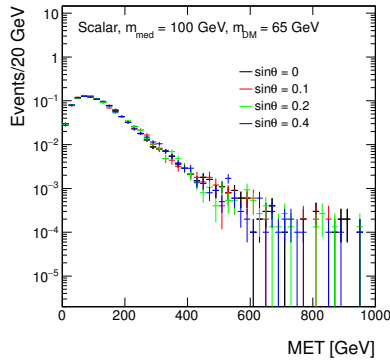


Figure 5.18: Missing transverse momentum distributions at generator level in the scalar mediator scenario: for different values of the mixing angle  $\sin \theta$ .

### 5.3.3 Higgs+MET signal from 2HDM model with a $Z'$ and a new pseudoscalar

In this simplified model [BLW14], a new  $Z'$  resonance decays to a Higgs boson  $h$  plus a heavy pseudoscalar state  $A$  in the 2HDM framework, which in turn decays to a DM pair. This model is represented in the diagram in Figure ??.

The motivation for coupling the dark matter to the pseudoscalar is that dark matter coupling to higgs or  $Z'$  is generically constrained by other signal channels and direct detection. An advan-

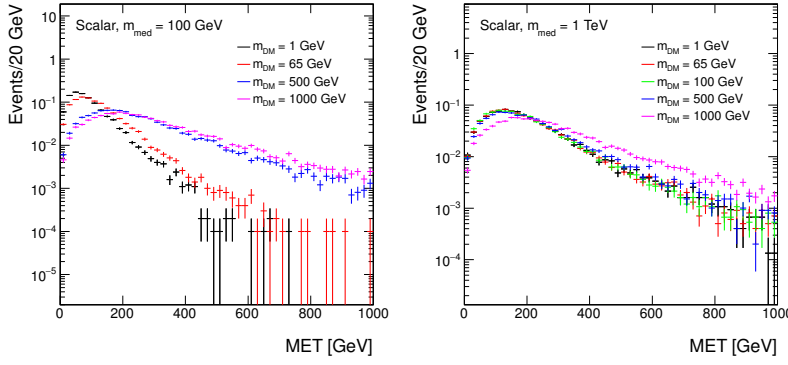


Figure 5.19: Missing transverse momentum distributions at generator level in the scalar mediator scenario: for different values of the dark matter mass  $m_{DM}$  and a mediator mass of  $m_{med} = 100$  GeV (left) and  $m_{med} = 1$  TeV (right).

tage of including this model is that it has different kinematics due to the on-shell  $Z'$  production, where for heavy  $Z'$  masses the MET and pT spectra are much harder. This model can satisfy electroweak precision tests and constraints from dijet resonance searches, and still give a potentially observable Higgs+MET signal.

This model comprises two doublets, where  $\Phi_u$  couples to up-type quarks and  $\Phi_d$  couples to down-type quarks and leptons:

$$-\mathcal{L} \supset y_u Q \Phi_u \bar{u} + y_d Q \Phi_d \bar{d} + y_e L \Phi_d \bar{e} + \text{h.c.} \quad (5.12)$$

After electroweak symmetry breaking, the Higgs doublets attain vevs  $v_u$  and  $v_d$ , and in unitary gauge the doublets are parametrized as

$$\begin{aligned} \Phi_d &= \frac{1}{\sqrt{2}} \begin{pmatrix} -\sin \beta H^+ \\ v_d - \sin \alpha h + \cos \alpha H - i \sin \beta A^0 \end{pmatrix} , \\ \Phi_u &= \frac{1}{\sqrt{2}} \begin{pmatrix} \cos \beta H^+ \\ v_u + \cos \alpha h + \sin \alpha H + i \cos \beta A^0 \end{pmatrix} \end{aligned} \quad (5.13)$$

where  $h, H$  are neutral CP-even scalars and  $A^0$  is a neutral CP-odd scalar. In this framework,  $\tan \beta \equiv v_u/v_d$ , and  $\alpha$  is the mixing angle that diagonalizes the  $h - H$  mass squared matrix. We take  $\alpha = \beta - \pi/2$ , in the limit where  $h$  has SM-like couplings to fermions and gauge bosons as per Ref. [?], and  $\tan \beta \geq 0.3$  as implied from the perturbativity of the top Yukawa coupling. The Higgs vevs lead to  $Z - Z'$  mass mixing, with a mixing parameter given by

$$\begin{aligned} \epsilon &\equiv \frac{1}{M_{Z'}^2 - M_Z^2} \frac{g g_z}{2 \cos \theta_w} (z_d v_d^2 + z_u v_u^2) \\ &= \frac{(M_Z^0)^2}{M_{Z'}^2 - M_Z^2} \frac{2 g_z \cos \theta_w}{g} z_u \sin^2 \beta. \end{aligned} \quad (5.14)$$

The production cross section for this model scales as  $(g_z)^2$ , as the decay width for this process to leading order in  $\epsilon$  (Eq. 5.14) is

$$\Gamma_{Z' \rightarrow h A^0} = (g_z \cos \alpha \cos \beta)^2 \frac{|p|}{24\pi} \frac{|p|^2}{M_{Z'}^2}. \quad (5.15)$$

where the center of mass momentum for the decay products  $|p| = \frac{1}{2M_{Z'}} \lambda^{1/2}(M_{Z'}^2, m_h^2, m_{A^0}^2)$ , and  $\lambda$  is the Källén triangle function.

### 5.3.3.1 Parameter scan

The model is described by five parameters:

- the pseudoscalar mass  $M_{A^0}$ ,
- the DM mass  $m_{DM}$ ,
- the  $Z'$  mass,  $M_{Z'}$ ,
- $\tan \beta (\equiv v_u/v_d)$ ,
- the  $Z'$  coupling strength  $g_z$ .

To study the signal production and kinematic dependencies on these parameters, we produced signal samples varying each of the five parameters through MadGraph for the matrix element, PYTHIA for the parton shower, and DELPHES[?] for a parameterized detector-level simulation.

As seen in Fig. 5.20, variations of  $\tan \beta$  does not lead to any kinematic difference and the production cross section simply scales as a function of  $\tan \beta$ . Hence we recommend to fix  $\tan \beta$  to unity in the signal generation.

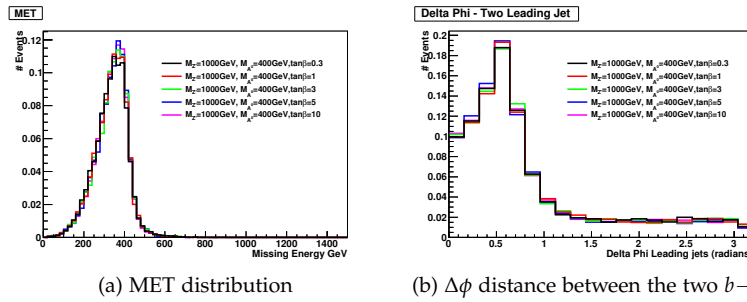


Figure 5.20: Kinematic distributions of the signal process varying  $\tan \beta$ , in the case of a Higgs boson decaying into two  $b$  quarks, after parameterized detector simulation: no kinematic dependency is observed

Similarly, variations of  $g_z$  do not lead to any kinematic changes.

The value of  $g_z$  for a given  $M_{Z'}$  and  $\tan \beta$  can be set according to the maximum value allowed by electroweak global fits and dijet constraints, as described in [BLW14]. Since this parameter does not influence the kinematics, we leave it up to individual analyses on whether they generate benchmark points only according to these external constraints [TODO: add link to section as in summary].

**This is the same sentence we will put in for the mono-b model].**

Since the DM pair are produced as a result of the decay of  $A^0$ , there are minimal kinematic changes when varying  $M_{DM}$  as long as  $M_{DM} < M_{A^0}/2$  so that  $A^0$  production is on-shell, as shown in Fig. 5.21 and 5.22 (before detector simulation).

We recommend to produce signal events for a fixed  $g_z = 0.8$ ,  $\tan \beta = 1$  and  $M_{DM} = 100$  GeV. For these values, we scan the 2-D parameter space of  $M_{Z'}, M_{A^0}$  with  $M_{Z'} = 600, 800, 1000, 1200, 1400$  GeV, and  $M_{A^0} = 300, 400, 500, 600, 700, 800$  GeV with  $M_{A^0} < M_{Z'} - m_h$ , for a total of 24 points. The choice of scan is justified by the sensitivity study in ??: the expected LHC sensitivity for Run-2 is up to  $M_{Z'} \sim 1.5$  TeV. For the parameter scan, the DM mass is fixed to 100 GeV. For two  $M_{Z'}, M_{A^0}$  value sets, we vary the DM mass to obtain

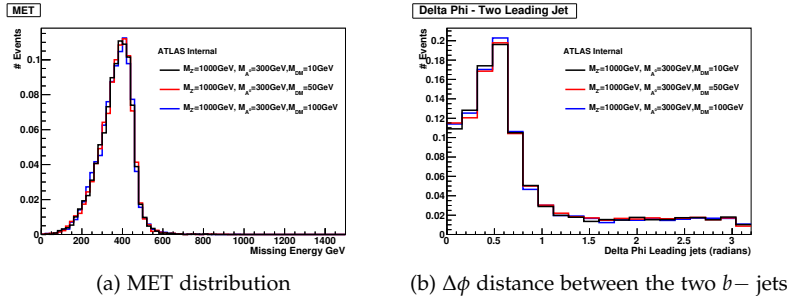


Figure 5.21: Kinematic distributions of the signal process varying  $M_{DM}$ : minimal kinematic dependency on  $M_{DM}$  as expected when  $A^0$  is produced on-shell. Plots shown for  $M_{Z'} = 1000$  GeV,  $M_{A^0} = 300$  GeV.

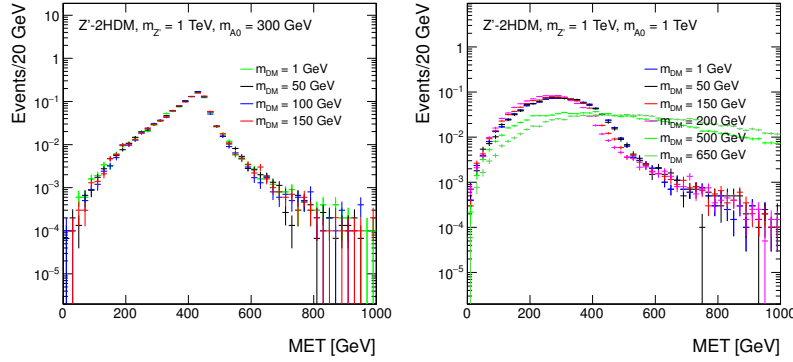


Figure 5.22: Missing transverse momentum distributions at generator level in the  $Z'+2HDM$  scenario for different values of the dark matter mass  $m_{DM}$ , with  $m_{Z'} = 1$  TeV and  $m_{A^0} = 300$  GeV (left) and  $m_{A^0} = 1$  TeV (right).

sample cross section for rescaling results. All LO cross sections for the various parameter scan points are reported in Appendix B. The parameter scan excludes the off-shell region, as the cross-sections are suppressed and the LHC would not have any sensitivity to these benchmark points in early data.

The kinematic distributions with varying  $M_{Z'}$  for fixed  $M_{A^0}$  are shown in Fig. 5.23, while the dependency on  $M_{A^0}$  is shown in Fig. 5.24.

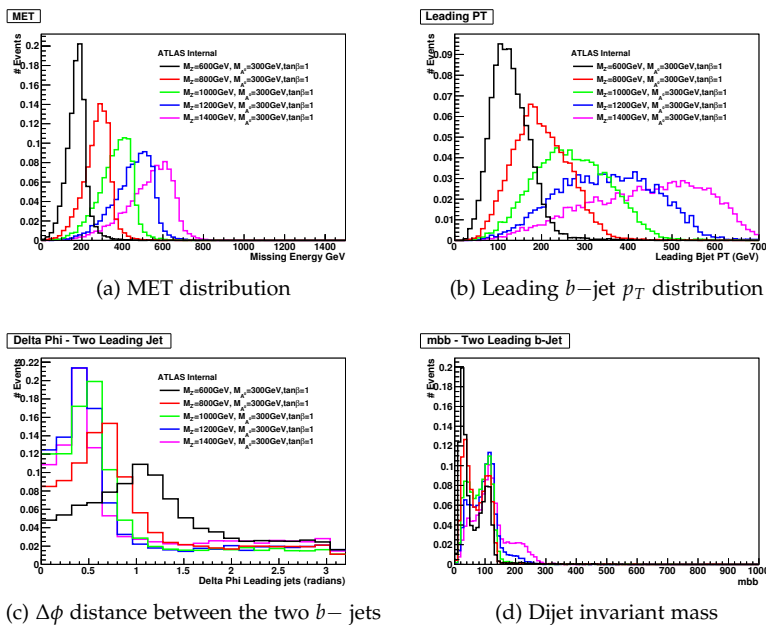


Figure 5.23: Kinematic distributions of the signal process varying  $M_{Z'}$ , for  $M_{DM} = 100$  GeV,  $M_{A^0} = 300$  GeV.

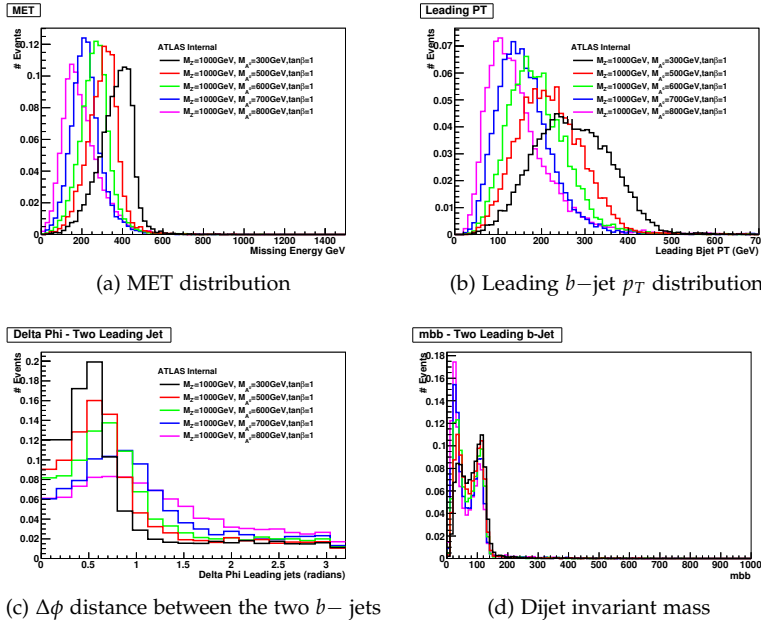


Figure 5.24: Kinematic distributions of the signal process varying  $M_{A^0}$ , for  $M_{DM} = 100$  GeV,  $M_{Z'} = 1000$  GeV.

This model also allows for an additional source of Higgs plus MET signal with a similar kinematics (Fig. 5.25, shown with detector simulation samples) to the signal process from the decay of  $Z' \rightarrow hZ$ , where the  $Z$  decays invisibly. The partial decay width for the  $Z'$  is:

$$\Gamma_{Z' \rightarrow hZ} = (g_z \cos \alpha \sin \beta)^2 \frac{|p|}{24\pi} \left( \frac{|p|^2}{M_{Z'}^2} + 3 \frac{M_Z^2}{M_{Z'}^2} \right), \quad (5.16)$$

The values for the  $Z'$  masses scanned for those samples should follow those of the previous samples, namely values of  $M_{Z'} = 600, 800, 1000, 1200, 1400$  GeV. This signal process has no  $M_A$  dependence.

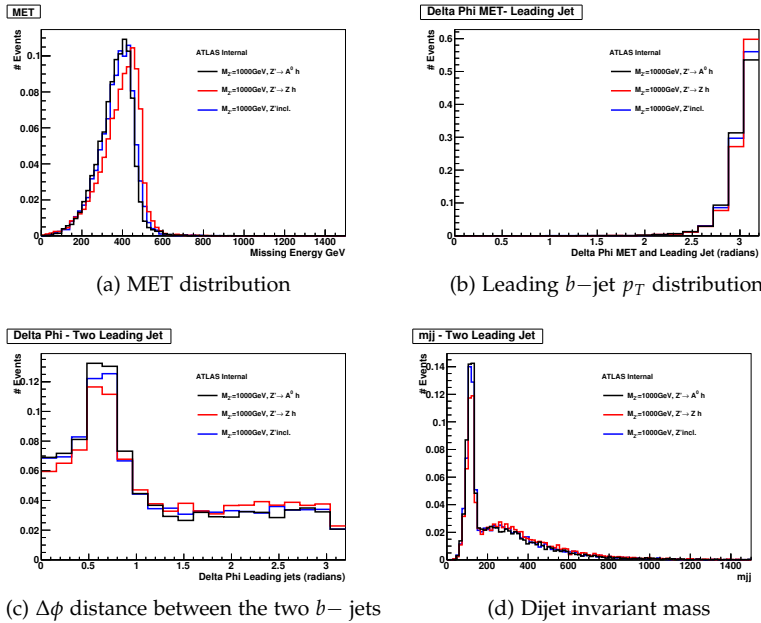


Figure 5.25: Kinematic distributions of  $Z' \rightarrow A^0 h$  exclusive production,  $Z' \rightarrow Zh$  exclusive production and  $Z'$  inclusive production for  $M_{Z'} = 1000$  GeV and  $M_{A^0} = 300$  GeV

#### 5.3.4 Model implementation

All three Higgs+MET models are generated at leading order with MadGraph 2.2.2, using Pythia8 for the parton shower. The MadGraph implementations of the scalar and vector models can be found on the Forum SVN repository [? ], while the 2HDM model can be found at this link [? ].

In all cases, it is recommended not to handle the  $h$  decay through MadGraph as it does not include the proper  $h$  branching ratios, or, if using MadGraph, then the resulting cross section should be rescaled to match onto the correct branching ratio.

##### *Madgraph details for scalar mediator Higgs+MET model*

In this model, the contribution from the  $gghS$  box is included through an effective Lagrangian evaluated in the large  $m_t$  limit. This may overestimate the rates of  $h + \cancel{E}_T$  signal [? ], but a full evaluation is left to future studies.

##### *Madgraph details for 2HDM Higgs+MET model*

The two couplings that can be changed in the Madgraph model follow the nomenclature below:

- $Tb - \tan \beta$
- $gz - g_z$ , gauge coupling of  $Z'$  to quarks

The other couplings are not changed, including  $gx$  (the  $A\tilde{\chi}\chi$  coupling) which has little impact on the signal.  $\sin \alpha$  is fixed internally such that  $\cos(\beta - \alpha) = 0$ . The width of the  $Z'$  and  $A$  can be computed automatically within Madgraph. The couplings here don't affect the signal kinematics, so they can be fixed to default values and then the signal rates can be scaled appropriately.

The nomenclature for the masses in the Madgraph model is:

- $MZp$  - PDG ID 32 -  $Z'$
- $MA0$  - PDG ID 28 -  $A$
- $MX$  - PDG ID 1000022 - dark matter particle

The other masses are unchanged and do not affect the result. Both  $Z' \rightarrow hZ(\bar{\nu}\nu)$  and  $Z' \rightarrow hA(\tilde{\chi}\chi)$  contribute to the final state, scaling different with model parameters. We recommend to generate them separately, and then add the two signal processes together weighted by cross sections.





## Validity of EFT approach

Effective Field Theories (EFTs) are an extremely useful tool for DM searches at the LHC. Given the current lack of indications about the nature of the DM particle and its interactions, a model independent interpretation of the collider bounds appears mandatory, especially in complementarity with the reinterpretation of the exclusion limits within a choice of simplified models, which cannot exhaust the set of possible completions of an effective Lagrangian. However EFTs must be used with caution at LHC energies, where the energy scale of the interaction is at a scale where the EFT approximation can no longer be assumed to be valid. Here we summarise some methods that can be used to ensure the validity of the EFT approximation. These methods are described in detail in Refs. [BDSMR14, BDSJ<sup>+</sup>14, A<sup>+</sup>15, RWZ15].

### 6.1 Outline of the procedure described in Refs. [A<sup>+</sup>15]

For a tree-level interaction between DM and the Standard Model (SM) via some mediator with mass  $M$ , the EFT approximation corresponds to expanding the propagator in powers of  $Q_{\text{tr}}^2/M^2$ , truncating at lowest order, and combining the remaining parameters into a single parameter  $M_*$  (also called  $\Lambda$ ). For an example scenario with a  $Z'$ -type mediator (leading to some combination of operators D5 to D8 in the EFT limit) this corresponds to setting

$$\frac{g_{\text{DM}}g_q}{Q_{\text{tr}}^2 - M^2} = -\frac{g_{\text{DM}}g_q}{M^2} \left( 1 + \frac{Q_{\text{tr}}^2}{M^2} + \mathcal{O}\left(\frac{Q_{\text{tr}}^4}{M^4}\right) \right) \simeq -\frac{1}{M_*^2}, \quad (6.1)$$

where  $Q_{\text{tr}}$  is the momentum carried by the mediator, and  $g_{\text{DM}}, g_q$  are the DM-mediator and quark-mediator couplings respectively. Similar expressions exist for other operators. Clearly the condition that must be satisfied for this approximation to be valid is that  $Q_{\text{tr}}^2 < M^2 = g_{\text{DM}}g_q M_*^2$ .

We can use this condition to enforce the validity of the EFT approximation by restricting the signal (after the imposition of the cuts of the analysis) to events for which  $Q_{\text{tr}}^2 < M^2$ . This truncated signal can then be used to derive the new, truncated limit on  $M_*$  as a function of  $(m_{\text{DM}}, g_{\text{DM}}g_q)$ .

For the example D5-like operator,  $\sigma \propto M_*^{-4}$ , and so there is a simple rule for converting a rescaled cross section into a rescaled

constraint on  $M_*$  if the original limit is based on a simple cut-and-count procedure. Defining  $\sigma_{\text{EFT}}^{\text{cut}}$  as the cross section truncated such that all events pass the condition  $\sqrt{g_{\text{DM}}g_q}M_*^{\text{rescaled}} > Q_{\text{tr}}$ , we have

$$M_*^{\text{rescaled}} = \left( \frac{\sigma_{\text{EFT}}}{\sigma_{\text{EFT}}^{\text{cut}}} \right)^{1/4} M_*^{\text{original}}, \quad (6.2)$$

1107 which can be solved for  $M_*^{\text{rescaled}}$  via either iteration or a scan (note  
 1108 that  $M_*^{\text{rescaled}}$  appears on both the LHS and RHS of the equation).  
 1109 Similar relations exist for a given UV completion of each operator.  
 1110 The details and application of this procedure to ATLAS results  
 1111 can be found in Ref. [A<sup>+</sup>15] for a range of operators. Since this  
 1112 method uses the physical couplings and energy scale  $Q_{\text{tr}}$ , it gives  
 1113 the strongest possible constraints in the EFT limit while remaining  
 1114 robust by ensuring the validity of the EFT approximation.

## 6.2 Outline of the procedure described in Ref. [RWZ15]

In [RWZ15] a procedure to extract model independent and consistent bounds within the EFT is described. This procedure can be applied to any effective Lagrangian describing the interactions between the DM and the SM, and provides limits that can be directly reinterpreted in any completion of the EFT.

The range of applicability of the EFT is defined by a mass scale  $M_{\text{cut}}$ , a parameter which marks the upper limit of the range of energy scales at which the EFT can be used reliably, independently of the particular completion of the model. Regardless of the details of the full theory, the energy scale probing the validity of the EFT is less than or equal to the centre-of-mass energy  $E_{\text{cm}}$ , the total invariant mass of the hard final states of the reaction. Therefore, the condition ensuring the validity of the EFT is, by definition of  $M_{\text{cut}}$ ,

$$E_{\text{cm}} < M_{\text{cut}}. \quad (6.3)$$

For example, in the specific case of a tree level mediation with a single mediator,  $M_{\text{cut}}$  can be interpreted as the mass of that mediator.

There are then at least three free parameters describing an EFT: the DM mass  $m_{\text{DM}}$ , the scale  $M_*$  of the interaction, and the cutoff scale  $M_{\text{cut}}$ .

We can use the same technique as above to restrict the signal to the events for which  $E_{\text{cm}} < M_{\text{cut}}$ , using only these events to derive the exclusion limits on  $M_*$  as a function of  $(m_{\text{DM}}, M_{\text{cut}})$ . We can also define an *effective coupling strength*  $M_{\text{cut}} = g_* M_*$ , where  $g_*$  is a free parameter that substitutes the parameter  $M_{\text{cut}}$ , and therefore derive exclusions on  $M_*$  as a function of  $(m_{\text{DM}}, g_*)$ . This allows us to see how much of the theoretically allowed parameter space has been actually tested and how much is still unexplored; For example, in the  $Z'$ -type model considered above,  $g_*$  is equal to  $\sqrt{g_{\text{DM}} g_q}$ . The resulting plots are shown in [RWZ15] for a particular effective operator.

The advantage of this procedure is that the obtained bounds can be directly and easily recast in any completion of the EFT, by computing the parameters  $M_*$ ,  $M_{\text{cut}}$  in the full model as functions of the parameters of the complete theory. On the other hand, the resulting limits will be weaker than those obtained using  $Q_{\text{tr}}$  and a specific UV completion.

## 6.3 EFT validity recommendations

## 6.4 Recommendation for contact interaction theories with simplified models available

...to be written...

## 6.5 Recommendation for truncation of theories with no simplified models available

$M_{\text{cut}}$  is related to physical couplings and masses only in a UV complete theory, and so is effectively a free parameter. It makes sense to choose  $M_{\text{cut}}$  such that we identify the transition region where the EFT stops being a good description of UV complete theories. This can be done using  $R$ , which is defined as the fraction of events for which  $\hat{s} > M_{\text{cut}}^2$ .

For large values of  $M_{\text{cut}}$ , no events are thrown away in the truncation procedure, and  $R=1$ . As  $M_{\text{cut}}$  becomes smaller, eventually all events are thrown away in the truncation procedure, i.e.  $R=0$ , and the EFT gives no exclusion limits for the chosen acceptance.

We propose a rough scan over  $M_{\text{cut}}$ , such that we find the values of  $M_{\text{cut}}$  for which  $R$  ranges from, say, 0.1 to 1. We can then perform a scan over (several, your choice) values of  $M_{\text{cut}}$ , showing the truncated limit for each one.

When  $R=0$ , there is no limit. When  $R$  reaches 1, the truncated limit is identical to the original limit.

# A

## *Appendix: Detailed studies on mono-jet signatures*

### *A.1 CKKW parton matching implementation*

The parton matching techniques are implemented in the mono-jet like MC generation in order to avoid double counting the partons from matrix elements and parton showering. The CKKW matching is better developed and preferred [A<sup>+</sup><sub>14c</sub>] [A<sup>+</sup><sub>08</sub>]. As the illustration sample, the EFT D5 samples are generated with MadGraph5\_aMC@NLO version 2.2.2. The technical implementations are shown as below.

On the generator side, i.e., MadGraph5\_aMC@NLO:

- ickkw = 0
- ktdurham = matching scale
- dparameter = 0.4
- dokt = T
- ptj=20
- drjj=0
- mmjj=0
- ptj1min=0

On the parton showering side, i.e., Pythia 8:

- Merging:ktType = 1
- Merging:TMS = matching scale
- 1000022:all = chi chi 2 0 0 30.0 0.0 0.0 0.0 0.0
- 1000022:isVisible = false
- Merging:doKTMerging = on
- Merging:Process = pp>chi,1000022chi , -1000022
- Merging:nJetMax = 2

The matching scales should be the same for the generation and parton showering. In MadGraph5\_aMC@NLO, the particle data group ID 1000022 is used for weakly interacting dark matter candidates, which should be informed to Pythia 8.

In this test we are generating the process with up to two parton emissions, so the command `Merging:nJetMax = 2` is applied to Pythia 8. The different parton emission cases are generated separately:

- $p p \rightarrow \chi \chi$
- $p p \rightarrow \chi \chi j$
- $p p \rightarrow \chi \chi j j$

Two matching scales are tested at 30 and 80 GeV. The differential jet rates are shown in Fig. A.1 for matching scale 30 GeV and Fig. A.2 for 80 GeV. The 80 GeV matching scale gives smoother distribution, which is desired to avoid artificial effect due to parton matching. There will be a small peak around the matching scale for both cases.

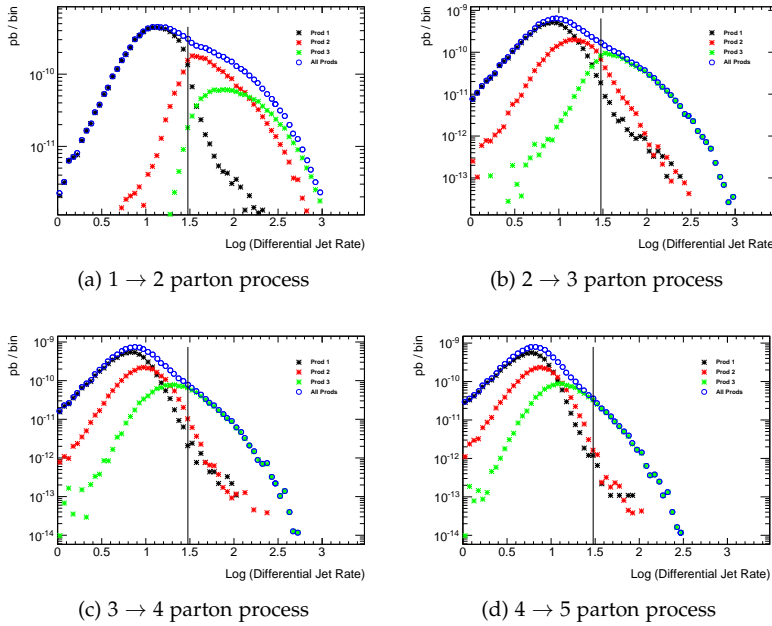


Figure A.1: Jet differential rates distributions for EFT D5 sample with CKKW matching scale at 30 GeV. 0-, 1- and 2-parton emission cases are generated separately. A vertical line is drawn at the matching scale.

To compare the effect in a finer step, the matching scales at 30, 50, 70, 80 and 90 GeV are plotted in FigA.3. Globally good agreement is seen among different matching scales, with some difference observed around the matching scale. A closer look in this range shows that the 80 and 90 GeV matching scales produce very close distributions, so it is safe to use 80 GeV as the baseline matching scale.

The MC distributions for the missing transverse energy and transverse momenta for the leading and subleading jets are plotted in Fig.. For the mono-jet analysis, usually a missing transverse energy cut larger than 300 GeV is applied for offline selection, which makes the contribution of the 0-parton emission case negligible in the mono-jet analysis.

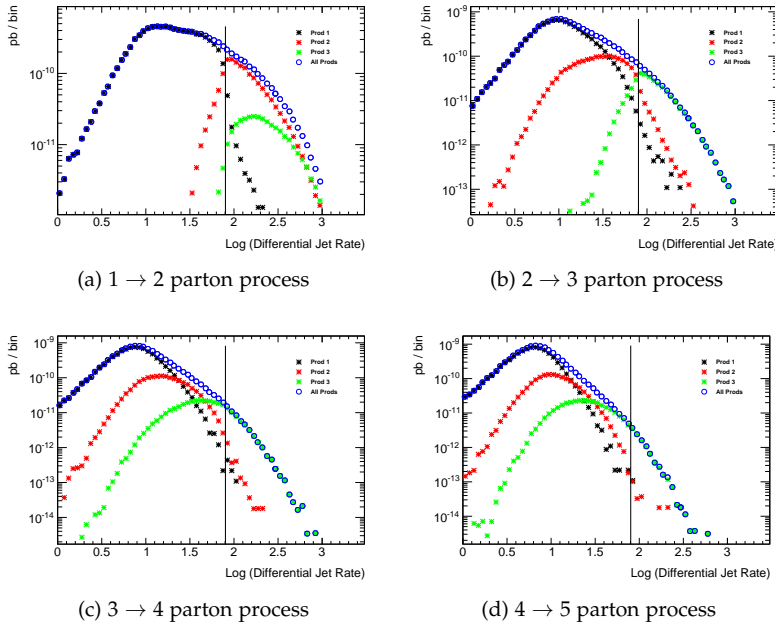


Figure A.2: Jet differential rates distributions for EFT D5 sample with CKKW matching scale at 80 GeV. 0-, 1- and 2-parton emission cases are generated separately. A vertical line is drawn at the matching scale.

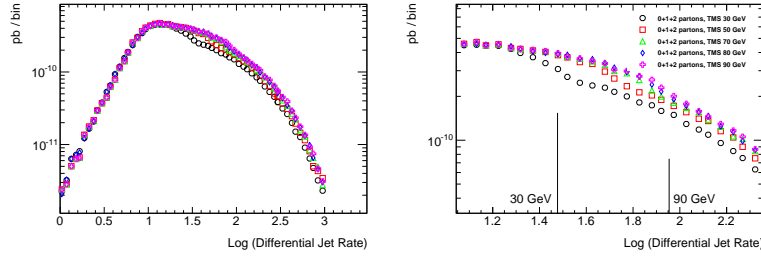
## A.2 Parton emission generation

In order to describe the signal kinematics correctly and save time in MC generation, the parton emissions will only be generated up to a certain numbers of parton and ignore the cases with more partons. The later ones usually have cross sections small enough and limited contribution in the interested kinematic regions.

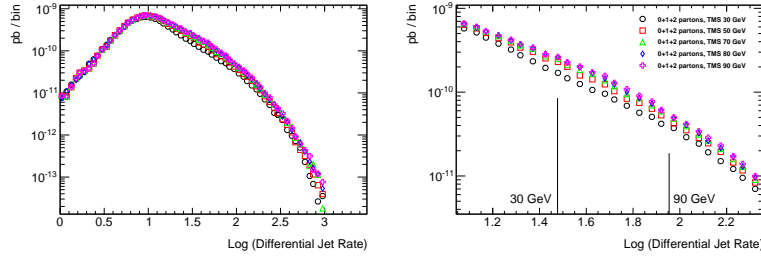
It is found that the 3- or more-parton emission cases are negligible in our interested regions, but the 2-parton emission case has significant contributions. The 0- and 1-parton emissions are out of discussion since they give the baseline signature in this analysis. The impacts of 2- and 3-parton emissions are quantified in this section.

Here the 0-, 1-, 2- and 3-parton emissions are generated separately and requested in matching step with `Merging:nJetMax=3` and scale at 80 GeV in Pythia8 for 0+1+2+3 parton emission case, while `Merging:nJetMax=2` requested for 0+1+2 case and `Merging:nJetMax=1` requested for 0+1 case. The MET distribution is plotted in Fig.A.5, while the jet multiplicity is shown in Fig.A.6.

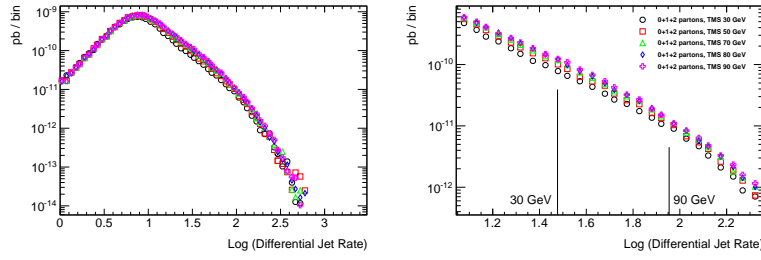
With the ATLAS run-I baseline cut (MET and leading jet  $p_T$  larger than 250 GeV, less than 4 jets), the 0+1 parton emission has 17.4% yield less compared to 0+1+2+3 parton emission, while the 0+1+2 has 2.2% less. With  $MET > 400$  GeV, 0+1 parton emission has 16.8% yield less and 0+1+2 parton emission has 2.4% less compared to 0+1+2+3 parton emission. With  $MET > 600$  GeV, 0+1 parton emission has 16.5% yield less and 0+1+2 parton emission has 2.9% less compared to 0+1+2+3 parton emission. The same numbers hold if a symmetric cut is added on leading jet transverse momentum.



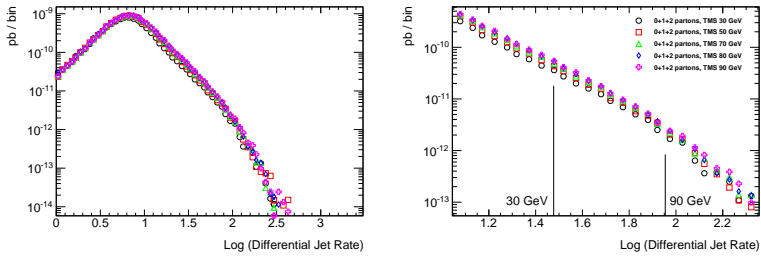
(a)  $1 \rightarrow 2$  parton process



(b)  $2 \rightarrow 3$  parton process



(c)  $3 \rightarrow 4$  parton process



(d)  $4 \rightarrow 5$  parton process

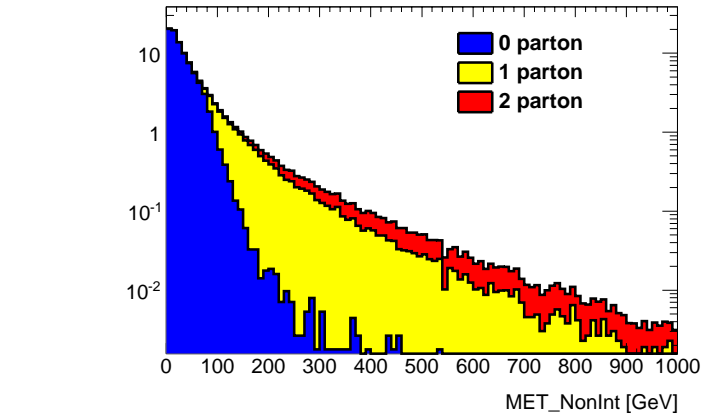


Figure A.3: Jet differential rates distributions for EFT D5 sample with CKKW matching scale at 30, 50, 70, 80 and 90 GeV. 0-, 1- and 2-parton emission cases are generated separately and the total merged contribution is shown. A closer look is shown around the matching scale.

Figure A.4: Missing transverse momentum distributions for EFT D5 sample with CKKW matching scale at 80 GeV. 0-, 1- and 2-parton emission cases are generated separately and added together by cross sections. The 0-parton emission case has very limited contribution for missing transverse energy larger than 300 GeV region.



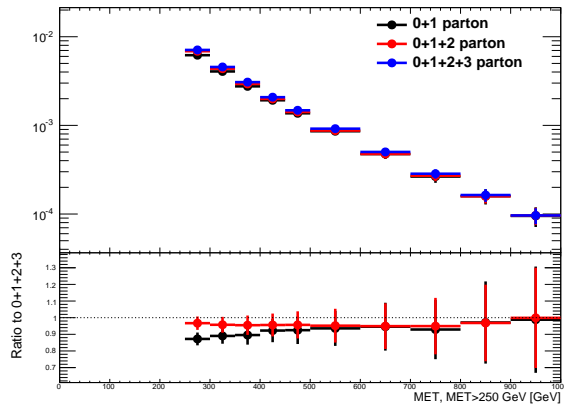


Figure A.5: Missing transverse momentum distributions for EFT D5 sample with CKKW matching scale at 80 GeV. 0-, 1-, 2- and 3-parton emission cases are generated separately and added together by cross sections.

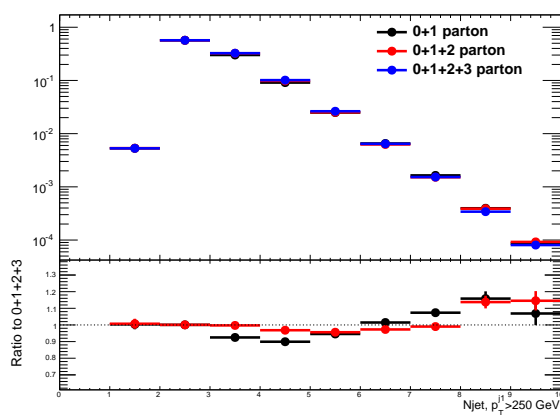


Figure A.6: Jet multiplicity distribution for EFT D5 sample with CKKW matching scale at 80 GeV. 0-, 1-, 2- and 3-parton emission cases are generated separately and added together by cross sections.



## Appendix: Detailed studies for EW models

### B.1 Further W+MET models with possible cross-section enhancements

As pointed out in Ref. [BCD<sup>+</sup>15], the mono- $W$  signature can probe the iso-spin violating interactions of dark matter with quarks. The relevant operators after the electroweak symmetry breaking is

$$\frac{1}{\Lambda^2} \bar{\chi} \gamma_\mu \chi (\bar{u}_L \gamma^\mu u_L + \xi \bar{d}_L \gamma^\mu d_L). \quad (\text{B.1})$$

Here, we only keep the left-handed quarks because the right-handed quarks do not radiate a  $W$ -gauge boson from the weak interaction. As the LHC constraints the cutoff to higher values, it is also important to know the corresponding operators before the electroweak symmetry. At the dimension-six level, the following operator

$$\frac{c_6}{\Lambda^2} \bar{\chi} \gamma_\mu \chi \bar{Q}_L \gamma^\mu Q_L \quad (\text{B.2})$$

conserves iso-spin and provides us  $\xi = 1$  [?]. At the dimension-eight level, new operators appear to induce iso-spin violation and can be

$$\frac{c_8^d}{\Lambda^4} \bar{\chi} \gamma_\mu \chi (H \bar{Q}_L) \gamma^\mu (Q_L H^\dagger) + \frac{c_8^u}{\Lambda^4} \bar{\chi} \gamma_\mu \chi (\tilde{H} \bar{Q}_L) \gamma^\mu (Q_L \tilde{H}^\dagger). \quad (\text{B.3})$$

After inputting the vacuum expectation value of the Higgs field, we have

$$\xi = \frac{c_6 + c_8^d v_{\text{EW}}^2 / 2\Lambda^2}{c_6 + c_8^u v_{\text{EW}}^2 / 2\Lambda^2}. \quad (\text{B.4})$$

For a nonzero  $c_6$  and  $v_{\text{EW}} \ll \Lambda$ , the iso-spin violation effects are suppressed. On the other hand, the values of  $c_6$ ,  $c_8^d$  and  $c_8^u$  depend on the UV-models.

There is one possible UV-model to obtain a zero value for  $c_6$  and non-zero values for  $c_8^d$  and  $c_8^u$ . One can have the dark matter and the SM Higgs field charged under a new  $U(1)'$ . There is a small mass mixing between SM  $Z$ -boson and the new  $Z'$  with a mixing angle of  $\mathcal{O}(v_{\text{EW}}^2 / M_{Z'}^2)$ . After integrating out  $Z'$ , one has different effective dark matter couplings to  $u_L$  and  $d_L$  fields, which are proportional to their couplings to the  $Z$  boson. For this model, we have  $c_6 = 0$  and

$$\xi = \frac{-\frac{1}{2} + \frac{1}{3} \sin^2 \theta_W}{\frac{1}{2} - \frac{2}{3} \sin^2 \theta_W} \approx -2.7 \quad (\text{B.5})$$

and order of unity.

## B.2 Tabulated cross-sections

### B.2.1 Higgs+MET signal, vector mediator model

Figure B.1 shows the cross sections in this vector mediator model in the  $m_{med}$  vs  $m_{DM}$  plane. The tabulated values can be found in Table B.1

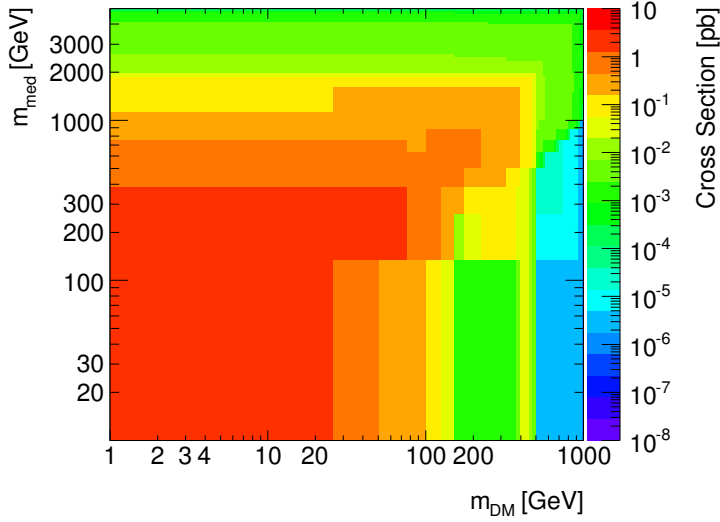


Figure B.1: Cross section of the  $pp \rightarrow H\chi\bar{\chi}$  process in units of pico-barn for the vector mediator model.

### B.2.2 Higgs+MET signal, scalar mediator model

Figure B.2 shows the cross sections of the  $pp \rightarrow H\chi\bar{\chi}$  process in this vector mediator model in the  $m_{med}$  vs  $m_{DM}$  plane. The tabulated values can be found in Table B.2

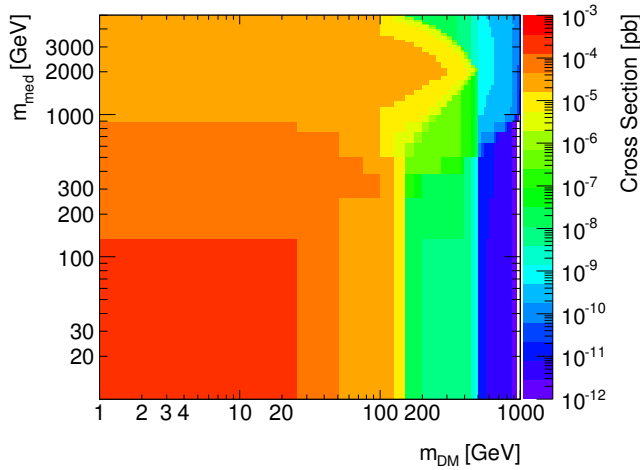


Figure B.2: Cross section of the  $pp \rightarrow H\chi\bar{\chi}$  process in units of pico-barn for the scalar mediator model.

$m_{DM}$ [GeV]	$m_{med}$ [GeV]	$\sigma_{pp \rightarrow h\chi\bar{\chi}}$ [pb]
1	10	0.0003835
1	20	0.0003177
1	50	0.0001467
1	100	0.0001065
1	200	6.867e-05
1	300	7.388e-05
1	500	7.858e-05
1	1000	4.327e-05
1	2000	4.018e-05
1	5000	3.336e-05
10	10	3.603e-06
10	15	1.477e-05
10	50	0.0001547
10	100	0.0001104
10	5000	4.5e-05
50	10	1.401e-07
50	50	2.099e-07
50	95	2.813e-05
50	200	4.82e-05
50	300	7.485e-05
50	5000	3.384e-05
150	10	4.833e-09
150	295	3.65e-08
150	500	6.463e-07
150	5000	2.407e-08
500	10	8.672e-12
500	500	1.157e-11
500	995	5.254e-10
500	2000	7.138e-10
500	5000	5.87e-10
1000	10	5.946e-14
1000	1000	1.546e-13
1000	1995	8.316e-12
1000	5000	2.112e-11

Table B.1: Cross section of the  $pp \rightarrow h\chi\bar{\chi}$  process in units of pico-barn for the vector mediator model.

$m_{DM}$ [GeV]	$m_{med}$ [GeV]	$\sigma_{pp \rightarrow h\chi\bar{\chi}}$ [pb]
1	10	2.389
1	20	2.483
1	50	2.98
1	100	2.881
1	200	2.344
1	300	2.041
1	500	0.9328
1	1000	0.1524
1	2000	0.008919
1	5000	1.39e-05
10	10	0.01895
10	15	0.7378
10	50	2.929
10	100	2.875
10	5000	1.387e-05
50	10	0.0003215
50	50	0.01127
50	95	0.2784
50	200	1.868
50	300	1.759
50	5000	1.391e-05
150	10	4.786e-06
150	200	0.004841
150	295	0.156
150	500	0.575
150	5000	1.391e-05
500	10	6.296e-09
500	500	2.855e-05
500	995	0.008244
500	2000	0.007899
500	5000	1.355e-05
1000	10	3.78e-11
1000	1000	7.372e-07
1000	1995	0.0004346
1000	5000	1.245e-05

Table B.2: Cross section of the  $pp \rightarrow h\chi\bar{\chi}$  process in units of pico-barn for the scalar mediator.

### B.2.3 Higgs+MET signal from 2HDM model with a $Z'$ and a new pseudoscalar

The leading order cross-sections from the Madgraph generator for the signal samples are listed in Tables B.3, B.4, B.5, for the various scan points recommended.

$M_{Z'}$ (GeV)	$M_{A^0}$ (GeV)	$\sigma$ [pb]
600	300	1.55E-01
600	400	2.18E-02
800	300	8.30E-02
800	400	2.72E-02
800	500	1.09E-02
800	600	2.98E-03
1000	300	3.74E-02
1000	400	1.53E-02
1000	500	8.91E-03
1000	600	4.89E-03
1000	700	2.21E-03
1000	800	7.05E-04
1200	300	1.70E-02
1200	400	7.65E-03
1200	500	5.14E-03
1200	600	3.52E-03
1200	700	2.25E-03
1200	800	1.27E-03
1400	300	8.00E-03
1400	400	3.79E-03
1400	500	2.75E-03
1400	600	2.09E-03
1400	700	1.58E-03
1400	800	1.06E-03

Table B.3: LO cross-sections for  $Z' \rightarrow A^0 h$  samples, varying  $M_{Z'}$  and  $M_{A^0}$ , keeping the DM mass fixed to 100 GeV. The columns from left to right describe  $M_{Z'}$ ,  $M_{A^0}$  and the sample cross section in pb.

$M_{Z'}$ (GeV)	$M_{A^0}$ (GeV)	$M_{DM}$ (GeV)	$\sigma$ [pb]
1000	300	10	3.76E-02
1000	300	50	3.75E-02
1200	600	10	3.64E-03
1200	600	20	3.07E-03

Table B.4: LO cross-sections for  $Z' \rightarrow A^0 h$  samples, when varying  $M_{DM}$ . The columns from left to right describe  $M_{Z'}$ ,  $M_{A^0}$ ,  $M_{DM}$ , and the sample cross section in pb.

$M_{Z'}$ (GeV)	$\sigma$ [pb]
600	1.15E-01
800	3.21E-02
1000	1.13E-02
1200	4.54E-03
1400	2.00E-03

Table B.5: LO cross-sections for  $Z' \rightarrow Zh$  exclusive samples, varying  $M_{Z'}$ . The columns from left to right describe  $M_{Z'}$  and the sample cross section in pb.





# Appendix: Table of cross sections for $t\bar{t}$ +MET searches

All tables need to be adjusted with right number of significant digits

Coupling (g)	$m_{\phi}$ [GeV]	$m_{\chi}$ [GeV]	$\Gamma_{min}$ [GeV]	$\sigma$
0.1	10	1	0.00374318	$0.207 \pm 0.0006846$
0.1	20	1	0.00784569	$0.1121 \pm 0.0003285$
0.1	50	1	0.01987	$0.03211 \pm 0.0001005$
0.1	100	1	0.0398141	$0.007325 \pm 2.416e-05$
0.1	150	1	0.0597437	$0.002396 \pm 7.419e-06$
0.1	200	1	0.0796724	$0.001018 \pm 3.398e-06$
0.1	300	1	0.119549	$0.0003394 \pm 1.234e-06$
0.1	500	1	0.310863	$6.802e-05 \pm 2.343e-07$
0.1	1000	1	0.881329	$5.817e-06 \pm 2.356e-08$
0.1	1500	1	1.40417	$8.942e-07 \pm 3.832e-09$
0.1	10	10	0.000100	$1.007e-05 \pm 3.761e-08$
0.1	20	10	0.000100	$3.491e-05 \pm 1.012e-07$
0.1	50	10	0.0153395	$0.03212 \pm 0.0001037$
0.1	100	10	0.0374747	$0.007343 \pm 2.011e-05$
0.1	150	10	0.0581752	$0.002389 \pm 7.654e-06$
0.1	200	10	0.0784937	$0.001018 \pm 6.258e-06$
0.1	300	10	0.118762	$0.0003373 \pm 1.448e-06$
0.1	500	10	0.310391	$6.773e-05 \pm 2.326e-07$
0.1	1000	10	0.881093	$5.81e-06 \pm 2.245e-08$
0.1	1500	10	1.40401	$8.937e-07 \pm 4.013e-09$
0.1	50	50	0.0000233555	$2.581e-07 \pm 1.214e-09$
0.1	100	50	0.0000492402	$1.526e-06 \pm 7.038e-09$
0.1	150	50	0.0247905	$0.002387 \pm 8.272e-06$
0.1	200	50	0.051794	$0.00102 \pm 3.216e-06$
0.1	300	50	0.100226	$0.0003366 \pm 1.393e-06$
0.1	500	50	0.299052	$6.679e-05 \pm 2.406e-07$
0.1	1000	50	0.875378	$5.764e-06 \pm 2.472e-08$
0.1	1500	50	1.4002	$8.866e-07 \pm 3.257e-09$
0.1	100	150	0.0000492402	$1.246e-08 \pm 5.121e-11$
0.1	150	150	0.0000765167	$1.393e-08 \pm 6.653e-11$
0.1	200	150	0.000106902	$1.693e-08 \pm 8.493e-11$
0.1	300	150	0.000190543	$7.557e-08 \pm 2.171e-10$

Continued on next page

Table C.1 – continued from previous page

Coupling (g)	$m_{\text{Phi}}$ [GeV]	$m_{\chi}$ [GeV]	$\Gamma_{\text{min}}$ [GeV]	$\sigma$
0.1	500	150	0.213784	$5.063\text{e-}05 \pm 1.724\text{e-}07$
0.1	1000	150	0.828844	$5.365\text{e-}06 \pm 2.028\text{e-}08$
0.1	1500	150	1.36872	$8.603\text{e-}07 \pm 3.769\text{e-}09$
0.1	200	300	0.000106902	$1.415\text{e-}09 \pm 5.97\text{e-}12$
0.1	300	300	0.000190543	$1.64\text{e-}09 \pm 7.878\text{e-}12$
0.1	500	300	0.111924	$3.078\text{e-}09 \pm 1.482\text{e-}11$
0.1	1000	300	0.687162	$3.828\text{e-}06 \pm 1.416\text{e-}08$
0.1	1500	300	1.26683	$7.579\text{e-}07 \pm 3.041\text{e-}09$
0.1	500	500	0.111924	$1.784\text{e-}10 \pm 1.105\text{e-}12$
0.1	1000	500	0.483444	$1.98\text{e-}09 \pm 9.199\text{e-}12$
0.1	1500	500	1.05448	$4.92\text{e-}07 \pm 2.14\text{e-}09$
0.3	10	1	0.0336886	$1.876 \pm 0.006611$
0.3	20	1	0.0706112	$1.006 \pm 0.003894$
0.3	50	1	0.17883	$0.2886 \pm 0.0009285$
0.3	100	1	0.358327	$0.06598 \pm 0.000182$
0.3	150	1	0.537693	$0.0214 \pm 6.701\text{e-}05$
0.3	200	1	0.717052	$0.009216 \pm 3.533\text{e-}05$
0.3	300	1	1.07594	$0.003044 \pm 1.194\text{e-}05$
0.3	500	1	2.79777	$0.0006105 \pm 2.187\text{e-}06$
0.3	1000	1	7.93196	$5.256\text{e-}05 \pm 2.165\text{e-}07$
0.3	1500	1	12.6376	$8.048\text{e-}06 \pm 3.473\text{e-}08$
0.3	10	10	5.69808	$0.0008143 \pm 3.272\text{e-}06$
0.3	20	10	0.0000630938	$0.002836 \pm 9.724\text{e-}06$
0.3	50	10	0.138055	$0.2869 \pm 0.0008971$
0.3	100	10	0.337272	$0.06606 \pm 0.0002407$
0.3	150	10	0.523576	$0.02145 \pm 8.01\text{e-}05$
0.3	200	10	0.706443	$0.009222 \pm 2.807\text{e-}05$
0.3	300	10	1.06886	$0.003051 \pm 1.001\text{e-}05$
0.3	500	10	2.79352	$0.0006115 \pm 2.268\text{e-}06$
0.3	1000	10	7.92983	$5.24\text{e-}05 \pm 1.964\text{e-}07$
0.3	1500	10	12.6361	$8.053\text{e-}06 \pm 3.203\text{e-}08$
0.3	10	50	5.69808	$1.704\text{e-}05 \pm 7.077\text{e-}08$
0.3	20	50	0.0000630938	$1.746\text{e-}05 \pm 7.383\text{e-}08$
0.3	50	50	0.000210199	$2.071\text{e-}05 \pm 8.162\text{e-}08$
0.3	100	50	0.000443162	$0.0001245 \pm 3.888\text{e-}07$
0.3	150	50	0.223114	$0.02138 \pm 6.22\text{e-}05$
0.3	200	50	0.466146	$0.009186 \pm 3.168\text{e-}05$
0.3	300	50	0.902031	$0.003039 \pm 1.09\text{e-}05$
0.3	500	50	2.69146	$0.0005971 \pm 2.181\text{e-}06$
0.3	1000	50	7.8784	$5.222\text{e-}05 \pm 1.907\text{e-}07$
0.3	1500	50	12.6018	$7.947\text{e-}06 \pm 2.996\text{e-}08$
0.3	100	150	0.000443162	$1.004\text{e-}06 \pm 4.682\text{e-}09$
0.3	150	150	0.00068865	$1.132\text{e-}06 \pm 4.644\text{e-}09$
0.3	200	150	0.000962116	$1.349\text{e-}06 \pm 6.834\text{e-}09$
0.3	300	150	0.00171489	$6.08\text{e-}06 \pm 2.289\text{e-}08$

Continued on next page

Table C.1 – continued from previous page

Coupling (g)	$m_{\Phi}$ [GeV]	$m_{\chi}$ [GeV]	$\Gamma_{min}$ [GeV]	$\sigma$
0.3	500	150	1.92405	$0.000456 \pm 2.064e-06$
0.3	1000	150	7.45959	$4.818e-05 \pm 1.84e-07$
0.3	1500	150	12.3185	$7.796e-06 \pm 2.802e-08$
0.3	200	300	0.000962116	$1.144e-07 \pm 4.635e-10$
0.3	300	300	0.00171489	$1.324e-07 \pm 6.534e-10$
0.3	500	300	1.00732	$2.5e-07 \pm 1.113e-09$
0.3	1000	300	6.18446	$3.439e-05 \pm 1.376e-07$
0.3	1500	300	11.4014	$6.834e-06 \pm 2.623e-08$
0.3	500	500	1.00732	$1.449e-08 \pm 5.536e-11$
0.3	1000	500	4.35099	$1.487e-07 \pm 6.617e-10$
0.3	1500	500	9.49035	$4.374e-06 \pm 1.739e-08$
0.7	10	1	0.183416	$10.2 \pm 0.03649$
0.7	20	1	0.384439	$5.462 \pm 0.02022$
0.7	50	1	0.97363	$1.558 \pm 0.004491$
0.7	100	1	1.95089	$0.3568 \pm 0.001143$
0.7	150	1	2.92744	$0.1161 \pm 0.0003685$
0.7	200	1	3.90395	$0.04995 \pm 0.0001494$
0.7	300	1	5.85789	$0.01649 \pm 5.579e-05$
0.7	500	1	15.2323	$0.003313 \pm 1.464e-05$
0.7	1000	1	43.1851	$0.0002823 \pm 1.233e-06$
0.7	1500	1	68.8045	$4.481e-05 \pm 1.885e-07$
0.7	10	10	0.0000310229	$0.02403 \pm 0.0001038$
0.7	20	10	0.000343511	$0.08347 \pm 0.0004742$
0.7	50	10	0.751635	$1.553 \pm 0.004764$
0.7	100	10	1.83626	$0.3569 \pm 0.0009501$
0.7	150	10	2.85058	$0.1165 \pm 0.0004139$
0.7	200	10	3.84619	$0.04984 \pm 0.0001855$
0.7	300	10	5.81933	$0.01649 \pm 6.843e-05$
0.7	500	10	15.2092	$0.003301 \pm 1.289e-05$
0.7	1000	10	43.1735	$0.0002815 \pm 1.129e-06$
0.7	1500	10	68.7967	$4.491e-05 \pm 2.108e-07$
0.7	10	50	0.0000310229	$0.000511 \pm 1.977e-06$
0.7	20	50	0.000343511	$0.0005184 \pm 2.146e-06$
0.7	50	50	0.00114442	$0.0006176 \pm 3.053e-06$
0.7	100	50	0.00241277	$0.003681 \pm 1.333e-05$
0.7	150	50	1.21473	$0.1156 \pm 0.0003755$
0.7	200	50	2.53791	$0.04988 \pm 0.0001824$
0.7	300	50	4.91106	$0.01651 \pm 6.317e-05$
0.7	500	50	14.6535	$0.003218 \pm 1.523e-05$
0.7	1000	50	42.8935	$0.0002794 \pm 1.049e-06$
0.7	1500	50	68.6098	$4.46e-05 \pm 1.989e-07$
0.7	100	150	0.00241277	$2.968e-05 \pm 1.364e-07$
0.7	150	150	0.00374932	$3.327e-05 \pm 1.594e-07$
0.7	200	150	0.00523819	$4.04e-05 \pm 1.861e-07$
0.7	300	150	0.00933663	$0.0001787 \pm 7.694e-07$

Continued on next page

Table C.1 – continued from previous page

Coupling (g)	$m_{\Phi}$ [GeV]	$m_{\chi}$ [GeV]	$\Gamma_{min}$ [GeV]	$\sigma$
0.7	500	150	10.4754	$0.00243 \pm 1.128\text{e-}05$
0.7	1000	150	40.6133	$0.0002573 \pm 1.014\text{e-}06$
0.7	1500	150	67.0675	$4.239\text{e-}05 \pm 1.707\text{e-}07$
0.7	100	300	0.00241277	$3.132\text{e-}06 \pm 1.547\text{e-}08$
0.7	150	300	0.00374932	$3.227\text{e-}06 \pm 1.433\text{e-}08$
0.7	200	300	0.00523819	$3.393\text{e-}06 \pm 1.437\text{e-}08$
0.7	300	300	0.00933663	$3.918\text{e-}06 \pm 1.628\text{e-}08$
0.7	500	300	5.4843	$7.383\text{e-}06 \pm 2.87\text{e-}08$
0.7	1000	300	33.6709	$0.0001801 \pm 7.992\text{e-}07$
0.7	1500	300	62.0745	$3.644\text{e-}05 \pm 1.473\text{e-}07$
0.7	500	500	5.4843	$4.301\text{e-}07 \pm 1.836\text{e-}09$
0.7	1000	500	23.6887	$3.684\text{e-}06 \pm 2.358\text{e-}08$
0.7	1500	500	51.6697	$2.291\text{e-}05 \pm 9.843\text{e-}08$
1.	10	1	0.374318	$20.79 \pm 0.08102$
1.	20	1	0.784569	$11.08 \pm 0.0396$
1.	50	1	1.987	$3.146 \pm 0.01331$
1.	100	1	3.98141	$0.7199 \pm 0.002775$
1.	150	1	5.97437	$0.2354 \pm 0.0008189$
1.	200	1	7.96724	$0.1009 \pm 0.0003854$
1.	300	1	11.9549	$0.03369 \pm 0.0001155$
1.	500	1	31.0863	$0.006652 \pm 2.898\text{e-}05$
1.	1000	1	88.1329	$0.0005705 \pm 2.817\text{e-}06$
1.	1500	1	140.417	$9.244\text{e-}05 \pm 4.273\text{e-}07$
1.	10	10	0.000063312	$0.1009 \pm 0.00035$
1.	20	10	0.000701043	$0.3475 \pm 0.002265$
1.	50	10	1.53395	$3.139 \pm 0.01028$
1.	100	10	3.74747	$0.7158 \pm 0.002486$
1.	150	10	5.81752	$0.236 \pm 0.0007591$
1.	200	10	7.84937	$0.1013 \pm 0.0003668$
1.	300	10	11.8762	$0.03374 \pm 0.0001403$
1.	500	10	31.0391	$0.006631 \pm 2.585\text{e-}05$
1.	1000	10	88.1093	$0.0005663 \pm 2.515\text{e-}06$
1.	1500	10	140.401	$9.408\text{e-}05 \pm 4.698\text{e-}07$
1.	10	50	0.000063312	$0.00212 \pm 8.815\text{e-}06$
1.	20	50	0.000701043	$0.002149 \pm 9.604\text{e-}06$
1.	50	50	0.00233555	$0.002568 \pm 1.017\text{e-}05$
1.	100	50	0.00492402	$0.01523 \pm 5.043\text{e-}05$
1.	150	50	2.47905	$0.2351 \pm 0.0008404$
1.	200	50	5.1794	$0.09993 \pm 0.0003164$
1.	300	50	10.0226	$0.03349 \pm 0.0001351$
1.	500	50	29.9052	$0.006402 \pm 2.604\text{e-}05$
1.	1000	50	87.5378	$0.0005634 \pm 2.601\text{e-}06$
1.	1500	50	140.02	$9.211\text{e-}05 \pm 4.909\text{e-}07$
1.	100	150	0.00492402	$0.0001247 \pm 5.899\text{e-}07$
1.	150	150	0.00765167	$0.0001387 \pm 5.889\text{e-}07$

Continued on next page

Table C.1 – continued from previous page

Coupling (g)	$m_{Phi}$ [GeV]	$m_\chi$ [GeV]	$\Gamma_{min}$ [GeV]	$\sigma$
1.	200	150	0.0106902	$0.000168 \pm 7.656e-07$
1.	300	150	0.0190543	$0.0007464 \pm 2.977e-06$
1.	500	150	21.3784	$0.004856 \pm 1.95e-05$
1.	1000	150	82.8844	$0.0005122 \pm 1.98e-06$
1.	1500	150	136.872	$8.662e-05 \pm 3.821e-07$
1.	200	300	0.0106902	$1.422e-05 \pm 6.147e-08$
1.	300	300	0.0190543	$1.626e-05 \pm 6.865e-08$
1.	500	300	11.1924	$3.081e-05 \pm 1.244e-07$
1.	1000	300	68.7162	$0.0003534 \pm 1.392e-06$
1.	1500	300	126.683	$7.258e-05 \pm 3.651e-07$
1.	500	500	11.1924	$1.777e-06 \pm 9.67e-09$
1.	1000	500	48.3444	$1.331e-05 \pm 6.551e-08$
1.	1500	500	105.448	$4.443e-05 \pm 1.988e-07$
1.5	10	1	0.842215	$46.59 \pm 0.1797$
1.5	20	1	1.76528	$24.52 \pm 0.08387$
1.5	50	1	4.47075	$6.903 \pm 0.02244$
1.5	100	1	8.95817	$1.577 \pm 0.005493$
1.5	150	1	13.4423	$0.5224 \pm 0.002309$
1.5	200	1	17.9263	$0.2259 \pm 0.0008625$
1.5	300	1	26.8985	$0.07529 \pm 0.0003407$
1.5	500	1	69.9442	$0.01445 \pm 6.469e-05$
1.5	1000	1	198.299	$0.001234 \pm 5.694e-06$
1.5	1500	1	315.939	$0.0002179 \pm 1.024e-06$
1.5	10	10	0.000142452	$0.5117 \pm 0.002037$
1.5	20	10	0.00157735	$1.763 \pm 0.01031$
1.5	50	10	3.45138	$6.906 \pm 0.02283$
1.5	100	10	8.4318	$1.568 \pm 0.006489$
1.5	150	10	13.0894	$0.5162 \pm 0.001934$
1.5	200	10	17.6611	$0.2249 \pm 0.0008153$
1.5	300	10	26.7214	$0.07541 \pm 0.0002941$
1.5	500	10	69.8379	$0.01447 \pm 6.923e-05$
1.5	1000	10	198.246	$0.001242 \pm 6.739e-06$
1.5	1500	10	315.903	$0.0002157 \pm 8.805e-07$
1.5	10	50	0.000142452	$0.01068 \pm 4.527e-05$
1.5	20	50	0.00157735	$0.01093 \pm 6.079e-05$
1.5	50	50	0.00525498	$0.01302 \pm 6.649e-05$
1.5	100	50	0.011079	$0.07677 \pm 0.0002445$
1.5	150	50	5.57786	$0.5195 \pm 0.001577$
1.5	200	50	11.6536	$0.2195 \pm 0.0006711$
1.5	300	50	22.5508	$0.07353 \pm 0.0003291$
1.5	500	50	67.2866	$0.0139 \pm 6.13e-05$
1.5	1000	50	196.96	$0.001209 \pm 7.038e-06$
1.5	1500	50	315.045	$0.0002109 \pm 8.631e-07$
1.5	100	150	0.011079	$0.0006295 \pm 3.008e-06$
1.5	150	150	0.0172162	$0.000706 \pm 3.661e-06$

Continued on next page

Table C.1 – continued from previous page

Coupling (g)	$m_{\Phi}$ [GeV]	$m_{\chi}$ [GeV]	$\Gamma_{min}$ [GeV]	$\sigma$
1.5	200	150	0.0240529	$0.00086 \pm 3.608\text{e-}06$
1.5	300	150	0.0428723	$0.003751 \pm 1.304\text{e-}05$
1.5	500	150	48.1013	$0.01046 \pm 4.013\text{e-}05$
1.5	1000	150	186.49	$0.001072 \pm 4.469\text{e-}06$
1.5	1500	150	307.963	$0.0001931 \pm 1.022\text{e-}06$
1.5	200	300	0.0240529	$7.176\text{e-}05 \pm 3.641\text{e-}07$
1.5	300	300	0.0428723	$8.3\text{e-}05 \pm 3.627\text{e-}07$
1.5	500	300	25.183	$0.000155 \pm 6.658\text{e-}07$
1.5	1000	300	154.611	$0.0007234 \pm 2.773\text{e-}06$
1.5	1500	300	285.036	$0.0001529 \pm 7.694\text{e-}07$
1.5	500	500	25.183	$9.099\text{e-}06 \pm 4.301\text{e-}08$
1.5	1000	500	108.775	$5.335\text{e-}05 \pm 2.699\text{e-}07$
1.5	1500	500	237.259	$8.736\text{e-}05 \pm 4.268\text{e-}07$
2.	10	1	1.49727	$82.65 \pm 0.3408$
2.	20	1	3.13828	$43.1 \pm 0.1487$
2.	50	1	7.948	$11.84 \pm 0.04278$
2.	100	1	15.9256	$2.712 \pm 0.01209$
2.	150	1	23.8975	$0.9056 \pm 0.004237$
2.	200	1	31.869	$0.3952 \pm 0.001653$
2.	300	1	47.8195	$0.132 \pm 0.0004713$
2.	500	1	124.345	$0.02461 \pm 0.0001101$
2.	1000	1	352.532	$0.002071 \pm 1.061\text{e-}05$
2.	1500	1	561.669	$0.0003815 \pm 1.4\text{e-}06$
2.	10	10	0.000253248	$1.627 \pm 0.005672$
2.	20	10	0.00280417	$5.528 \pm 0.03152$
2.	50	10	6.13579	$11.98 \pm 0.04005$
2.	100	10	14.9899	$2.696 \pm 0.01091$
2.	150	10	23.2701	$0.8981 \pm 0.004067$
2.	200	10	31.3975	$0.3921 \pm 0.001675$
2.	300	10	47.5047	$0.1312 \pm 0.0005524$
2.	500	10	124.156	$0.02454 \pm 0.0001302$
2.	1000	10	352.437	$0.002051 \pm 9.73\text{e-}06$
2.	1500	10	561.606	$0.0003797 \pm 1.522\text{e-}06$
2.	10	50	0.000253248	$0.03397 \pm 0.0001354$
2.	20	50	0.00280417	$0.03452 \pm 0.0001623$
2.	50	50	0.00934219	$0.04088 \pm 0.0001623$
2.	100	50	0.0196961	$0.24 \pm 0.0008579$
2.	150	50	9.9162	$0.8991 \pm 0.002903$
2.	200	50	20.7176	$0.382 \pm 0.001411$
2.	300	50	40.0903	$0.1287 \pm 0.0005596$
2.	500	50	119.621	$0.02328 \pm 0.0001255$
2.	1000	50	350.151	$0.001995 \pm 1.184\text{e-}05$
2.	1500	50	560.08	$0.0003671 \pm 1.741\text{e-}06$
2.	10	150	0.000253248	$0.001822 \pm 7.946\text{e-}06$
2.	20	150	0.00280417	$0.001842 \pm 8.453\text{e-}06$

Continued on next page

Table C.1 – continued from previous page

Coupling (g)	$m_{\Phi}$ [GeV]	$m_{\chi}$ [GeV]	$\Gamma_{min}$ [GeV]	$\sigma$
2.	50	150	0.00934219	$0.00187 \pm 8.818\text{e-}06$
2.	100	150	0.0196961	$0.001985 \pm 8.101\text{e-}06$
2.	150	150	0.0306067	$0.002231 \pm 1.131\text{e-}05$
2.	200	150	0.0427607	$0.002694 \pm 1.215\text{e-}05$
2.	300	150	0.0762174	$0.01186 \pm 4.862\text{e-}05$
2.	500	150	85.5134	$0.01769 \pm 8.02\text{e-}05$
2.	1000	150	331.538	$0.001716 \pm 7.617\text{e-}06$
2.	1500	150	547.49	$0.0003242 \pm 1.537\text{e-}06$
2.	100	300	0.0196961	$0.0002092 \pm 8.197\text{e-}07$
2.	150	300	0.0306067	$0.0002152 \pm 8.37\text{e-}07$
2.	200	300	0.0427607	$0.0002275 \pm 8.607\text{e-}07$
2.	300	300	0.0762174	$0.0002609 \pm 1.05\text{e-}06$
2.	500	300	44.7698	$0.0004931 \pm 2.01\text{e-}06$
2.	1000	300	274.865	$0.001119 \pm 5.167\text{e-}06$
2.	1500	300	506.731	$0.0002432 \pm 1.053\text{e-}06$
2.	300	500	0.0762174	$2.367\text{e-}05 \pm 1.206\text{e-}07$
2.	500	500	44.7698	$2.871\text{e-}05 \pm 1.09\text{e-}07$
2.	1000	500	193.378	$0.000131 \pm 5.569\text{e-}07$
2.	1500	500	421.793	$0.0001323 \pm 5.222\text{e-}07$
2.5	10	1	2.33949	$128.4 \pm 0.4393$
2.5	20	1	4.90356	$65.92 \pm 0.2248$
2.5	50	1	12.4187	$17.77 \pm 0.0663$
2.5	100	1	24.8838	$4.051 \pm 0.01562$
2.5	150	1	37.3398	$1.364 \pm 0.004927$
2.5	200	1	49.7953	$0.6008 \pm 0.002928$
2.5	300	1	74.718	$0.2036 \pm 0.0008994$
2.5	500	1	194.29	$0.03629 \pm 0.0001865$
2.5	1000	1	550.831	$0.002918 \pm 1.235\text{e-}05$
2.5	1500	1	877.608	$0.0005639 \pm 2.327\text{e-}06$
2.5	10	10	0.0003957	$3.918 \pm 0.0159$
2.5	20	10	0.00438152	$13.54 \pm 0.05349$
2.5	50	10	9.58718	$18.03 \pm 0.06068$
2.5	100	10	23.4217	$4.025 \pm 0.01458$
2.5	150	10	36.3595	$1.36 \pm 0.00698$
2.5	200	10	49.0586	$0.5979 \pm 0.002445$
2.5	300	10	74.2262	$0.2016 \pm 0.0006995$
2.5	500	10	193.994	$0.03579 \pm 0.0001738$
2.5	1000	10	550.683	$0.002902 \pm 1.515\text{e-}05$
2.5	1500	10	877.509	$0.0005651 \pm 2.275\text{e-}06$
2.5	10	50	0.0003957	$0.08298 \pm 0.000365$
2.5	20	50	0.00438152	$0.08474 \pm 0.0003631$
2.5	50	50	0.0145972	$0.09986 \pm 0.000455$
2.5	100	50	0.0307751	$0.5855 \pm 0.001667$
2.5	150	50	15.4941	$1.359 \pm 0.005802$
2.5	200	50	32.3712	$0.5728 \pm 0.002188$

Continued on next page

Table C.1 – continued from previous page

Coupling (g)	$m_{\text{Phi}}$ [GeV]	$m_\chi$ [GeV]	$\Gamma_{\text{min}}$ [GeV]	$\sigma$
2.5	300	50	62.6411	$0.1938 \pm 0.0008665$
2.5	500	50	186.907	$0.03384 \pm 0.0001589$
2.5	1000	50	547.111	$0.002773 \pm 1.645\text{e-}05$
2.5	1500	50	875.125	$0.0005349 \pm 3.534\text{e-}06$
2.5	10	150	0.0003957	$0.004461 \pm 1.951\text{e-}05$
2.5	20	150	0.00438152	$0.004473 \pm 2.159\text{e-}05$
2.5	50	150	0.0145972	$0.00451 \pm 1.808\text{e-}05$
2.5	100	150	0.0307751	$0.00486 \pm 1.984\text{e-}05$
2.5	150	150	0.0478229	$0.00548 \pm 2.35\text{e-}05$
2.5	200	150	0.0668136	$0.006545 \pm 2.81\text{e-}05$
2.5	300	150	0.11909	$0.02878 \pm 0.0001168$
2.5	500	150	133.615	$0.02572 \pm 0.00011$
2.5	1000	150	518.027	$0.002339 \pm 1.101\text{e-}05$
2.5	1500	150	855.453	$0.0004622 \pm 2.297\text{e-}06$
2.5	100	300	0.0307751	$0.0005104 \pm 2.62\text{e-}06$
2.5	150	300	0.0478229	$0.000526 \pm 2.091\text{e-}06$
2.5	200	300	0.0668136	$0.0005503 \pm 2.402\text{e-}06$
2.5	300	300	0.11909	$0.0006368 \pm 2.911\text{e-}06$
2.5	500	300	69.9528	$0.001197 \pm 4.697\text{e-}06$
2.5	1000	300	429.476	$0.001499 \pm 6.445\text{e-}06$
2.5	1500	300	791.767	$0.0003277 \pm 1.439\text{e-}06$
2.5	300	500	0.11909	$5.773\text{e-}05 \pm 2.645\text{e-}07$
2.5	500	500	69.9528	$6.973\text{e-}05 \pm 3.037\text{e-}07$
2.5	1000	500	302.152	$0.0002498 \pm 1.042\text{e-}06$
2.5	1500	500	659.052	$0.000172 \pm 8.531\text{e-}07$
3.	10	1	3.36886	$185.9 \pm 0.8608$
3.	20	1	7.06112	$92.49 \pm 0.3581$
3.	50	1	17.883	$24.38 \pm 0.08507$
3.	100	1	35.8327	$5.551 \pm 0.02275$
3.	150	1	53.7693	$1.878 \pm 0.008801$
3.	200	1	71.7052	$0.8398 \pm 0.004651$
3.	300	1	107.594	$0.2856 \pm 0.001301$
3.	500	1	279.777	$0.04861 \pm 0.0002143$
3.	1000	1	793.196	$0.003716 \pm 1.874\text{e-}05$
3.	1500	1	1263.76	$0.0007294 \pm 3.217\text{e-}06$
3.	10	10	0.000569808	$8.181 \pm 0.03184$
3.	20	10	0.00630938	$28.05 \pm 0.09412$
3.	50	10	13.8055	$24.97 \pm 0.07128$
3.	100	10	33.7272	$5.485 \pm 0.01916$
3.	150	10	52.3576	$1.858 \pm 0.007406$
3.	200	10	70.6443	$0.8336 \pm 0.003435$
3.	300	10	106.886	$0.2832 \pm 0.001293$
3.	500	10	279.352	$0.04802 \pm 0.0003129$
3.	1000	10	792.983	$0.003669 \pm 1.542\text{e-}05$
3.	1500	10	1263.61	$0.0007221 \pm 3.036\text{e-}06$

Continued on next page



Table C.1 – continued from previous page

Coupling (g)	$m_{Phi}$ [GeV]	$m_\chi$ [GeV]	$\Gamma_{min}$ [GeV]	$\sigma$
3.	10	50	0.000569808	$0.1714 \pm 0.0007653$
3.	20	50	0.00630938	$0.1751 \pm 0.000689$
3.	50	50	0.0210199	$0.2073 \pm 0.001019$
3.	100	50	0.0443162	$1.21 \pm 0.003153$
3.	150	50	22.3114	$1.896 \pm 0.007571$
3.	200	50	46.6146	$0.787 \pm 0.002939$
3.	300	50	90.2031	$0.2685 \pm 0.001344$
3.	500	50	269.146	$0.04468 \pm 0.0002221$
3.	1000	50	787.84	$0.003505 \pm 1.861e-05$
3.	1500	50	1260.18	$0.0006823 \pm 3.857e-06$
3.	10	150	0.000569808	$0.009285 \pm 4.234e-05$
3.	20	150	0.00630938	$0.00924 \pm 4.234e-05$
3.	50	150	0.0210199	$0.009462 \pm 3.85e-05$
3.	100	150	0.0443162	$0.01017 \pm 4.443e-05$
3.	150	150	0.068865	$0.01124 \pm 5.221e-05$
3.	200	150	0.0962116	$0.01366 \pm 6.834e-05$
3.	300	150	0.171489	$0.05937 \pm 0.0002495$
3.	500	150	192.405	$0.03448 \pm 0.0001467$
3.	1000	150	745.959	$0.00288 \pm 1.359e-05$
3.	1500	150	1231.85	$0.0005735 \pm 3.925e-06$
3.	50	300	0.0210199	$0.001039 \pm 3.982e-06$
3.	100	300	0.0443162	$0.001056 \pm 4.834e-06$
3.	150	300	0.068865	$0.001096 \pm 4.922e-06$
3.	200	300	0.0962116	$0.001147 \pm 5.869e-06$
3.	300	300	0.171489	$0.001327 \pm 6.728e-06$
3.	500	300	100.732	$0.00245 \pm 9.636e-06$
3.	1000	300	618.446	$0.001853 \pm 7.863e-06$
3.	1500	300	1140.14	$0.0003934 \pm 2.083e-06$
3.	150	500	0.068865	$0.0001123 \pm 4.327e-07$
3.	200	500	0.0962116	$0.000114 \pm 5.127e-07$
3.	300	500	0.171489	$0.0001206 \pm 5.124e-07$
3.	500	500	100.732	$0.0001447 \pm 6.102e-07$
3.	1000	500	435.099	$0.0004016 \pm 1.656e-06$
3.	1500	500	949.035	$0.0002061 \pm 8.548e-07$
3.5	10	1	4.58539	$257.5 \pm 0.9241$
3.5	20	1	9.61097	$123.8 \pm 0.4645$
3.5	50	1	24.3407	$31.59 \pm 0.09614$
3.5	100	1	48.7723	$7.04 \pm 0.02954$
3.5	150	1	73.186	$2.417 \pm 0.01038$
3.5	200	1	97.5987	$1.089 \pm 0.004308$
3.5	300	1	146.447	$0.3709 \pm 0.001616$
3.5	500	1	380.808	$0.06035 \pm 0.0003762$
3.5	1000	1	1079.63	$0.004345 \pm 2.711e-05$
3.5	1500	1	1720.11	$0.0008581 \pm 3.653e-06$
3.5	10	10	0.000775572	$15.08 \pm 0.0569$

Continued on next page

Table C.1 – continued from previous page

Coupling (g)	$m_{\text{Phi}}$ [GeV]	$m_\chi$ [GeV]	$\Gamma_{\text{min}}$ [GeV]	$\sigma$
3.5	20	10	0.00858777	$51.42 \pm 0.1478$
3.5	50	10	18.7909	$32.56 \pm 0.1113$
3.5	100	10	45.9065	$6.963 \pm 0.03199$
3.5	150	10	71.2646	$2.38 \pm 0.009493$
3.5	200	10	96.1548	$1.079 \pm 0.004244$
3.5	300	10	145.483	$0.369 \pm 0.001602$
3.5	500	10	380.229	$0.05978 \pm 0.0003017$
3.5	1000	10	1079.34	$0.004302 \pm 2.412\text{e-}05$
3.5	1500	10	1719.92	$0.0008525 \pm 3.878\text{e-}06$
3.5	10	50	0.000775572	$0.3176 \pm 0.001314$
3.5	20	50	0.00858777	$0.3229 \pm 0.001215$
3.5	50	50	0.0286105	$0.3857 \pm 0.001618$
3.5	100	50	0.0603192	$2.228 \pm 0.00751$
3.5	150	50	30.3684	$2.477 \pm 0.008787$
3.5	200	50	63.4476	$1.025 \pm 0.003864$
3.5	300	50	122.776	$0.3483 \pm 0.001614$
3.5	500	50	366.338	$0.05534 \pm 0.0003035$
3.5	1000	50	1072.34	$0.004076 \pm 2.371\text{e-}05$
3.5	1500	50	1715.24	$0.0008077 \pm 4.889\text{e-}06$
3.5	10	150	0.000775572	$0.01719 \pm 9.115\text{e-}05$
3.5	20	150	0.00858777	$0.01719 \pm 8.334\text{e-}05$
3.5	50	150	0.0286105	$0.01754 \pm 8.239\text{e-}05$
3.5	100	150	0.0603192	$0.01855 \pm 8.371\text{e-}05$
3.5	150	150	0.0937329	$0.02099 \pm 0.0001038$
3.5	200	150	0.130955	$0.0252 \pm 0.0001138$
3.5	300	150	0.233416	$0.1096 \pm 0.0006465$
3.5	500	150	261.885	$0.04374 \pm 0.0002091$
3.5	1000	150	1015.33	$0.00334 \pm 1.751\text{e-}05$
3.5	1500	150	1676.69	$0.0006583 \pm 3.614\text{e-}06$
3.5	10	300	0.000775572	$0.001925 \pm 9.279\text{e-}06$
3.5	20	300	0.00858777	$0.001916 \pm 1.026\text{e-}05$
3.5	50	300	0.0286105	$0.001918 \pm 8.166\text{e-}06$
3.5	100	300	0.0603192	$0.001958 \pm 7.426\text{e-}06$
3.5	150	300	0.0937329	$0.002036 \pm 8.81\text{e-}06$
3.5	200	300	0.130955	$0.002123 \pm 8.379\text{e-}06$
3.5	300	300	0.233416	$0.002448 \pm 9.259\text{e-}06$
3.5	500	300	137.107	$0.004413 \pm 2.588\text{e-}05$
3.5	1000	300	841.774	$0.002184 \pm 1.014\text{e-}05$
3.5	1500	300	1551.86	$0.0004471 \pm 2.349\text{e-}06$
3.5	10	500	0.000775572	$0.0002016 \pm 7.906\text{e-}07$
3.5	20	500	0.00858777	$0.0002011 \pm 9.138\text{e-}07$
3.5	50	500	0.0286105	$0.0002018 \pm 9.929\text{e-}07$
3.5	100	500	0.0603192	$0.0002033 \pm 8.104\text{e-}07$
3.5	150	500	0.0937329	$0.0002067 \pm 8.026\text{e-}07$
3.5	200	500	0.130955	$0.0002106 \pm 8.439\text{e-}07$

Continued on next page

Table C.1 – continued from previous page

Coupling (g)	$m_{\Phi}$ [GeV]	$m_{\chi}$ [GeV]	$\Gamma_{min}$ [GeV]	$\sigma$
3.5	300	500	0.233416	$0.0002225 \pm 9.256\text{e-}07$
3.5	500	500	137.107	$0.0002686 \pm 1.162\text{e-}06$
3.5	1000	500	592.219	$0.0005877 \pm 2.823\text{e-}06$
3.5	1500	500	1291.74	$0.0002318 \pm 1.11\text{e-}06$



## Bibliography

- [A<sup>+</sup>08] J. Alwall et al. Comparative study of various algorithms for the merging of parton showers and matrix elements in hadronic collisions. *Eur.Phys.J.*, C53(2):473–500, 2008.
- [A<sup>+</sup>14a] Georges Aad et al. Search for new particles in events with one lepton and missing transverse momentum in  $pp$  collisions at  $\sqrt{s} = 8$  TeV with the ATLAS detector. *JHEP*, 1409:037, 2014.
- [A<sup>+</sup>14b] Jalal Abdallah et al. Simplified Models for Dark Matter and Missing Energy Searches at the LHC. *arXiv:1409.2893*, 2014.
- [A<sup>+</sup>14c] J. Alwall et al. The automated computation of tree-level and next-to-leading order differential cross sections, and their matching to parton shower simulations. *JHEP*, 07(2):079, 2014.
- [A<sup>+</sup>15] Georges Aad et al. Search for new phenomena in final states with an energetic jet and large missing transverse momentum in  $pp$  collisions at  $\sqrt{s} = 8$  TeV with the ATLAS detector. 2015.
- [AAB<sup>+</sup>14] Jean-Laurent Agram, Jeremy Andrea, Michael Buttignol, Eric Conte, and Benjamin Fuks. Monotop phenomenology at the Large Hadron Collider. *Phys.Rev.*, D89(1):014028, 2014.
- [Aad14a] Search for dark matter in events with a hadronically decaying W or Z boson and missing transverse momentum in  $pp$  collisions at  $\sqrt{s} = 8$  TeV with the ATLAS detector. *Phys.Rev.Lett.*, 112(4):041802, 2014.
- [Aad14b] Search for dark matter in events with a Z boson and missing transverse momentum in  $pp$  collisions at  $\sqrt{s}=8$  TeV with the ATLAS detector. *Phys.Rev.*, D90(1):012004, 2014.
- [Aad15] Search for new phenomena in events with a photon and missing transverse momentum in  $pp$  collisions at  $\sqrt{s} = 8$  TeV with the ATLAS detector. *Phys.Rev.*, D91(1):012008, 2015.

- [ADR<sup>+</sup>14] Mohammad Abdullah, Anthony DiFranzo, Arvind Rajaraman, Tim M.P. Tait, Philip Tanedo, et al. Hidden on-shell mediators for the Galactic Center  $\gamma$ -ray excess. *Phys.Rev.*, D90(3):035004, 2014.
- [AFM11] J. Andrea, B. Fuks, and F. Maltoni. Monotops at the LHC. *Phys.Rev.*, D84:074025, 2011.
- [ATL14] Sensitivity to WIMP Dark Matter in the Final States Containing Jets and Missing Transverse Momentum with the ATLAS Detector at 14 TeV LHC. Technical Report ATL-PHYS-PUB-2014-007, CERN, Geneva, Jun 2014.
- [AWZ14] Haipeng An, Lian-Tao Wang, and Hao Zhang. Dark matter with  $t$ -channel mediator: a simple step beyond contact interaction. *Phys. Rev. D*, 89:115014, 2014.
- [BB13] Yang Bai and Joshua Berger. Fermion Portal Dark Matter. *JHEP*, 11:171, 2013.
- [BCD<sup>+</sup>15] Nicole F. Bell, Yi Cai, James B. Dent, Rebecca K. Leane, and Thomas J. Weiler. Dark matter at the LHC: EFTs and gauge invariance. 2015.
- [BCDF15] Idir Boucheneb, Giacomo Cacciapaglia, Aldo Deandrea, and Benjamin Fuks. Revisiting monotop production at the LHC. *JHEP*, 1501:017, 2015.
- [BDSJ<sup>+</sup>14] Giorgio Busoni, Andrea De Simone, Thomas Jacques, Enrico Morgante, and Antonio Riotto. On the Validity of the Effective Field Theory for Dark Matter Searches at the LHC Part III: Analysis for the  $t$ -channel. *JCAP*, 1409:022, 2014.
- [BDSMR14] Giorgio Busoni, Andrea De Simone, Enrico Morgante, and Antonio Riotto. On the Validity of the Effective Field Theory for Dark Matter Searches at the LHC. *Phys.Lett.*, B728:412–421, 2014.
- [BFG15] Matthew R. Buckley, David Feld, and Dorival Goncalves. Scalar Simplified Models for Dark Matter. *Phys.Rev.*, D91(1):015017, 2015.
- [BLW14] Asher Berlin, Tongyan Lin, and Lian-Tao Wang. Mono-Higgs Detection of Dark Matter at the LHC. *JHEP*, 1406:078, 2014.
- [BT13] Yang Bai and Tim M.P. Tait. Searches with Mono-Leptons. *Phys.Lett.*, B723:384–387, 2013.
- [CDM<sup>+</sup>14] Linda Carpenter, Anthony DiFranzo, Michael Mulhearn, Chase Shimmin, Sean Tulin, et al. Mono-Higgs-boson: A new collider probe of dark matter. *Phys.Rev.*, D89(7):075017, 2014.

- [CEHL14] Spencer Chang, Ralph Edezhath, Jeffrey Hutchinson,  
and Markus Luty. Effective WIMPs. *Phys. Rev. D*,  
89:015011, 2014.
- [CHH15] Andreas Crivellin, Ulrich Haisch, and Anthony Hibbs.  
LHC constraints on gauge boson couplings to dark  
matter. 2015.
- [CHLR13] R.C. Cotta, J.L. Hewett, M.P. Le, and T.G. Rizzo.  
Bounds on Dark Matter Interactions with Electroweak  
Gauge Bosons. *Phys.Rev.*, D88:116009, 2013.
- [CNS<sup>+</sup>13] Linda M. Carpenter, Andrew Nelson, Chase Shimmin,  
Tim M.P. Tait, and Daniel Whiteson. Collider searches  
for dark matter in events with a Z boson and missing  
energy. *Phys.Rev.*, D87(7):074005, 2013.
- [CRTW14] Randel C. Cotta, Arvind Rajaraman, Tim M. P. Tait,  
and Alexander M. Wijangco. Particle Physics Implica-  
tions and Constraints on Dark Matter Interpretations  
of the CDMS Signal. *Phys.Rev.*, D90(1):013020, 2014.
- [DNRT13] Anthony DiFranzo, Keiko I. Nagao, Arvind Rajara-  
man, and Tim M. P. Tait. Simplified Models for Dark  
Matter Interacting With Quarks. *JHEP*, 1311, 2013.
- [Fuk] Benjamin Fuks. Monotop Effective Theory: MadGraph  
model. <http://feynrules.irmp.ucl.ac.be/wiki/Monotops>.
- [GIR<sup>+</sup>10] Jessica Goodman, Masahiro Ibe, Arvind Rajaraman,  
William Shepherd, Tim M.P. Tait, et al. Constraints on  
Dark Matter from Colliders. *Phys.Rev.*, D82:116010,  
2010.
- [HKR13] Ulrich Haisch, Felix Kahlhoefer, and Emanuele Re.  
QCD effects in mono-jet searches for dark matter.  
*JHEP*, 1312:007, 2013.
- [HR15] Ulrich Haisch and Emanuele Re. Simplified dark  
matter top-quark interactions at the LHC. 2015.
- [K<sup>+</sup>14] Vardan Khachatryan et al. Search for physics beyond  
the standard model in final states with a lepton and  
missing transverse energy in proton-proton collisions  
at  $\sqrt{s} = 8$  TeV. 2014.
- [Kha14] Search for new phenomena in monophoton final states  
in proton-proton collisions at  $\sqrt{s} = 8$  TeV. 2014.
- [NCC<sup>+</sup>14] Andy Nelson, Linda M. Carpenter, Randel Cotta,  
Adam Johnstone, and Daniel Whiteson. Confronting  
the Fermi Line with LHC data: an Effective Theory  
of Dark Matter Interaction with Photons. *Phys.Rev.*,  
D89(5):056011, 2014.

- 1397 [PVZ<sub>14</sub>] Michele Papucci, Alessandro Vichi, and Kathryn M.  
1398 Zurek. Monojet versus the rest of the world I:  $t$ -  
1399 channel models. *JHEP*, 2014.
- 1400 [RWZ<sub>15</sub>] Davide Racco, Andrea Wulzer, and Fabio Zwirner.  
1401 Robust collider limits on heavy-mediator Dark Matter.  
1402 2015.
- 1403 [ZBW<sub>13</sub>] Ning Zhou, David Berge, and Daniel Whiteson. Mono-  
1404 everything: combined limits on dark matter produc-  
1405 tion at colliders from multiple final states. *Phys.Rev.*,  
1406 D87(9):095013, 2013.



